

Fundamental studies on electrophoretic methods
with poly(ethylene glycol)-based materials

Chenchen Liu

2021

Contents

<i>General introduction</i>	1
<i>Chapter I</i>	
Online fluorescence imaging method by reducing the inequivalent photobleaching for a quantitative capillary electrophoresis	11
<i>Chapter II</i>	
Controllable molecular sieving by <i>copoly</i> (poly(ethylene glycol) acrylate/poly(ethylene glycol) diacrylate) based hydrogels via capillary electrophoresis for DNA fragments	29
<i>Chapter III</i>	
<i>Copoly</i> (poly(ethylene glycol) diacrylate/poly(ethylene glycol) acrylate) based molecularly imprinted polymer for the specific adsorption and selective electrophoretic separation of native cytochrome c	53
<i>Chapter IV</i>	
Fabrication of protein recognition structures by grafting molecularly imprinted polymer on a crosslinked hydrogel	73
<i>General conclusion</i>	85
<i>List of publications</i>	87
<i>Acknowledgments</i>	89

General introduction

1. Background

1.1 Electrophoresis

In the field of analytical chemistry, electrophoresis is one of powerful methods to separate analytes via an electric force. Generally, the charged analytes are moved by the electric force and distinguished by the migration distance or migration mobility resulting the qualitatively or quantitatively determination. An electrophoresis equipment is composed of a power supplier to provide the electric field, a background electrolyte to guarantee the analytes participate in the electric circuit, and a detection system to detect the signal of analytes (Fig. 1). Categorizing by the form of equipment, different kinds of electrophoresis are presented. The separation in free flow electrophoresis (FFE)¹ and slab gel electrophoresis (SGE)² occur in a two-dimensional (2D) flat space. Capillary electrophoresis (CE) employs a thin fused silica capillary (inner diameter < 100 μm) as a separation channel to confine the background electrolyte³. The integration of electrophoretic analysis with the upward and downward analysis into a micro-total analysis system ($\mu\text{-TAS}$) is one trend at present^{4, 5}. With the advancing of separation methods and detection methods, the three-dimensional (3D) form of electrophoresis has been realized with the assistance of a 3D microfluidic device and the confocal/light-sheet imaging technology⁶.

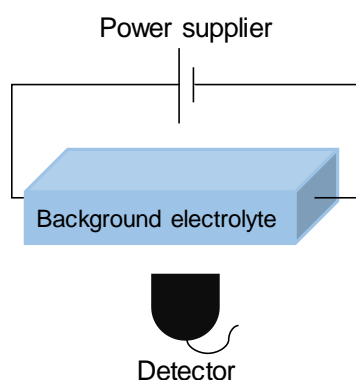


Fig. 1 Basic equipment elements used in an electrophoretic analysis.

Electrophoresis is versatile to analyze a variety of components, including ions⁷, nucleic acids^{8, 9}, proteins^{10, 11}, polysaccharides¹², nanoparticles^{13, 14}, cells¹⁵⁻¹⁷, etc. To accommodate the nature property of the analytes, various separation modes have been developed, so that the analytes would be separated by

the charge to mass ratio, size, or affinity to a ligand. Here the author would like to introduce two major separation techniques: gel electrophoresis¹⁸ and affinity electrophoresis¹⁹, which are involved in this study. In a constant electric field and a constant background electrolyte, the migration velocity of an analyte depends on its charge to mass ratio. While, some molecules such as nucleic acids, their charge to mass ratios are too close to be distinguished. Gel electrophoresis takes the polymer network in a hydrogel as sieving matrix. When the pore size of the polymer network discriminates the size of the analytes, and then fractional effects occurs, thereby the size sieving of analytes can be realized. Gel electrophoresis, including SGE, capillary gel electrophoresis (CGE), and capillary polymer electrophoresis (CPE), has become a workhorse in the field of biomolecule analysis. Recent studies related with gel electrophoresis concerns new protocols for the determination of a specified analyte^{20, 21}, involving new size sieving materials to facilitate experimental operation^{22, 23}, improve the separation performance²⁴⁻²⁸, realize new functionality²⁹ for the design of new methods and devices for μ -TAS³⁰⁻³², etc.

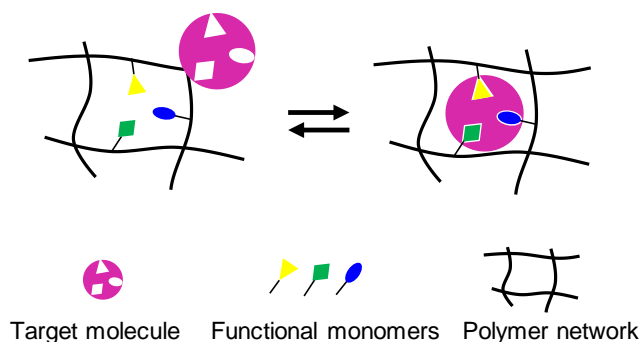


Fig. 2 Schematic diagram of molecularly imprinting polymer and its specific recognition of target molecule.

Affinity electrophoresis is generally suitable for specific binding, separation, and determination of bio-related molecules. The mobility of a molecule varies according to whether or not they interact with the affinity ligand. Molecules with a similar size are separated depending on their affinity activities with the ligand; the kinetic interaction between the ligands and targets are measurable³³. The affinity ligand is complexed into a hydrogel or coated on the inner surface of a capillary³⁴. When plotting affinity electrophoresis, the choice of a proper ligand is indispensable because the separation is based on the difference of the affinity strength between molecules and ligands. Variety of ligands including small molecules like metal complex^{35, 36}, boronic compounds³⁷, and macromolecules³⁸⁻⁴⁰ such as nucleic acids, enzymes, antibodies, and antigens, have been previously reported. As a novel form of a ligand, a molecularly imprinted polymer (MIP) (Fig. 2) is available, which is an artificial molecular recognition

material that can be fabricated with the presence of a template molecule under polymer networks^{41, 42}. MIPs, especially for biomolecules, memorize the surface information of the template molecule and shows high affinity to target molecule. Compared to some ligands obtained from nature source, MIPs have merits of cost effective, easy to obtain, structurally stable, and designable specificity. Therefore, the author expects that MIPs will be a promising prospect as the affinity material in the electrophoretic separation⁴³⁻⁴⁶.

1.2.1 Hydrogel in electrophoresis

A hydrogel is one type of 3D networks formed by the hydrophilic polymers absorbing a substantial amount of aqueous solution (Fig. 3 (a)). Depending on the chemical composition of the polymer, the hydrogel can possess tunable physical and chemical properties, release physical or biochemical signal spontaneously or upon external stimuli, allow for spatiotemporal control⁴⁷. Usually, the background electrolyte in an electrophoretic analysis is an aqueous solution, thus when absorbing the background electrolyte, a hydrogel may serve as a sieving matrix and/or a scaffold of affinity ligand (Fig. 3 (b), (c)). Agarose gels and crosslinked polyacrylamide gels are used as hydrogels. Replaceable polymer solutions, which can provide an entangled polymer network and flushed after each run, are frequently employed in CPE and microfluidic devices⁴.

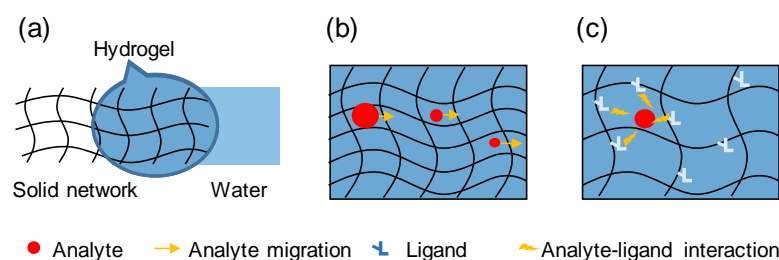


Fig. 3 (a) Illustration of hydrogel which is composed of a solid polymer network absorbing an aqueous solution. (b) Illustration of size sieving matrix using a hydrogel to separate molecules by size. (c) Illustration of affinity ligand attached on a hydrogel network.

With the advances in adjustable synthesis, novel hydrogels have been widely developed to promote the electrophoretic technology with improved separation performance, facile operation, rapid analysis, and high compactness form. For example, high pressure (1000 psi) is required in the column filling with a viscous sieving matrix, which is not applicable to microfluidic devices owing to their moderate pressure tolerance (<200 psi)⁴. Thermal responsive polymers showed dramatic viscosity alteration upon the

change of temperature, and were reported to be facile in column filling at one temperature and capable of high resolution separation at another temperature⁴⁸. As another example, multi-functional hydrogel served as size sieving matrix at one stage of the analysis and play as affinity binding scaffolds at another stage of analysis, with which the sample transformation between two stages of analysis was exempted and the compactness of the microfluidic device increased^{30, 31}. According to these achievements, the progress of hydrogel would bring new opportunities and possible breakthrough to the electrophoretic technology.

1.2.2 Poly(ethylene glycol) based hydrogel

A poly(ethylene glycol) (PEG)-based hydrogel is composed of hydrophilic PEG polymer subunits absorbable a high water content. The PEG-based hydrogel can be synthesized from different types of monomer, for example, the polycondensation of tetraamine-terminated PEG with tetra-*N*-hydroxysuccinimidyl-glutarate-terminated PEG⁴⁹, and the free radical polymerization of PEG diacrylate (PEGDA) and PEG acrylate (PEGA)⁵⁰. Thus, the different kinds of PEG polymer exist, such as linear PEG polymer and non-linear PEG polymer (Fig. 4)⁵¹. Especially, the structure of non-linear poly(PEGA) polymer is composed of carbon-carbon backbone and oligo(ethylene glycol) side chains. A precise modification of its functionality becomes simple by just changing the chemical composition of the side chain segment. For example, as the PEG methacrylate (PEGMA) oligo has a thermal responsive character and show various lower critical solution temperature (LCST) ranging from 26 to 90 °C depending on the oligo length and polymer concentration⁵¹. To precisely modify the LCST of poly(PEGMA), it just requires a random copolymerization of different oligo with a stoichiometric amount⁵².

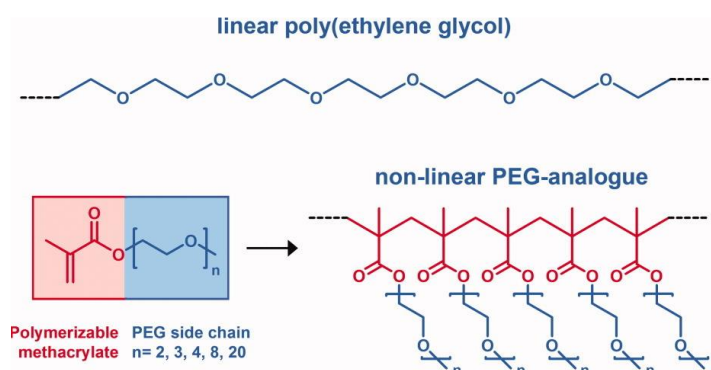


Fig. 4 Molecular structure of standard linear PEG and nonlinear PEG-analogues constructed with oligo(ethylene glycol) (macro)monomers⁵¹. Copyright (2008) obtained from Wiley.

The PEG material is well recognized as its biocompatibility with the evidences of not elicit an immune response and not induce cell death⁵³. Thus, PEG is widely applied for biological applications, such as the modification of therapeutic proteins and peptides, the coating of drug delivery carriers, the scaffold for *in vivo* cell culture, etc. On the standing point of analytical chemistry, the PEG polymer is also suitable for analysis of biomolecule because of showing less unspecific hydrogen interactions. So far, the PEG polymer solutions and PEG-based hydrogels have been reported as size sieving matrix with highly efficient separations^{54, 55}. Previous studies also demonstrated the possibility to apply PEG-based hydrogels to the stimuli-responsive MIP materials^{56, 57}. In this work, the author continues to use the novel PEG-based materials as size sieving matrix (Chapter I). In addition, the author also attempts to develop new PEG-based materials for molecular size sieving (Chapter II) and affinity recognition (Chapters III and IV).

1.3 Online fluorescence detection and the photobleaching phenomenon

The fluorescence detection is a method to detect the fluorescent emission of the analyte under an excitation wavelength. The analyte may be self-fluorescence or complexed with fluorophores. As the emission wavelength is different to its excitation length, the sensitive detection is obtained owing to filtering the background noise. In most CE and microfluidic electrophoretic systems, an online detection manner is usually employed for the signal collection from a detection window opened on the separation channel. The signal collection is processed while the analytes are migrating; the obtained electropherogram reflects the signal intensity in the detection window. According to previous studies, these features of online fluorescence detection should be carefully handled otherwise the detection sensitivity and quantitative determination are affected.

The photobleaching of fluorophores is an inevitable photoinduced oxidation process accompanied with the fluorescent excitation. As the online fluorescence detection taking the analyte's fluorescent intensity for quantitative analysis, the effect of photobleaching on the profile of electrophoretic peaks requires a deep understanding. Previous studies showed that the photobleaching affects the sensitivity of CE^{58, 59}. Hirschfeld's theoretical study predicted that a high signal-to-noise ratio (SNR) could be achieved even for low quantum efficiency fluorophores, as long as a complete photobleaching could be implemented⁶⁰. Because the analytes pass through the detection window at different velocities, the faster one will be exposed by a shorter time duration and the slower one by a longer time duration. Consequently, inequivalent photobleaching occurs with a velocity dependence. Other reports demonstrated that the

inequivalent photobleaching in online detection affects the accuracy of quantitative analysis⁶¹⁻⁶³. One solution is to tune the excitation power accordingly with the analyte's velocity^{61, 62}. Another approach is to reduce the total photodegradation of fluorophores. A few studies included the use of a high migration velocity, the use of the fluorophores with high photostability, the use of the photostabilizing buffer additives, or the use of a low-power laser beam^{61, 63}. Besides, reducing the length of the detection window helps to reduce the time duration for excitation. However, this is at a trade for the detection sensitivity, because the total time for collecting fluorescent emissions will also be reduced⁶⁴.

2. Contents of this thesis

The contents of this thesis contain fundamental studies of electrophoresis with the aim of providing approaches to an accurate quantitative CE (qCE) analysis, an efficient size sieving separation, and a selective separation for target molecule. In detail, chapter I concentrates on reducing the interference of inequivalent photobleaching with qCE. An online fluorescent imaging detection method was set up to trace the real-time fluorescent intensity of migrating analytes, so that the accuracy of qCE would be guaranteed by collecting the fluorescent intensities under identical photo exposure duration. Chapter II reports the separation performance of a new size sieving material via CE. The proposed *copoly*(PEG diacrylate/PEG acrylate) (*copoly*(PEGDA/PEGA)) hydrogel was demonstrated to have a comparable size sieving ability as well as a high repeatability compared with the authentic polyacrylamide (PA) gel. Chapter III and chapter IV focus on the fabrication of PEG-based MIP hydrogels for the specific recognition to target proteins, and then MIP hydrogels could be used as affinity materials in electrophoretic separations. Chapter III shows the *copoly*(PEGDAPEGA) hydrogel as a new MIP material; the compositions of the *copoly*(PEGDAPEGA) hydrogel were investigated for a high specific molecular recognition. A hybrid slab gel was developed containing a MIP gel zone and a PA zone, with which a selective separation of target protein (cytochrome c) was realized. Chapter IV proposes a new approach to fabricate an MIP material by a postmodification of a crosslinked hydrogel. The MIP structure was grafted on a polymer network strand via the atom transfer radical polymerization. Although future work is still demanded to demonstrate selective electrophoretic separations, current result shows the possibility to use the resulting MIP hydrogel for the specific adsorption of target proteins (cytochrome c and trypsin).

References

- (1) Johnson, A. C.; Bowser, M. T., Micro free flow electrophoresis. *Lab Chip* **2018**, *18*, 27-40.
- (2) Zarei, M.; Zarei, M.; Ghasemabadi, M., Nanoparticle improved separations: From capillary to slab gel electrophoresis. *Trends Anal. Chem.* **2017**, *86*, 56-74.
- (3) Voeten, R. L. C.; Ventouri, I. K.; Haselberg, R.; Somsen, G. W., Capillary Electrophoresis: Trends and Recent Advances. *Anal. Chem.* **2018**, *90*, 1464-1481.
- (4) Chung, M.; Kim, D.; Herr, A. E., Polymer sieving matrices in microanalytical electrophoresis. *Analyst* **2014**, *139*, 5635-5654.
- (5) Wenclawiak, B. W.; Puschl, R., Sample injection for capillary electrophoresis on a micro fabricated device/on chip CE injection. *Anal. Lett.* **2006**, *39*, 3-16.
- (6) Grist, S. M.; Mourdoukoutas, A. P.; Herr, A. E., 3D projection electrophoresis for single-cell immunoblotting. *Nat. Commun.* **2020**, *11*, 6237.
- (7) Mai, T. D.; Le, M. D.; Sáiz, J.; Duong, H. A.; Koenka, I. J.; Pham, H. V.; Hauser, P. C., Triple-channel portable capillary electrophoresis instrument with individual background electrolytes for the concurrent separations of anionic and cationic species. *Anal. Chim. Acta* **2016**, *911*, 121-128.
- (8) Liu, C.; Yamaguchi, Y.; Zhu, X.; Li, Z.; Ni, Y.; Dou, X., Analysis of small interfering RNA by capillary electrophoresis in hydroxyethylcellulose solutions. *Electrophoresis* **2015**, *36*, 1651-1657.
- (9) Liu, C.; Li, Z.; Meng, F.; Ni, Y.; Dou, X.; Yamaguchi, Y., Capillary Electrophoresis of DNA in Hydroxyethylcellulose. *Acta Chim. Sinica* **2013**, *71*, 265-270.
- (10) Bao, J.; Krylova, S. M.; Cherney, L. T.; Hale, R. L.; Belyanskaya, S. L.; Chiu, C. H.; Arico-Muendel, C. C.; Krylov, S. N., Prediction of protein-DNA complex mobility in gel-free capillary electrophoresis. *Anal. Chem.* **2015**, *87*, 2474-9.
- (11) Jonasdottir, H. S.; Papan, C.; Fabritz, S.; Balas, L.; Durand, T.; Hardardottir, I.; Freysdottir, J.; Giera, M., Differential mobility separation of leukotrienes and protectins. *Anal. Chem.* **2015**, *87*, 5036-40.
- (12) Kubo, T.; Nishimura, N.; Furuta, H.; Kubota, K.; Naito, T.; Otsuka, K., Tunable separations based on a molecular size effect for biomolecules by poly(ethylene glycol) gel-based capillary electrophoresis. *J. Chromatogr. A* **2017**, *1523*, 107-113.
- (13) Hanauer, M.; Pierrat, S.; Zins, I.; Lotz, A.; Sönnichsen, C., Separation of Nanoparticles by Gel Electrophoresis According to Size and Shape. *Nano Lett.* **2007**, *7*, 2881-2885.
- (14) Kang, Y.; Kim, J., Electrochemiluminescence of Glutathione-Stabilized Au Nanoclusters Fractionated by Gel Electrophoresis in Water. *ChemElectroChem* **2020**, *7*, 1058-1058.
- (15) van Tricht, E.; Geurink, L.; Pajic, B.; Nijenhuis, J.; Backus, H.; Germano, M.; Somsen, G. W.; Sanger-van de Griend, C. E., New capillary gel electrophoresis method for fast and accurate identification and quantification of multiple viral proteins in influenza vaccines. *Talanta* **2015**, *144*, 1030-1035.
- (16) Phung, S. C.; Cabot, J. M.; Macka, M.; Powell, S. M.; Guijt, R. M.; Breadmore, M., Isotachophoretic Fluorescence in Situ Hybridization of Intact Bacterial Cells. *Anal. Chem.* **2017**, *89*, 6513-6520.
- (17) Zhang, C.-X.; Meagher, M. M., Sample Stacking Provides Three Orders of Magnitude

- Sensitivity Enhancement in SDS Capillary Gel Electrophoresis of Adeno-Associated Virus Capsid Proteins. *Anal. Chem.* **2017**, *89*, 3285-3292.
- (18) Issaq, H. J.; Veenstra, T. D., Two-dimensional polyacrylamide gel electrophoresis (2D-PAGE): advances and perspectives. *Biotechniques* **2008**, *44*, 697-+.
- (19) Takeo, K., Affinity electrophoresis: Principles and applications. *Electrophoresis* **1984**, *5*, 187-195.
- (20) Bharti; Gopmandal, P. P.; Bhattacharyya, S.; Ohshima, H., A simplified model for gel electrophoresis of a hydrophobic rigid colloid. *Soft Matter*.
- (21) Filep, C.; Szigeti, M.; Farsang, R.; Haberger, M.; Reusch, D.; Guttman, A., Multilevel capillary gel electrophoresis characterization of new antibody modalities. *Anal. Chim. Acta* **2021**, *1166*.
- (22) Wan, F.; He, W.; Zhang, J.; Chu, B., Reduced matrix viscosity in DNA sequencing by CE and microchip electrophoresis using a novel thermo-responsive copolymer. *Electrophoresis* **2009**, *30*, 2488-2498.
- (23) Sudor, J.; Barbier, V.; Thiro, S.; Godfrin, D.; Hourdet, D.; Millequant, M.; Blanchard, J.; Viovy, J.-L., New block-copolymer thermoassociating matrices for DNA sequencing: Effect of molecular structure on rheology and resolution. *Electrophoresis* **2001**, *22*, 720-728.
- (24) Li, X.; Khairulina, K.; Chung, U.-i.; Sakai, T., Electrophoretic mobility of double-stranded DNA in polymer solutions and gels with tuned structures. *Macromolecules* **2014**, *47*, 3582-3586.
- (25) Zarei, M.; Goharshadi, E. K.; Ahmadzadeh, H.; Samiee, S., Improvement of heat dissipation in agarose gel electrophoresis by metal oxide nanoparticles. *RSC Adv.* **2015**, *5*, 88655-88665.
- (26) Sajjadi, S. H.; Goharshadi, E. K.; Ahmadzadeh, H., Heat dissipation in slab gel electrophoresis: The effect of embedded TiO₂ nanoparticles on the thermal profiles. *J. Chromatogr. B* **2019**, *1118-1119*, 63-69.
- (27) Shaabani, N.; Jemere, A. B.; Harrison, D. J., Size - based proteins separation using polymer - entrapped colloidal self - assembled nanoparticles on - chip. *Electrophoresis* **2016**, *37*, 2602-2609.
- (28) Guo, Y.; Huang, L.; Baeyens, W. R. G.; Delanghe, J. R.; He, D.; Ouyang, J., Novel Application of Carbon Nanotubes for Improving Resolution in Detecting Human Serum Proteins with Native Polyacrylamide Gel Electrophoresis. *Nano Lett.* **2009**, *9*, 1320-1324.
- (29) He, M.; Herr, A. E., Automated microfluidic protein immunoblotting. *Nat. Protoc.* **2010**, *5*, 1844-1856.
- (30) Hughes, A. J.; Lin, R. K. C.; Peehl, D. M.; Herr, A. E., Microfluidic integration for automated targeted proteomic assays. *Proc. Natl. Acad. Sci. U. S. A.* **2012**, *109*, 5972-5977.
- (31) Kang, C.-C.; Yamauchi, K. A.; Vlassakis, J.; Sinkala, E.; Duncombe, T. A.; Herr, A. E., Single cell-resolution western blotting. *Nat. Protoc.* **2016**, *11*, 1508-1530.
- (32) Hou, C.; Herr, A. E., Ultrashort separation length homogeneous electrophoretic immunoassays using on-chip discontinuous polyacrylamide gels. *Anal. Chem.* **2010**, *82*, 3343-3351.
- (33) Kinoshita, E.; Kinoshita-Kikuta, E.; Koike, T., The Cutting Edge of Affinity Electrophoresis Technology. *Proteomes* **2015**, *3*, 42-55.
- (34) Baba, Y., Capillary affinity gel electrophoresis: new technique for specific recognition of DNA sequence and the mutation detection on DNA. *J. Biochem. Biophys. Methods* **1999**, *41*, 91-101.
- (35) Kinoshita, E.; Takahashi, M.; Takeda, H.; Shiro, M.; Koike, T., Recognition of phosphate monoester dianion by an alkoxide-bridged dinuclear zinc(ii) complex. *Dalton Trans.* **2004**, 1189-1193.

- (36) Kinoshita, E.; Kinoshita-Kikuta, E.; Koike, T., Separation and detection of large phosphoproteins using Phos-tag SDS-PAGE. *Nat. Protoc.* **2009**, *4*, 1513-1521.
- (37) Li, D.; Chen, Y.; Liu, Z., Boronate affinity materials for separation and molecular recognition: structure, properties and applications. *Chem. Soc. Rev.* **2015**, *44*, 8097-8123.
- (38) Awada, C.; Sato, T.; Takao, T., Affinity-Trap Polyacrylamide Gel Electrophoresis: A Novel Method of Capturing Specific Proteins by Electro-Transfer. *Anal. Chem.* **2010**, *82*, 755-761.
- (39) Zhang, C.; Woolfork, A. G.; Suh, K.; Ovbude, S.; Bi, C.; Elzoeiry, M.; Hage, D. S., Clinical and pharmaceutical applications of affinity ligands in capillary electrophoresis: A review. *J. Pharm. Biomed. Anal.* **2020**, *177*, 112882.
- (40) Pont, L.; Benavente, F.; Barbosa, J.; Sanz-Nebot, V., On-line immunoaffinity solid-phase extraction capillary electrophoresis mass spectrometry using Fab antibody fragments for the analysis of serum transthyretin. *Talanta* **2017**, *170*, 224-232.
- (41) Chen, L.; Xu, S.; Li, J., Recent advances in molecular imprinting technology: current status, challenges and highlighted applications. *Chem. Soc. Rev.* **2011**, *40*, 2922-42.
- (42) Chen, L.; Wang, X.; Lu, W.; Wu, X.; Li, J., Molecular imprinting: perspectives and applications. *Chem. Soc. Rev.* **2016**, *45*, 2137-211.
- (43) Lin, J. M.; Nakagama, T.; Uchiyama, K.; Hobo, T., Molecularly imprinted polymer as chiral selector for enantioseparation of amino acids by capillary gel electrophoresis. *Chromatographia* **1996**, *43*, 585-591.
- (44) Moreno-Gonzalez, D.; Lara, F. J.; Gamiz-Gracia, L.; Garcia-Campana, A. M., Molecularly imprinted polymer as in-line concentrator in capillary electrophoresis coupled with mass spectrometry for the determination of quinolones in bovine milk samples. *J. Chromatogr. A* **2014**, *1360*, 1-8.
- (45) Lara, F. J.; Lynen, F.; Sandra, P.; Garcia-Campana, A. M.; Ales-Barrero, F., Evaluation of a molecularly imprinted polymer as in-line concentrator in capillary electrophoresis. *Electrophoresis* **2008**, *29*, 3834-3841.
- (46) An, J. Y.; Azizov, S.; Kumar, A. P.; Lee, Y. I., Quantitative Analysis of Artificial Sweeteners by Capillary Electrophoresis with a Dual-Capillary Design of Molecularly Imprinted Solid-Phase Extractor. *Bull. Korean Chem. Soc.* **2018**, *39*, 1315-1319.
- (47) Zhang, Y. S.; Khademhosseini, A., Advances in engineering hydrogels. *Science* **2017**, *356*, eaaf3627.
- (48) Durney, B. C.; Lounsbury, J. A.; Poe, B. L.; Landers, J. P.; Holland, L. A., A Thermally Responsive Phospholipid Pseudogel: Tunable DNA Sieving with Capillary Electrophoresis. *Anal. Chem.* **2013**, *85*, 6617-6625.
- (49) Sakai, T.; Matsunaga, T.; Yamamoto, Y.; Ito, C.; Yoshida, R.; Suzuki, S.; Sasaki, N.; Shibayama, M.; Chung, U. I., Design and fabrication of a high-strength hydrogel with ideally homogeneous network structure from tetrahedron-like macromonomers. *Macromolecules* **2008**, *41*, 5379-5384.
- (50) Kinoshita, T.; Ishigaki, Y.; Nakano, K.; Yamaguchi, K.; Akita, S.; Nii, S.; Kawaizumi, F., Application of acrylate gel having poly(ethylene glycol) side chains to recovery of gold from hydrochloric acid solutions. *Sep. Purif. Technol.* **2006**, *49*, 253-257.
- (51) Lutz, J.-F., Polymerization of oligo(ethylene glycol) (meth)acrylates: Toward new generations of smart biocompatible materials. *J. Polym. Sci., Part A: Polym. Chem.* **2008**, *46*, 3459-3470.
- (52) Lutz, J.-F.; Hoth, A., Preparation of Ideal PEG Analogues with a Tunable Thermosensitivity by

- Controlled Radical Copolymerization of 2-(2-Methoxyethoxy)ethyl Methacrylate and Oligo(ethylene glycol) Methacrylate. *Macromolecules* **2006**, *39*, 893-896.
- (53) Lutz, J.-F.; Andrieu, J.; Üzgün, S.; Rudolph, C.; Agarwal, S., Biocompatible, Thermoresponsive, and Biodegradable: Simple Preparation of “All-in-One” Biorelevant Polymers. *Macromolecules* **2007**, *40*, 8540-8543.
- (54) Yamaguchi, Y.; Li, Z.; Zhu, X.; Liu, C.; Zhang, D.; Dou, X., Polyethylene Oxide (PEO) and Polyethylene Glycol (PEG) Polymer Sieving Matrix for RNA Capillary Electrophoresis. *PLoS One* **2015**, *10*, e0123406.
- (55) Li, X.; Khairulina, K.; Chung, U.-i.; Sakai, T., Migration Behavior of Rodlike dsDNA under Electric Field in Homogeneous Polymer Networks. *Macromolecules* **2013**, *46*, 8657-8663.
- (56) Kubo, T.; Arimura, S.; Tominaga, Y.; Naito, T.; Hosoya, K.; Otsuka, K., Molecularly imprinted polymers for selective adsorption of lysozyme and cytochrome c using a PEG-based hydrogel: selective recognition for different conformations due to pH conditions. *Macromolecules* **2015**, *48*, 4081-4087.
- (57) Tominaga, Y.; Kubo, T.; Sueyoshi, K.; Hosoya, K.; Otsuka, K., Synthesis of poly(ethylene glycol)-based hydrogels and their swelling/shrinking response to molecular recognition. *J. Polym. Sci., Part A: Polym. Chem.* **2013**, *51*, 3153-3158.
- (58) Johnson, M. E.; Landers, J. P., Fundamentals and practice for ultrasensitive laser-induced fluorescence detection in microanalytical systems. *Electrophoresis* **2004**, *25*, 3513-3527.
- (59) Ramsay, L. M.; Dickerson, J. A.; Dada, O.; Dovichi, N. J., Femtomolar concentration detection limit and zeptomole mass detection limit for protein separation by capillary isoelectric focusing and laser-induced fluorescence detection. *Anal. Chem.* **2009**, *81*, 1741-1746.
- (60) Hirschfeld, T., Quantum efficiency independence of the time integrated emission from a fluorescent molecule. *Appl. Opt.* **1976**, *15*, 3135-3139.
- (61) White, J. C.; Stryer, L., Photostability studies of phycobiliprotein fluorescent labels. *Anal. Biochem.* **1987**, *161*, 442-452.
- (62) Shear, J. B.; Dadoo, R.; Fishman, H. A.; Scheller, R. H.; Zare, R. N., Optimizing fluorescence detection in chemical separations for analyte bands traveling at different velocities. *Anal. Chem.* **1993**, *65*, 2977-2982.
- (63) Wu, S.; Dovichi, N. J., High-sensitivity fluorescence detector fluorescein isothiocyanate derivatives of amino acids separated by capillary zone electrophoresis. *J. Chromatogr.* **1989**, *480*, 141-155.
- (64) Altria, K., D., In *Capillary electrophoresis guidebook*, Humana Press: Totowa, New Jersey, **1995**; Vol. 52, pp 71-82.

Chapter I

Online fluorescence imaging method by reducing the inequivalent photobleaching for quantitative capillary electrophoresis

Abstract

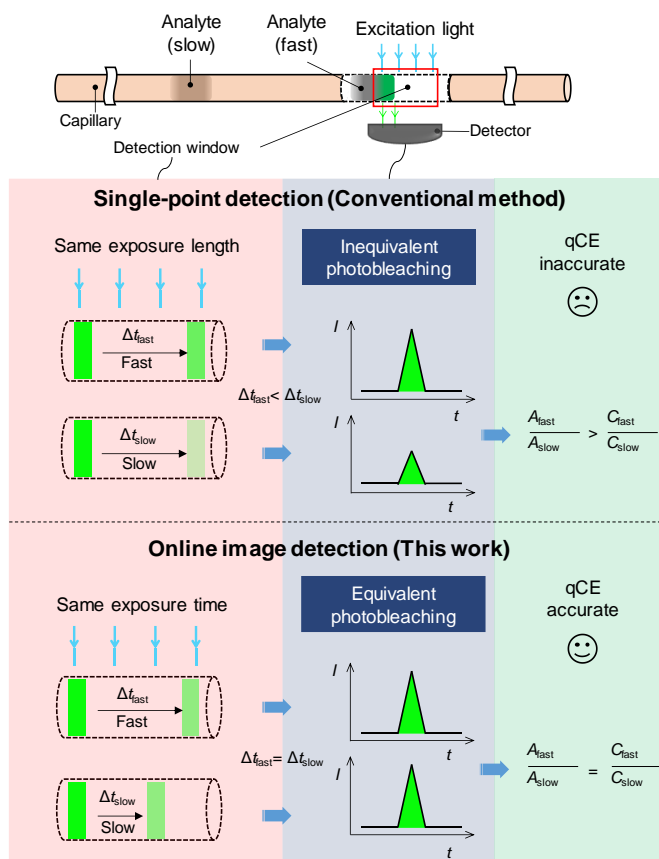
In traditional capillary electrophoresis (CE) by fluorescence detection, the difference of the migration time of analytes leads to the inequivalent photobleaching, therefore the quantitative determination of the analytes is usually difficult. Especially, when an internal standard (IS) is used, the fluorescent intensities of analytes are hardly comparable to that of IS if the inequivalent photobleaching is not restricted. We propose a practical approach to reduce the effect of inequivalent photobleaching via an online fluorescence imaging system coupled with the IS method. The detection was operated by the acquisitions of the fluorescent intensities from the divided small section array in the detection window and the electropherograms were obtained from the integrated each acquisition. Compared with the traditional CE detection method, the proposed method demonstrates a real-time detection to collect the fluorescence signals of different analytes under the definite exposure time, rather than the same traversing length. Experimental demonstration for the proposed method was carried out by using DNA-dye conjugations. As result, our method provided a lower relative error of peak area ratio of 0.3-3.2% and a more practical operation because the efforts to restrict the photobleaching are exempted.

1. Introduction

Quantitative capillary electrophoresis (qCE) by a fluorescence-detection is a molecular detection technology which has merits of high sensitivity, high specificity, high precision, and multi-target feasibility¹⁻³. Accurate quantification of biomolecules, such as nucleic acids, proteins, and polysaccharides, promotes the early diagnosis, the study of disease progress and the study of single cells. Thus the fluorescence-detection based qCE (FL-qCE) has a wide application in precision medicine⁴, biomolecule diagnosis^{2, 5, 6}, and cell analysis⁷. Besides, the FL-qCE's integrative and cost-effective properties have attracted considerable attention in the development of miniaturized assemblies, including the microchip electrophoresis⁸⁻¹¹. The most portable microsystems for sample-to-answer analysis, which applies to the point of need analysis¹² of pathogen detection and forensic genotyping, are coupled with FL-qCE¹³⁻¹⁶.

The photobleaching of fluorophores is an inevitable photoinduced oxidation process accompany with the fluorescent excitation. As the qCE takes the analyte's fluorescent intensity for quantitative analysis, the effect of photobleaching on the profile of electrophoretic peaks requires a deep understanding. Previous works showed that the photobleaching affects the sensitivity of FL-qCE¹⁷⁻²⁰. Studies also have been carried out focusing on improving the quantitative properties by restricting the inequivalent photobleaching. One solution is to tune the excitation power accordingly with the analyte's velocity^{21, 22}. Another approach is to reduce the total photodegradation of fluorophores. The reported measures include the use of a high migration velocity, the use of the fluorophores with high photostability, the use of the photostabilizing buffer additives, or the use of a low-power laser beam^{21, 23}. Besides, reducing the length of the detection window helps to reduce the time duration for excitation, as well as to improve the detection resolution²⁴. However, this is at a trade for the detection sensitivity, because the total time for collecting fluorescent emissions will also be reduced²⁵. It is noted that some measures are not feasible for quantitative analysis, although they can yield a higher SNR. For example, the pulsed laser helps to yield high SNR, but not applicable for producing a linear relation over a wide range of concentration²⁶. In summary, the existing methods can be efficient to restrict the influence of inequivalent photobleaching on the quantitative analysis, but the detection conditions/apparatus are complexed, the choice of fluorophores is limited or the detection sensitivity is sacrificed.

It can be seen that a more practical qCE measure is appealed to avoid the undesired influence from the photobleaching of analytes, which is the main target in this work. The internal standard (IS) method



Scheme 1. A comparison schematic diagram of the conventional single-point detection method and the online fluorescence imaging method in this work. These two methods integrate the fluorescent emission with different manners, resulting in different peak area ratios of the fast to the slow analytes (A_{fast}/A_{slow}). While both methods can perform migration velocity analysis. The latter one can record the equivalent photobleaching of analytes and provide a more accurate quantitative analysis. Δt , exposure time; C , analyte concentration; I , fluorescent intensity; t , migration time.

is a convenient self-calibration approach for the quantitative analysis, which doesn't require the construction of a calibration curve²⁷. Within a single CE run, the concentration of the analyte can be calculated from the peak area ratio (R) of the analytes to the IS. As the analytes and IS have different migration velocities, the inequivalent photobleaching between the analyte and IS will introduce inaccuracy to the calculation of the IS method. In this work, an online fluorescence imaging method is proposed to study the photobleaching of migrating analytes. While an online fluorescence imaging system is commonly employed in the self-assembled CE apparatus for image capture^{28,29}, this work employs it to record the real-time fluorescent intensities of the moving analytes; and scripts an image analysis program for tracing the change in peak profiles upon photobleaching. As is shown by the online image detection in Scheme 1, the proposed method will be applied to the IS method for avoiding

the inequivalent-photobleaching-induced error. Providing the IS and the analyte have the an identical photodegrading rate, quantum efficiency, buffer environment, and close concentration, practically they will experience the same rate of photobleaching²². Using the online fluorescence image detection method to index their fluorescent intensities under an equal time-duration of illumination, the inequivalent-photobleaching-induced error could be avoided. Therefore, this paper attempts to experimentally demonstrate the IS-online fluorescence image method by using DNA-dye conjugations as a standard sample.

At first, we briefly demonstrate our method to use an online fluorescence image detection system in FL-qCE. Then, we experimentally confirm the role of photobleaching in alternating the peak areas. The photodegrading rates of peak areas under various conditions are examined, including the intensity of excitation irradiance, the type of fluorophore and the migration velocity. The method to collect the fluorescent intensities at equivalent photoalteration is demonstrated. Then, we introduce the principle of the IS-online fluorescence image method for quantitative analysis.

2. Experimental

2.1 Method

2.1.1 The online fluorescence imaging method

The online fluorescence imaging method employed an online fluorescence imaging system and the corresponding imaging analysis method. The construction of the online fluorescence imaging-qCE system is described in our previously published work⁴. The method of image analysis was realized by using a self-scripted MatLAB program. In brief, the program equally sectioned the image of the detection window into a designable number. The fluorescent intensity in each *section* was integrated and thereby a series of electropherograms were derived. As an analog to the conventional CE detection systems, these *sections* could be regarded as independent and successive detection regions with identical volume, i.e. an array of fluorescence sensors. The real-time change in the peak profile, including the peak area, peak width and resolution, are recorded when the analyte was passing by the detection array.

Notes: (1) Peak areas obtained from the electropherogram were divided by the corresponding migration times to compensate for the dependence of the residence time in the detector on the

migration velocity of the analyte³⁰. (2) The peak area derived from each *section* was divided by the peak area obtained in the first *section* the analyte passed through. Thus, the initial peak area was normalized to 1 at the beginning of the elapse time. Similar data processing was implemented for analyzing the *Rs*. (3) The length of sections could be decided as short as possible, thus, it is not supposed to raise an issue for detection resolution.

The term irradiance distance (D_r) is defined as a length parameter starting from the analyte enters the excitation irradiance area. D_r was calculated by accumulating the length of sections that the analyte passed through. In this work, we used DNA fragments conjugated with dyes as analytes. We hypothesized (1) the number of dyes labeled on DNAs is proportional to the length of the DNA fragment (2) DNA-dye conjugations were photodegraded with first-order kinetics so that the photobleaching of their peak areas could be fitted with the exponential function³¹. The fitting lines were simulated using the Microsoft Excel software.

We manipulated the intensity of excitation irradiance by using the objective lens on the microscope. Data measured by an illuminometer (UT383s, UNI-T, Guangdong, China) showed that the excitation irradiance intensity using the 60x objective lens (UplanFLN 60x/0.90) was average 8700 lux, 10x objective lens (UPLanFL N 10x/0.30, Olympus) 8825 lux, and using the 4x lens (UPLanFL N 4x/0.13, Olympus), 5661 lux. The capillary had an inner diameter of 75 μm , and was tailored with a 5 mm window by removing the polyimide coat. The diameter of excitation irradiance (L_s) was adjusted to be smaller than the sensing field of CCD (L_d) by sizing the diaphragm on the microscope.

2.1.2 The conventional CE detection method

The conventional CE system employs a single-point detection manner, which integrates the fluorescent intensity from a detection window with a certain length of volume. The proposed online fluorescence imaging system was also applied to conventional CE detection. As mentioned in section 2.1.1, each *section* can be regarded as a single-point detection window for the conventional CE detection. The position of the *section*, i.e. the D_r , represented the length of the detection window.

2.1.3 Capillary coating

The inner wall of the capillary was conditioned before use to reduce the electroosmotic flow and

avoid the adsorption of analytes on the wall. The capillary was flushed successively with 1 M NaOH for 5 min, water for 5 min, 1 M HCl for 5 min, and the coating buffer for 20 min³². The coating buffer contains 0.25% 7M (molecular weight) polyethylene oxide (PEO) and 0.1 M HCl in water.

2.2 Chemicals

100 bp DNA ladder, 20 bp DNA ladder, and TBE buffer powder were purchased from Takara (Dalian, China). Different types of fluorophores, including Sybr Green I (SG I), YOYO-1, and Cy 3 (Thermo Fisher Scientific, Waltham, MA, USA) were employed for dyeing DNAs. SG I was mixed with DNA fragments with a final 10 \times concentration before CE detection. The methods for labeling YOYO-1 and Cy3 on DNAs were following the manual provided by the manufacturer, respectively. The 7M PEO polymer was purchased from Aladdin (Shanghai, China), tetra-polyethylene glycol (tetra-PEG) polymers, including PET-200HS and PET-200HS, were from NOF (Tokyo, Japan). Deionized water was prepared by a Milli-Q Direct-Q 3UV system (Merck Millipore, Tokyo, Japan).

3. Results and discussion

3.1 Real-time fluorescence detection with the online fluorescence imaging system

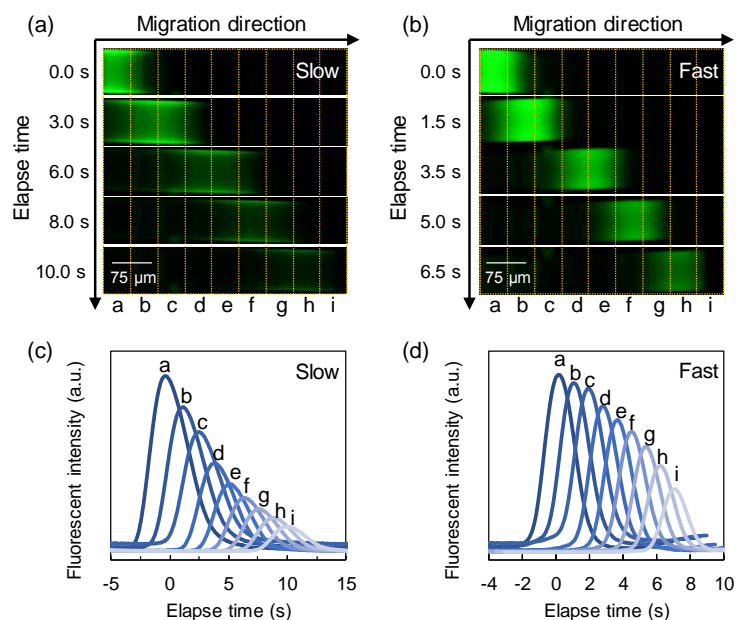


Fig. 1 Images of DNA bands passing through an excitation irradiance area with (a) a slow migration velocity, and (b) a fast migration velocity, respectively. Electropherograms derived by using the self-script program from the recorded images of the DNA band with (c) the slow migration velocity, and (d) the fast migration velocity, respectively.

The representing images recorded by the online fluorescence imaging system and the illustration of data analysis are shown in (Fig. 1). The self-scripted MatLAB program divided the image of the detection window into equal sections (Fig. 1 (a, b)); from each section, an electropherogram was obtained (Fig. 1 (c, d)). Both Figs. 1(a) and 1(b) show that the peak area decreased after the band traveled from one end to the other end of the detection window. It was also observed that, although the peak area always decreased, sometimes peak width increased during the detection (data not shown). Band broadening is a common phenomenon during CE separation, which might also be a reason to cause the peak area decreases. In case the band broadening effect interferes with the exponential fitting of the photobleaching effect, we attempted to separate these two effects by the following experiments.

3.2 Band broadening vs photobleaching

After the electrophoretic band of the 100 bp DNA fragment passed through the detection window, we applied a pulsed power, so that the electrophoretic band could pass through the detection window back and forth (see Fig. 2 (a)-(c)). The peak area (A) was integrated every time the DNA band passed back and forth. The declination of peak area (D) was examined. This experiment involves two tests, test (i) and test (ii). During the test (i), the excitation irradiance was switched off at t_1 for 2 min. The test (ii) was conducted with the excitation irradiance kept on. The A s obtained from the test (i) and test (ii) are plotted against the time as shown in Fig. 2 (d) and (e), respectively.

Among the factors that cause band broadening, including molecular diffusion, microheterogeneity, eddy diffusion, electro-diffusion, *etc.*, there are reversible and irreversible processes³³. This experiment examines the A of a single band when it passed back and forth a single detection volume. Thus, only the irreversible band broadening processes are considered here.

For test (i), at the time t_1 , the exposure was turned off; at the time t_2 , the exposure was turned on. Thus, D can be expressed as equation (1) and (2)

$$D(t_1) = D_d(t_1) + D_p(t_1) \quad (1)$$

$$D(t_2) = D_d(t_2) + D_p(t_1) \quad (2)$$

where $D(t)$ represents the loss of A at t . $D_d(t)$ and $D_p(t)$ represent the loss of A at t contributed by the band broadening effect and the photobleaching effect, respectively. From t_1 to t_2 the excitation irradiance was turned off, so there was no photobleaching process, while the band broadening process

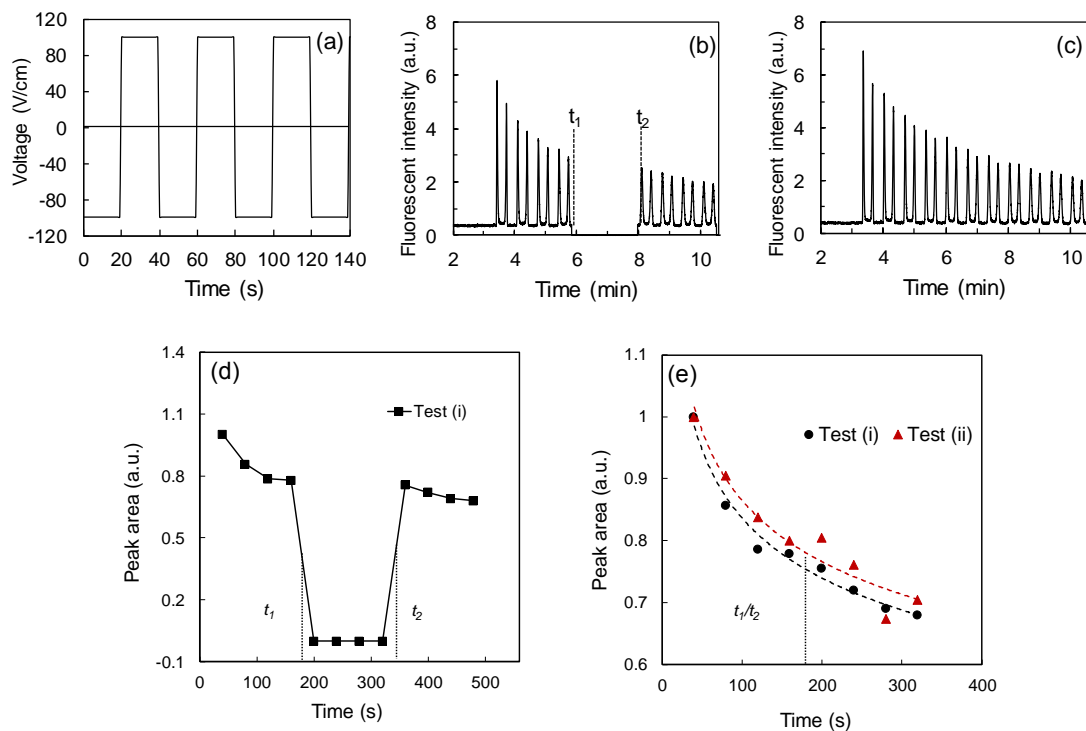


Fig. 2 (a) The pulsed power for driving the DNA band to migrate back and forth. (b) The electropherogram obtained from test (i). From t_1 to t_2 the excitation irradiance was switched off. (c) The electropherogram obtained from test (ii). Plots of normalized peak area in (d) test (i) and (e) test (ii) and replotted test (ii). Electrophoretic conditions: sample, 100 bp DNA fragment; objective lens, 60 \times ; sieving matrix, 1% PEO polymer in 0.5 \times TBE; dye, SG I; L_e , 6 cm; E , 100 V/cm.

still went on. The D that was caused only by the band broadening effect can be calculated by subtracting $D(t_1)$ from $D(t_2)$, as shown in equation (3):

$$D_d(t_2) - D_d(t_1) = D(t_2) - D(t_1) \quad (3)$$

For a better illustration, the line in Fig. 2 (d) was replotted after cutting off the data when the exposure was off, giving the plot labeled as the test (i) in Fig. 2 (e). In Fig. 2 (e), the declination rates of A at t_1/t_2 on the plot of the test (i) was $7.6 \times 10^{-4} \text{ s}^{-2}$, and at t_1 on the plot of the test (ii) was $7.5 \times 10^{-4} \text{ s}^{-2}$ (details of fitting line not shown here). It could be seen that the declination rates were very close. In other words, in the test (i) even an extra 2 min of irreversible band broadening process from t_1 to t_2 didn't cause a significant decrease in the peak area. Thus, it could be considered that, under the presented experimental conditions, the effect of the irreversible band broadening on the peak area is negligible.

As another supporting experiment, the data in reference [33] show that the band broadening, including the reversible and irreversible ones, might not cause the decrease of peak area. For example, in Table 1 of reference [33], the peak areas of peak 2/4 were bigger than those of peak 1/3 after the

bands broadened. The described work employed UV detection. In our paper, given the peak area's sensitive dependence upon excitation exposure, it is reasonable to hypothesize that the declination of the peak area is dominantly caused by the photobleaching effect.

3.3 Exponential simulation of the peak area on the elapse time scale

After confirming the dominating role of photobleaching in altering the peak area, this section attempted to simulate the real-time fluorescent intensities of the migrating DNA fragments. The peak area against the elapse time was investigated under different conditions, including the irradiance intensity, the type of fluorophores, the irradiance distance and the migration velocity. As a summary of the results, it is demonstrated that the plots of peak area against the elapse time could be fitted using an exponential function which was characterized by a half-life period (τ). Experimental results showed that the decay rate of peak areas is influenced by the excitation irradiance intensity (Fig.3 (a)): it speeded up when the excitation irradiance intensity increased from 5661 ($\tau=18$ s) to 8825 ($\tau=5$ s) lux. Different fluorophores exhibited different decay rates (Fig. 3 (b)): the fluorescent intensity of DNA-YOYO-1 conjugations showed a better photostability ($\tau=1250$ s), while the DNA-SG I conjugations ($\tau=42$ s) and DNA-Cy3 conjugations ($\tau=38$ s) were more apt to photobleaching.

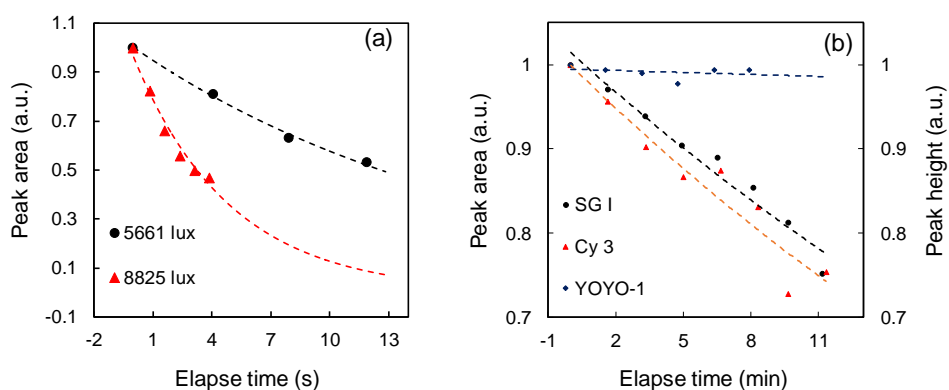


Fig. 3 (a) Comparison of the normalized peak area of 1.5 kbp DNA fragment under the 5661 lux and 8825 lux excitation irradiances. (b) Comparison of the normalized peak area/height of 500 bp DNA fragment dyed with SG I, Cy3, and YOYO-1. Other experimental conditions: sieving matrix, 1% PEO polymer in $0.5\times$ TBE; dye, SG I; L_e , 7 cm; E , 100 V/cm.

When the excitation irradiance intensity and the fluorophores were the same, it is found that the peak areas of different DNA fragments showed the same photodegrading rate (Fig. 4). As is illustrated by the equations (4) and (5), for the 100 and 400 bp DNA fragments, the simulation of their peak area

against elapse time yielded the same $\tau=37$ s, which is consistent with our hypothesis described in the section 2.1.1.

$$A = 1.0211 e^{-t/37} \quad (4)$$

$$A = 1.0072 e^{-t/37} \quad (5)$$

where the A is the peak area with an arbitrary unit, t is the elapse time in unit of second. This result suggests that the analysis on the elapse time scale exempted the inequivalent photobleaching from the analytes with different velocities. Thereby, with our online fluorescent imaging detection method, it is more accurate for the IS method to calculate the R_s .

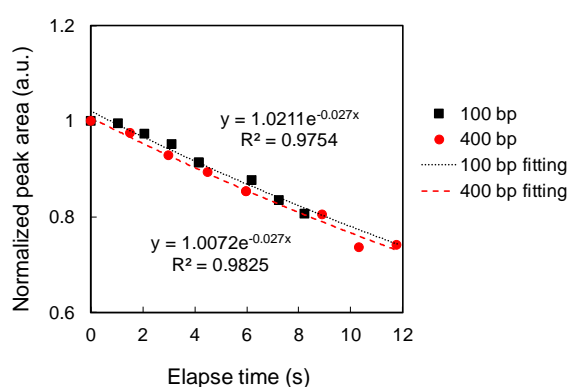


Fig. 4 The normalized peak areas of 100 and 400 bp DNA fragments against elapse time and their fitting lines. E , 100 V/cm. Other experimental conditions as in Fig. 3.

3.4 Internal standard-online fluorescence imaging method and its accuracy

Being able to collect the fluorescent intensities under the equivalent photobleaching process, this section describes the IS-online fluorescence imaging method. As a demonstration, the 100 bp DNA fragment in Fig. 4 was taken as the IS, and the 400 bp as the target analyte. First, their peak area-elapse time plots were fitted as shown in equations (4) and (5). Then, the equations (4) and (5) were integrated. Thereby, we obtained the fluorescence integrations of the analyte and IS against elapse time, given equations (6) and (7). Divide equation (7) by (6), there was a physical meaning of comparing the fluorescence integrations of 400 to 100 bp DNA fragments at the same elapse time.

$$A = 1.0211 (1 - e^{-t/37}) \quad (6)$$

$$A = 1.0072 (1 - e^{-t/37}) \quad (7)$$

where the A is the peak area with an arbitrary unit, t is the elapse time in unit of second. Other fitting parameters of 100 and 400 bp DNA-SG I conjugations under different electric field strengths (E_s) are listed in Table 1.

Table 1 Results of single exponential simulation $A = a e^{-t/\tau}$ under different E s, R^2 is the correlation coefficient.

E (V/cm)	DNA size (bp)	a	τ (s)	R^2
50	100	1.231	48	0.9698
	400	1.27	48	0.9958
100	100	1.0211	37	0.9754
	400	1.0072	37	0.9825
150	100	1.0255	36	0.8662
	400	1.0224	36	0.9515
200	100	1.0209	34	0.9014
	400	1.0184	31	0.9556

As demonstrated above, the mass ratio of the analyte to the IS would be equal to the experimental result (7)/(6), which represented the fluorescent intensity ratio of the analyte to the IS at an equivalent photobleaching status. In this work, the true value of equation (7)/(6) was normalized to 1. The relative error (δ) of R , which was the relative deviation of the experimental (7)/(6) from the true value, was employed to evaluate the accuracy of the IS-online fluorescence imaging method. A high accuracy method is accompanied by a low δ .

As illustrated in Fig. 5 (a), under a constant electric field strength ($E = 50, 100, 150$ V/cm, respectively), the δ remained a constant on the scale of elapse time. This result indicates that the R did not show a bias upon the elapse time, i.e. the influence from the unequal exposure time was avoided. Because the D_r is proportional to the elapse time, the IS-online fluorescence imaging method also exempted the dependence of R on D_r . In the situation of $E = 200$ V/cm, although the δ increased with elapse time, the increase was only little from 0.3 to 0.9%. As a contrast, the δ increased from 0.6 to 4.9% when the conventional single-point detection method was applied (Fig. 5 (b)). In conclusion, by collecting the fluorescent intensities at equal photobleaching duration, one can efficiently avoid the influence of inequivalent photodegradation among fluorophores.

In Fig. 5 (a), the δ s show a dependency on E . One reason for this dependency might be the inhomogeneous spatial distribution of the excitation irradiance. As is illustrated in Scheme 1, in the online fluorescence image detection method, the finish line of different analytes ended up at different D_r s. Thus, there might exist some inequivalent photodegradation rate/fluorescence response caused by the distribution of excitation irradiance. It is not difficult to infer that a lower E slowed down the migration of analytes, which might contribute to the accumulation of these inequivalence. It is expected

that future works would increase the spatial homogeneity of the excitation irradiance to release the influence of photobleaching on quantitative accuracy.

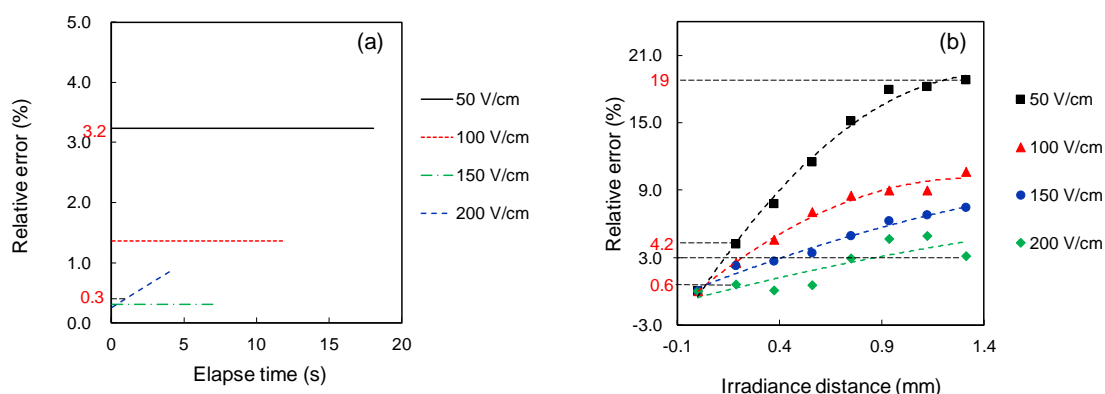


Fig. 5 Under different E s/migration velocities, the relative error against (a) elapse time and (b) D_r . In Fig. (b) the total last of elapse time was corresponding to the total illumination time of the 100 bp DNA fragment in Fig. 5. Objective lens, 4x; L_e , 7 cm; dye, SG I; other experimental conditions as in Fig. 3.

For comparison, the IS method coupled with the conventional single-point CE detection method was implemented. As is shown in Fig. 5(b), the δ was piled up from 0.6-4.2% to 3-19% by the increasing D_r . Consequently, efforts were required to minimize the difference between the analytes' excitation irradiance, for example, choose the internal standard with similar mobility, raise the E , shorten the D_r , etc. In contrast, the IS-online fluorescence image method showed a lower δ and more robust accuracy under the same separation conditions. The errors from the migration velocity of the analyte and the D_r were avoided. We note the practicality of the proposed method for many tedious works to minimize the photobleaching of fluorophores can be exempted.

3.5 Influence of photobleaching on the resolution and peak area ratio

We have demonstrated that in a conventional CE detection system the photobleaching could have a significant impact on the peak area, as well as the R . This section analyzes the electropherograms yielded from the successive *sections* and reports the fact that the peak width and resolution (see reference [27] for the calculation method) are influenced by the photobleaching of fluorophores. As shown in Fig. 6, the resolution substantially increased by a range from 28 to 81% after the 20 bp DNA ladder passed through a 0.96 mm D_r under the 8825 lux excitation irradiance. Data analysis showed that (1) the distance between two adjacent peaks was extended by a range from 2 to 10% as DNAs

migrated forth. (2) The peak width was largely narrowed down by a range from 11 to 43% (data not shown here). This indicated that the trimming down of the peak width caused by photobleaching effect outpaced band broadening effect, resulting in an improvement of graphical resolution. We emphasize that this narrow down of the peak width was graphical because a part of the electrophoretic band was just unseen rather than vanished or removed from the capillary column.

It is noted here that, while the peak area declined after the band traveled from the one end of the detection window to the other end. The calculated peak width would decrease under the electrophoretic conditions; it also would increase in other of our experiments (data not shown), which indicates that, in these cases, the band broadening was faster than the photobleaching narrowing³³. These attention-arising results mean that the photobleaching of an electrophoretic band could perplex the calculation of the observed peak width and resolution. Appropriate measurement approaches are required for deep understanding of the peak width and resolution in the FL-CE analysis.

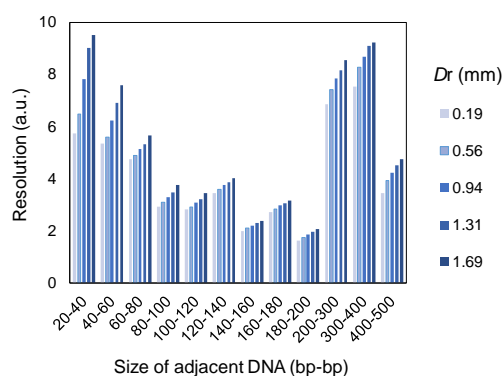


Fig. 6 Changes of the resolution between the adjacent DNA fragments along with the progress of photobleaching. Experimental conditions were the same as Fig. 1.

4. Conclusion

This work shows that the photobleaching of fluorophores could influence the peak area, peak width, resolution, and R in CE analysis. Especially, the R , which is a widely used parameter for quantitative analysis, is altered by the inequivalent photobleaching of analytes. The proposed system provides a real-time detection manner so that the fluorescent intensities of analytes at equal time duration of illumination can be indexed. The IS-online fluorescence image method calculates the quantities of analytes from their R to the IS under the equivalent photobleaching process. Results show that the δ remained a low value (0.3-3.2%) even when the analytes underwent a long term of photobleaching. Thereby, the proposed method promises practical operations because efforts to

minimize the photodegradation of fluorophores could be liberated. Unlike the conventional single-point CE detection, there will be no restriction to the photostability of dyes, migration velocity, separation voltage, and exposure distance. Consequently, the newly developed method is applicable for analytes that can be labeled with certain fluorophore to DNAs, proteins, and saccharides.

References

- (1) Li, L.; Li, P.; Fang, J.; Li, Q.; Xiao, H.; Zhou, H.; Tang, B., Simultaneous quantitation of Na⁺ and K⁺ in single normal and cancer cells using a new near-infrared fluorescent probe. *Anal. Chem.* **2015**, *87*, 6057-6063.
- (2) Hu, L.; Stasheuski, A. S.; Wegman, D. W.; Wu, N.; Yang, B. B.; Hayder, H.; Peng, C.; Liu, S. K.; Yousef, G. M.; Krylov, S. N., Accurate microRNA analysis in crude cell lysate by capillary electrophoresis-based hybridization assay in comparison with quantitative reverse transcription-polymerase chain reaction. *Anal. Chem.* **2017**, *89*, 4743-4748.
- (3) Shala-Lawrence, A.; Blanden, M. J.; Krylova, S. M.; Gangopadhyay, S. A.; Beloborodov, S. S.; Houglund, J. L.; Krylov, S. N., Simultaneous analysis of a non-lipidated protein and its lipidated counterpart: Enabling quantitative investigation of protein lipidation's impact on cellular regulation. *Anal. Chem.* **2017**, *89*, 13502-13507.
- (4) Liu, C.; Yamaguchi, Y.; Sekine, S.; Ni, Y.; Dou, X., Precise and simultaneous enumeration of multiplex pathogens using multiplex polymer chain reaction coupled with a novel quantitative capillary electrophoresis. *Sensors and Actuators B: Chemical* **2018**, *258*, 263-269.
- (5) Inoue, S.; Kaji, N.; Kataoka, M.; Shinohara, Y.; Okamoto, Y.; Tokeshi, M.; Baba, Y., Rapid qualitative evaluation of DNA transcription factor NF-kappa B by microchip electrophoretic mobility shift assay in mammalian cells. *Electrophoresis* **2011**, *32*, 3241-3247.
- (6) Cui, X. Z.; Ni, C. F.; Liang, C.; Gong, F. J.; Wang, R.; Chen, G. L.; Zhang, Y. R., Screening and quantitation of forty-six drugs of abuse and toxic compounds in human whole blood by capillary electrophoresis: Application to forensic cases. *Microchem. J.* **2019**, *144*, 403-410.
- (7) Fan, Y. Y.; Dong, D. F.; Li, Q. L.; Si, H. B.; Pei, H. M.; Li, L.; Tang, B., Fluorescent analysis of bioactive molecules in single cells based on microfluidic chips. *Lab Chip* **2018**, *18*, 1151-1173.
- (8) Nuchtavorn, N.; Suntornsuk, W.; Lunte, S. M.; Suntornsuk, L., Recent applications of microchip electrophoresis to biomedical analysis. *J. Pharm. Biomed. Anal.* **2015**, *113*, 72-96.
- (9) Beauchamp, M. J.; Nielsen, A. V.; Gong, H.; Nordin, G. P.; Woolley, A. T., 3D printed microfluidic devices for microchip electrophoresis of preterm birth biomarkers. *Anal. Chem.* **2019**, *91*, 7418-7425.
- (10) Kalish, H.; Phillips, T. M., Assessment of chemokine profiles in human skin biopsies by an immunoaffinity capillary electrophoresis chip. *Methods* **2012**, *56*, 198-203.
- (11) Yagi, Y.; Kakehi, K.; Hayakawa, T.; Suzuki, S., Application of microchip electrophoresis sodium dodecyl sulfate for the evaluation of change of degradation species of therapeutic antibodies in stability testing. *Anal. Sci.* **2014**, *30*, 483-488.
- (12) de Araujo, W. R.; Cardoso, T. M. G.; da Rocha, R. G.; Santana, M. H. P.; Munoz, R. A. A.; Richter, E. M.; Paixao, T.; Coltro, W. K. T., Portable analytical platforms for forensic chemistry: A review. *Anal. Chim. Acta* **2018**, *1034*, 1-21.
- (13) Chabynec, M. L.; Chiu, D. T.; McDonald, J. C.; Stroock, A. D.; Christian, J. F.; Karger, A. M.; Whitesides, G. M., An integrated fluorescence detection system in poly(dimethylsiloxane) for microfluidic applications. *Anal. Chem.* **2001**, *73*, 4491-4498.
- (14) Han, J.; Gan, W.; Zhuang, B.; Sun, J.; Zhao, L.; Ye, J.; Liu, Y.; Li, C. X.; Liu, P., A fully integrated microchip system for automated forensic short tandem repeat analysis. *Analyst* **2017**, *142*, 2004-2012.

- (15) Kim, Y. T.; Lee, D.; Heo, H. Y.; Sim, J. E.; Woo, K. M.; Kim, D. H.; Im, S. G.; Seo, T. S., Total integrated slidable and valveless solid phase extraction-polymerase chain reaction-capillary electrophoresis microdevice for mini Y chromosome short tandem repeat genotyping. *Biosens. Bioelectron.* **2016**, *78*, 489-496.
- (16) Lagally, E. T.; Scherer, J. R.; Blazej, R. G.; Toriello, N. M.; Diep, B. A.; Ramchandani, M.; Sensabaugh, G. F.; Riley, L. W.; Mathies, R. A., Integrated portable genetic analysis microsystem for pathogen/infectious disease detection. *Anal. Chem.* **2004**, *76*, 3162-3170.
- (17) Johnson, M. E.; Landers, J. P., Fundamentals and practice for ultrasensitive laser-induced fluorescence detection in microanalytical systems. *Electrophoresis* **2004**, *25*, 3513-3527.
- (18) Ramsay, L. M.; Dickerson, J. A.; Dada, O.; Dovichi, N. J., Femtomolar concentration detection limit and zeptomole mass detection limit for protein separation by capillary isoelectric focusing and laser-induced fluorescence detection. *Anal. Chem.* **2009**, *81*, 1741-1746.
- (19) Hirschfeld, T., Quantum efficiency independence of the time integrated emission from a fluorescent molecule. *Appl. Opt.* **1976**, *15*, 3135-3139.
- (20) Mathies, R. A.; Peck, K.; Stryer, L., Optimization of high-sensitivity fluorescence detection. *Anal. Chem.* **1990**, *62*, 1786-1791.
- (21) White, J. C.; Stryer, L., Photostability studies of phycobiliprotein fluorescent labels. *Anal. Biochem.* **1987**, *161*, 442-452.
- (22) Shear, J. B.; Dadoo, R.; Fishman, H. A.; Scheller, R. H.; Zare, R. N., Optimizing fluorescence detection in chemical separations for analyte bands traveling at different velocities. *Anal. Chem.* **1993**, *65*, 2977-2982.
- (23) Wu, S.; Dovichi, N. J., High-sensitivity fluorescence detector fluorescein isothiocyanate derivatives of amino acids separated by capillary zone electrophoresis. *J. Chromatogr.* **1989**, *480*, 141-155.
- (24) Huang, X. H.; Coleman, W. F.; Zare, R. N., Analysis of factors causing peak broadening in capillary zone electrophoresis. *J. Chromatogr.* **1989**, *480*, 95-110.
- (25) Altria, K., D., In *Capillary electrophoresis guidebook*, Humana Press: Totowa, New Jersey, **1995**; Vol. 52, pp 71-82.
- (26) Boutonnet, A.; Morin, A.; Petit, P.; Vicendo, P.; Poinot, V.; Couderc, F., Pulsed lasers versus continuous light sources in capillary electrophoresis and fluorescence detection studies: Photodegradation pathways and models. *Anal. Chim. Acta* **2016**, *912*, 146-155.
- (27) Liu, C.; Yamaguchi, Y.; Sekine, S.; Ni, Y.; Li, Z.; Zhu, X.; Dou, X., Gene analysis of multiple oral bacteria by the polymerase chain reaction coupled with capillary polymer electrophoresis. *J. Sep. Sci.* **2016**, *39*, 986-992.
- (28) Yasui, T.; Inoue, Y.; Naito, T.; Okamoto, Y.; Kaji, N.; Tokeshi, M.; Baba, Y., Inkjet injection of DNA droplets for microchannel array electrophoresis. *Anal. Chem.* **2012**, *84*, 9282-9286.
- (29) Dang, F.; Zhang, L.; Jabasini, M.; Kaji, N.; Baba, Y., Characterization of electrophoretic behavior of sugar isomers by microchip electrophoresis coupled with videomicroscopy. *Anal. Chem.* **2003**, *75*, 2433-2439.
- (30) Mammen, M.; Colton, I. J.; Carbeck, J. D.; Bradley, R.; Whitesides, G. M., Representing primary electrophoretic data in the 1/time domain: comparison to representations in the time domain. *Anal. Chem.* **1997**, *69*, 2165-2170.
- (31) Song, L.; Hennink, E. J.; Young, I. T.; Tanke, H. J., Photobleaching kinetics of fluorescein in

- quantitative fluorescence microscopy. *Biophys. J.* **1995**, *68*, 2588-2600.
- (32) Iki, N.; Yeung, E. S., Non-bonded poly(ethylene oxide) polymer-coated column for protein separation by capillary electrophoresis. *J. Chromatogr. A* **1996**, *731*, 273-282.
- (33) Terabe, S.; Shibata, O.; Isemura, T., Band broadening evaluation by back-and-forth capillary electrophoresis. *J. High. Resolut. Chromatogr.* **1991**, *14*, 52-55.

Chapter II

Controllable molecular sieving by *copoly*(poly(ethylene glycol) acrylate/poly(ethylene glycol) diacrylate) based hydrogels via capillary electrophoresis for DNA fragments

Abstract

This work proposes a controllable molecular sieving using the crosslinked *copoly*(poly(ethylene glycol) acrylate/poly(ethylene glycol) diacrylate) (*copoly*(PEGA/PEGDA)) hydrogels as the sieving matrix for DNAs in capillary electrophoresis (CE). Attempts were made to control the separation performance by using different gel components, including the initiator concentration (C_{APS}), total concentration (C_{t}) of monomers, the ratio (R) of PEGA to PEGDA, and the length of crosslinker (L_{c}). Results reveal that the molecular sieving effect in the *copoly*(PEGA/PEGDA) gel can be controlled by C_{t} , R , C_{APS} and L_{c} , especially the former two parameters. Higher C_{t} and lower R provided the smaller average pore size resulting better separation of small-size DNA fragments, while lower C_{t} and higher R allowed better separation of large-size DNA fragments. Moreover, by using a representing gel component, the repeated test showed a run-to-run precision of $\text{RSD} < 0.9\%$ ($n = 10$ tests), a column-to-column precision of $\text{RSD} < 5.9\%$ ($n = 5$ columns), and a day-to-day precision of $\text{RSD} < 5.2\%$ ($n = 25$ tests in 5 days) for migration time. The results also reveal a rapid and high resolution separation for 20-140 bp DNA fragments using the *copoly*(PEGA/PEGDA) gel when tune to a lower R and lower C_{t} . When high C_{t} was requested, the *copoly*(PEGA/PEGDA) gel capillary was found to have better repeatability and higher resolution than the authentic poly(acrylamide) gels owing to the better volume stability upon polymerization.

1. Introduction

Capillary gel/polymer electrophoresis (CGE/CPE) is an important separation technology for biomolecules and has a wide application in clinical chemistry,^{1,2} forensic medicine,³ biopharmaceutical developments,^{4,6} pathology study,⁷ food safety,^{8,9} etc. Because in CGE/CPE the band broadening is effectively suppressed by using a narrow capillary (< 300 μm inner diameter) for heat diffusion and a polymer matrix for anti-convection, and high voltage allowed the fast separation. CGE/CPE have advantages of high resolution, rapid analysis, cost effective, automatable, and integratable.¹⁰ In addition, current progress in CGE/CPE also pursues the microscale platform¹¹ and even higher performance separation. Among them, there are the miniaturized instruments using microchip electrophoresis for the rapid and point-of-need detection,^{12, 13} and capillary electrophoresis (CE)-mass spectrometry for informative molecular analysis.^{14, 15}

The natural biomolecules have a wide size/structure distribution, therefore, it is required to optimize the CPE/CGE conditions to adapt for the target sizes. The sieving matrix plays a key role in controlling the separation performance of CPE/CGE. Commonly used sieving matrices are polymer networks formed by a polymer gel or solution, for example a crosslinked poly(acrylamide) (PA) gel, agarose gel, non-crosslinked PA solution, and poly(ethylene glycol) (PEG) solution. As revealed by the tons of previous studies, a practical separation of target molecules requires the polymer network to present a suitable pore size for an efficient size sieving¹⁶⁻¹⁹ and a lower viscosity for a facile hydrodynamic filling.²⁰ The most commonly used method to tune the pore size is to adjust the polymer concentration. Higher polymer concentration affords a smaller pore size, and thus better separation for small molecules. However, high concentration of polymer solutions leads to difficulties to capillary filling due to increase of the viscosity. Polymer gels such as PA gel have low viscous precursor solutions, however, difficulties have to be conquered regarding to the volume shrinkage upon polymerization.^{21, 22} Consequently, the CPE/CGE sieving of small biomolecules faces technical difficulties for the lack of an applicability for the practical sieving matrix. Except for the pore size and facility in capillary filling, other properties are also taken into account when choosing a proper sieving matrix, including a stimuli responsive,^{23, 24} capillary-coating property²⁵, and molecular interaction with analytes.^{26, 27}

There are considerable interests in developing sieving gels for an enhanced separation²⁸⁻³² or a compact integration in a sophisticated structure.^{33, 34} Among the new sieving gels, another approach to

control the separation performance attracts attentions, which is to tune the length of network strand. Li *et. al.* tailored the network strand of the tetra-PEG hydrogel by changing the arm length of tetra-PEG monomers.^{28,29} Our previous study proposed a PEG dimethacrylate (PEGDMA) gel for the separation of DNA and saccharides.³¹ The PEGDMA monomer served as both crosslinker as well as a tunable polymer strand. It was revealed that the length of the PEGDMA monomer was found to have an influence on the DNAs' mobility. While the works about the tetra-PEG gel and the PEGDMA gel show the possibility to improve the separation performance without increasing the monomer concentration. The inconvenience is that tuning their network strand is cumbersome with the replacement of monomer with another length. In other words, a monomer with another molecular size has to be synthesized to tune the network strand. The authentic PA gels with higher crosslinker content are better at sieving small molecules. The average network strand between the two crosslinkers could be easily modified by tuning the content of crosslinker.^{35,36} However, the aqueous insolubility of the crosslinker (methylene *bis*-acrylamide) limits the further enrichment of short PA strands. Thus in this work, a *copoly*(poly(ethylene glycol) acrylate/PEGDA hydrogel (*copoly*(PEGA/PEGDA)) hydrogel, is proposed as a new sieving material for a practical control of the CGE separation.

The *copoly*(PEGA/PEGDA) hydrogel has a tunable crosslinked network with bottlebrush-like polymer strands as illustrated in Fig. 1. The main chain polyacrylate is formed through the polymerization of the vinyl groups from the PEGDA and PEGA. The PEGDAs, of which both vinyl groups get polymerized, serve as the crosslinkers. The reacted PEGAs and the PEGDAs, of which only one vinyl group get polymerized, serve as the side chains.^{37,38} The good water solubilities of both PEGDA and PEGA monomers allow to prepare the monomer ratio with a wide range, which afford a simple way to tune the length of network strand, *i.e.*, the distance between the two adjacent crosslinking points (D). To clarify in this work, the D parameter is limited to the main chain strands which have two crosslinking points at both ends, rather than to the ones which have only one end immobilized on the polymer network, nor to the side chains. As the former type of polymer stand. The network structure can also be tuned by changing the total monomer concentration and the length of monomer as alternative approaches. With such tunable networks, the *copoly*(PEGA/PEGDA) hydrogel is expected to own a controllable separation performance.

Previously, the proposed *copoly*(PEGA/PEGDA) gels were fabricated as functional materials,^{39,40} the beads for metal ions extraction,^{37,38} *etc.* Our preliminary tests found that the *copoly*(PEGA/PEGDA)

gel showed less volume shrinkage upon polymerization comparing to the PA gel. As volume shrinkage may cause bubble formation in a capillary and lead to poor separation repeatability. The use of a volume stable gel promises a possibility of higher CE reproducibility. Interested by the aforementioned characters, this study synthesizes the *copoly*(PEGA/PEGDA) gels in a 75 μm capillary for the size sieving based CE analysis. The investigations here include the different routes for controlling the separation performance of the *copoly*(PEGA/PEGDA) gel. Generally, the network structure is tuned via the different compositions, including the initiator concentration (C_{APS}), total monomer concentration (C_t) (Scheme 1 (a)), monomer ratio (R) (Scheme 1 (b)), and length of crosslinker (L_c) (Scheme 1 (c)). A DNA ladder widely ranging from 20 to 1500 bp is employed as sample biomolecule. The reproducibility of the gel capillaries is also examined. Finally, a comparison evaluation is carried out between the authentic PA gel and the *copoly*(PEGA/PEGDA) gel.

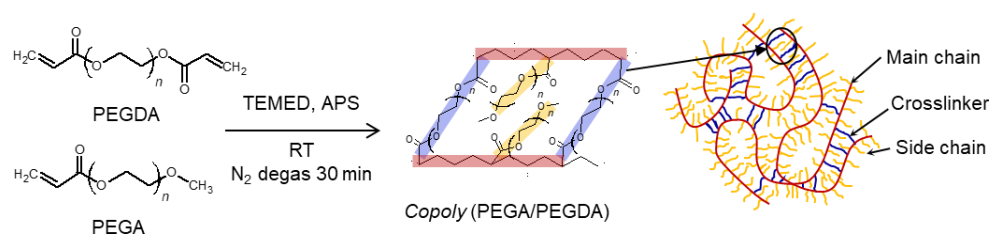
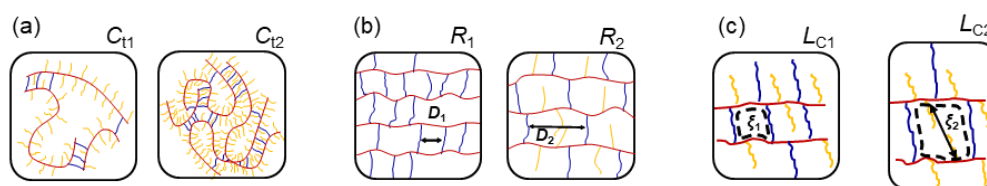


Fig. 1 Schematic diagram of the *copoly*(PEGA/PEGDA) synthesis and network structure.



Scheme 1. Different routes to tune the *copoly*(PEGA/PEGDA) gel structure for controlling the separation performance. (a) Total monomer concentration (C_t), where $C_{t2} > C_{t1}$. (b) PEGA/PEGDA ratio (R). At a fixed C_t (mol/v) and monomer length, when $R_2 > R_1$, there is $D_2 > D_1$. The average value D unavoidably has a distribution due to the inhomogeneity of the network, which is reflected by this illustration but not indicated by words. (c) Crosslinker length L_c . ξ is the average diameter of the pore bounded by the two adjacent crosslinkers and the main chain. Here the pores are also partially occupied by the side chains. As an approximation, we would like to consider it's negligible since the side chain is one-end free and may redirection when an analyte molecule passes by. At a fixed C_t (w/v), when $L_{c2} > L_{c1}$, there is $\xi_2 > \xi_1$.

2. Experimental

2.1 Chemicals

PEGDA monomers are named as “number”G’. The “numbers” are defined from the number of PEG units in each monomer. The PEGDA (MW= 508, 708, and 1108 for 9G’, 14G’, and 23G’, respectively) and PEGA (MW=468, number of PEGs is 9) were kindly donated from Shin-Nakamura Chemical (Wakayama, Japan), 3-(trimethoxysilyl)propylmethacrylate (γ -MAPS) was purchased from Tokyo Chemical Industry (Tokyo, Japan), ammonium peroxydisulfate (APS) and *N,N,N',N'*-tetramethylethylenediamine (TEMED) from Wako Pure Chemical Industries (Osaka, Japan), 40% (w/v) acrylamide/bis mixed (37.5:1) solution from Nacalai tesque (Kyoto Japan), TBE powder and DNA ladder from Takara (Shiga, Japan), and SYBR green II from Lonza (Rockland, ME, USA). The DNA sample mixture contains a 20 bp ladder from 20 to 200 bp, a 100 bp ladder from 200 to 1000 bp and a 1500 bp fragments. Deionized water was obtained from a Milli-QDirect-Q 3UV system (Merck Millipore, Tokyo, Japan). The fused-silica capillary was purchased from Polymicro Technologies (Phoenix, AZ, USA).

2.2 Preparation of gel capillaries.

The inner wall of a capillary was coated with γ -MAPS following a previously described protocol.³¹ The *copoly*(PEGA/PEGDA) gels were synthesized with PEGDA and PEGA as monomers, APS as an initiator, TEMED as a catalyst, and 0.5xTBE as a buffer solution. First, a solution with prescribed components were mixed without the addition of TEMED and bubbled by N₂ gas for 30 min. The TEMED was added and gently mixed via pipetting. Then, the precursor solution was filled into the capillary. Both ends of the capillary was sealed, keeping at room temperature for 24 h. The gel capillary was tested within 7 days after preparation. Before use, the gel capillary was checked with the assistance of a microscope under a 10x objective lens in case bubbles exist. One centimeter of each capillary end was cut off to remove the voids. The gel components were varied with different APS concentrations (C_{APS}), total monomer concentration (C_t), monomer ratio of PEGA/PEGDA (R), and length of crosslinker (L_c). A detailed list of composition was shown in Table 1-4. For a comparison study, the PA gel capillaries with different C_t were prepared following the compositions in Table 5.

Table 1 Compositions of *copoly*(PEGA/PEGDA) gels with different APS concentrations (C_{APS}).

C_{APS} (% (w/v))	20% APS (μL)	9G' (% (v/v))	0.5xTBE (mL)	TEMED (μL)
0.2	20			
0.14	14			
0.10	10			
0.08	8	10.7	2	1
0.02	2			
0.015	1.5			
0.0002	0.02			

Table 2 Compositions of *copoly*(PEGA/PEGDA) gels with different total monomer concentrations (C_t). The PEGA/PEGDA ratio $R = 5/5$ (mol/mol).

C_t (% (w/v))	9MG' (μL)	9G' (μL)	0.5xTBE (mL)	20% APS (μL)	TEMED (μL)
2.1	18	20.1			
6.0	54	60.4			
9.6	90	100.7	2	2	1
13.0	126	141			
16.1	162	181.3			

Table 3 Compositions of *copoly*(PEGA/PEGDA) gels with different PEGA/PEGDA ratios (R (mol/mol)). The total monomer concentration was 64.9 mM.

R (mol/mol)	9MG' (μL)	9G' (μL)	0.5xTBE (μL)	20% APS (μL)	TEMED (μL)
9.5/0.5	102.6	6.0	2005.8		
8/2	86.4	24.2	2003.9		
7/3	75.6	36.3	2002.6		
6/4	64.8	48.3	2001.3		
5/5	54	60.4	2114.4		
4/6	43.2	72.5	1998.7	2	1
3/7	32.4	84.6	1997.4		
2/8	21.6	96.7	1996.1		
1/9	10.8	108.8	1994.9		
0/10	0	120.8	1993.6		

Table 4 Compositions of *copoly*(PEGA/PEGDA) gels with different crosslinker lengths (L_c). The total monomer concentration was 6.0 (w/v).

L_c	Volume (μL)	9MG' (μL)	0.5xTBE (mL)	20% APS (μL)	TEMED (μL)
9MG'					
14MG'	60.4	54.0	2	2	1
23MG'					

Table 5 Compositions of PA gels with different total monomer concentrations (C_{tPA}).

C_{tPA} (% (w/v))	40% acrylamide/bis (μL)	10xTBE (μL)	Water (mL)	20% APS (μL)	TEMED (μL)
2	100	5	1.9		
8	400	20	1.6		
14	700	35	1.3	2	1
20	1000	50	1		

2.3 CE system and separation.

The CE tests were carried out via a self-built CE instrument as described in the previous work.⁴¹ The gel capillary was tailored to a 10 cm total length with a detection window at 6 cm from the injection end. The separation voltage was 200 V/cm if not specified. The 130 ng/ μL double strand DNA sample was dyed with 10x SYBR green II. The sample injection was conducted under a 200 V/cm voltage for 2 s.

2.4 Evaluation of the volume shrinkage.

The precursor solutions were prepared in glass tubes. Immediately after the precursor solution was degassed, put a volume of liquid paraffin (100-200 μL) onto the precursor solution for avoiding evaporation. Mark a line to indicate the interface between the precursor solution and the liquid paraffin. After the polymerization completed, the interface between the gel and liquid paraffin might move down to the mark owing to volume shrinkage. Take a picture for recording the distance between the mark and the gel-paraffin interface. This distance could be analyzed by an image analysis software such as image J. The longer this distance, the more volume shrinkage.

2.5 Probing the unreacted vinyl groups in the gel

Br_2 was employed to probe the unreacted vinyl group in the gel bulks. After washed by THF for 16 h, the sample gels were reacted with 1% (v/v) Br_2 in CCl_4 overnight. The reacted solutions were diluted by CCl_4 into 10 folds and then implemented UV spectrum detection (UV-2450 Shimadzu, Kyoto, Japan). The adsorption at 415 nm was taken as an indicator of the remaining amount of Br_2 in the reacted solution.

3. Results and discussion

3.1 Initiator concentration

For optimizing the polymer reaction, the influence of initiator concentration (C_{APS}) on the separation performance of the PEGDA gel capillary is discussed. Here, we employed the gels consisted only of PEGDA to understand the effect of the remaining vinyl groups due to C_{APS} . The value of C_{APS} ranged from 0.002 to 0.2% (w/v), which expanded three orders of magnitude (Table 1). After obtaining the electropherogram by using the PEGDA gel capillaries, the separation range, mobility, and resolution of the 20-1500 bp DNA fragments were discussed. Here, the separation range was defined as the size range of DNA fragments that could be separated with an above-zero resolution. The mobility and resolution were calculated as in reference 42. The evaluation and comparison of these parameters are taken for a comparison among the *copoly*(PEGA/PEGDA) gels with different compositions. For an overall understanding of the *copoly*(PEGA/PEGDA) gel's separation performance, a representative gel capillary will be compared with the traditional PA gel capillary at the end of this work. The repeatability of the gel capillary will be reported in an independent section titled Repeatability and Reusability, where a *copoly*(PEGA/PEGDA) gel columns with a typical composition was taken as demonstration.

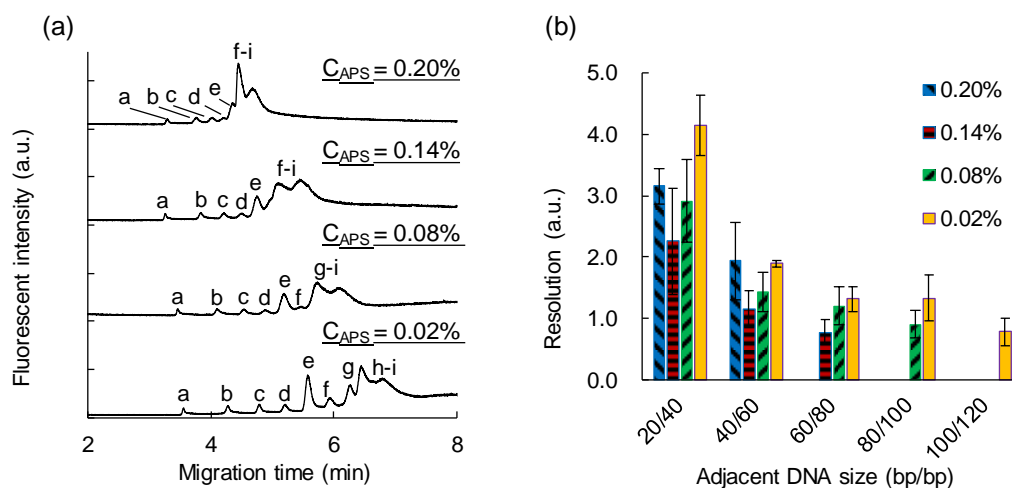


Fig. 2 (a) Electropherogram of the 20 bp DNA ladder under different C_{APS} on *poly*-PEGDA. The zero baselines were shifted for a comparative illustration, same operation Fig. 5 (a). Peaks and DNA sizes: a, 20 bp; b, 40 bp; c, 60 bp; d, 80 bp; e, 100 bp; f, 120 bp; g, 140 bp; h, 160 bp; i, 180-500 bp. (b) Resolution between adjacent DNA fragments under different C_{APS} .

The resulted electropherograms (Fig. 2 (a)) show that only the DNA fragments ranged from 20-80 bp were distinguished at high $C_{APS}=0.2\%$; along with the declination of C_{APS} , larger DNA fragments

(80-120 bp) could be resolved. Thus, it is found that the low C_{APS} of 0.02% led to an extension of separation range and an enhanced mobility difference. Meanwhile, the resolution diagram (Fig. 2 (b)) show that the DNA fragments were resolved with a higher resolution at low C_{APS} .

To explain this result, the amount of unreacted vinyl groups in the gels was estimated by using Br_2 as a probe. The result in Fig. 3 showed that the absorbance of Br_2 at 415 nm decreased under the lower C_{APS} after reaction with the gel samples, which indicates an increase of unreacted vinyl groups. This result suggested the presence of polymer strands with dangling PEGDA as side chains. We assumed that the dangling side chains tend to form long network strands and large pores. The presence of large pores in the network is consistent with the improved resolution for larger DNA fragments. As a summary, the separation range and the sieving resolution of the PEGDA gel capillary were improved by appropriately reducing C_{APS} .

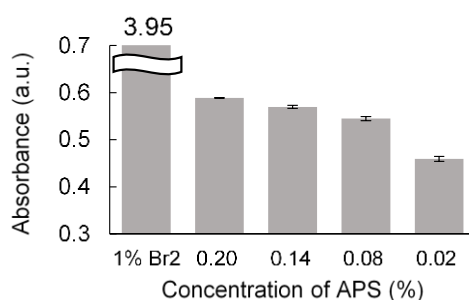


Fig. 3 The UV absorbance at 415 nm of the 1% Br_2 solution and the Br_2 solution reacted with the *copoly*(PEGA/PEGDA) gels fabricated with different C_{APS} .

3.2 The effect of total monomer concentration

This section studies the effect of total monomer concentration (C_t), which was the total concentration of PEGA and PEGDA, on the separation performance. As preliminary tests, an additional PEGA monomer was employed with a PEGA/PEGDA molar ratio of 5/5. The range of C_t employed here was from 2 to 13% (w/v) (Table 2). Results are described in the electropherograms (Fig. 4 (a)) and the resolution plots (Fig. 4 (b)). Generally, the migration velocity of each DNA fragment got slower as C_t increasing. For small DNA fragments (20-100 bp), higher C_t provided the better sieving resolution. For the middle DNA fragments (100-800 bp), an optimum resolution was found at 6% C_t . For larger DNA fragments (800-1500 bp), the resolution was less influenced by C_t at 200 V/cm of the electric field strength. After adjusting the electric field to 100 V/cm, it was found an optimum sieving resolution at around 6-10% C_t (data not shown). Under either electric field strength, the medium C_t (6%)

of *copoly*(PEGA/PEGDA) gels showed the ability to separate a wide size range of DNAs. The previous studies also showed similar tendency between the polymer concentration and the sieving resolution.^{43, 44} That was high concentration polymer solution could afford a high resolution for small DNAs; if a wide DNA size range is to be separated, a low concentration polymer solution was better. In brief, we confirmed the effectiveness of using C_t to control the separation performance of CGE.

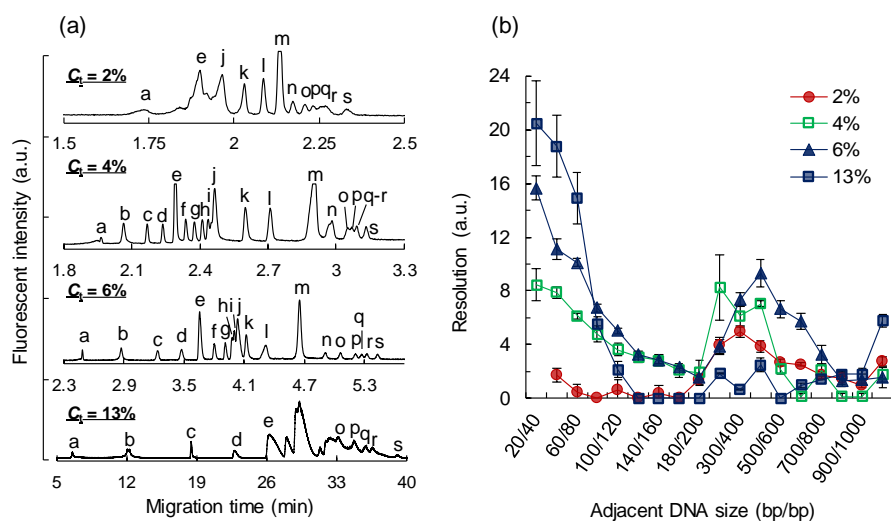


Fig. 4 (a) Electropherograms of the DNA ladder under different total monomer concentrations (C_t). Peaks and DNA sizes (bp): a, 20; b, 40, c, 60; d, 80; e, 100; f, 120; g, 140; h, 160; i, 180; j, 200; k, 300; l, 400; m, 500; n, 600; o, 700; p, 800; q, 900; r, 1000; s, 1500. (b) The resolution of the adjacent DNAs under different C_t .

3.3 The effect of PEGA/PEGDA ratio

The effect of molar ratio (R) of PEGA/PEGDA was investigated for controlling the separation performance of *copoly*(PEGA/PEGDA) gels. As is calculated in appendix Eq. (10) - (14) and illustrated in Scheme 1 (b), the average distance (D) between the two crosslinking sites, *i.e.*, the length of the polymer strand, would be modified by the prescribed R . Although in reality a distribution of D might exist due to the inhomogeneity⁴⁵ and incomplete reaction, an empirical study is presented. Here, the R ranged from 0/10 to 9.5/0.5 (mol/mol), and the total monomer concentration was fixed at 64.9 mM (Table 3). The electropherograms under different R (Fig. 5 (a)) showed that the separation range could be expanded from a range of 20-120 bp to 20-1500 bp as R increasing from 0/10 to 8/2. The resolution plots under different R showed that (Fig. 5 (b)), for small DNA fragments (20-140 bp), the optimum resolution was found at lower R of 2/8. The middle size of DNA fragments (200-700 bp) were finely separated when R was at higher around 5/5 to 8/2. For the large DNA fragments (700-1500 bp), the gels

with different R yielded a close resolution at 200 V/cm of the electric field strength. After adjusting the electric field strength to 100 V/cm, the 700-1500 bp DNA fragments were effectively separated with a range of R from 5/5 to 8/2 (data not shown). Fig. 5 illustrated that a wider separation range was obtained when R was ranged from 5/5 to 8/2.

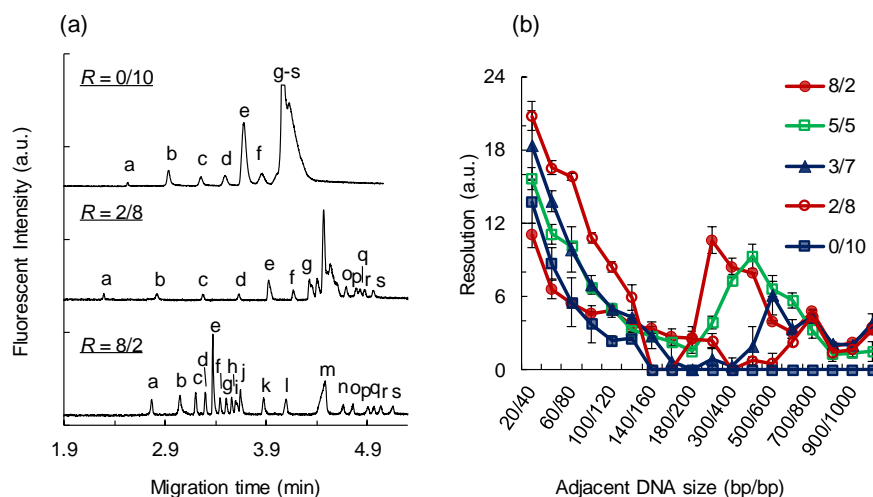


Fig. 5 (a) Electropherograms of the DNA ladder under different PEGA/PEGDA ratios (R). Peaks and DNA sizes were the same as in Fig. 4. (b) The resolution of the adjacent DNAs under different R .

It is noteworthy that although resolution was strongly influenced, the analysis time (20-1500 bp) was prolonged by only a little (< 1 min) at the optimum R . Back to the previous section, a similar resolution for 20-100 bp DNA fragments was also achieved by increasing C_t to 13% (Fig. 4), while this was at the cost of much longer analysis time. In a crosslinked network, increasing either the crosslinker (characterized with low R) or the monomer density (C_t) could yield a small average pore size. Thus, both approaches led to the improvement of resolution for small DNA fragments. While the former one allows the use of less monomers and thus is able to afford a fast separation. On the other hand, with low R , the molecular sieving pores are more likely to be built up via the covalent bonded crosslinker; with high C_t , the pores are more likely to be built up via the entangled/non-covalent bonded polymer strands. It's not difficult to suppose that the former approach provides a more stable structure and showed more efficient molecular sieving effect at the same cost of monomers.

The change in the mobility plots is discussed for a better understanding about the influence of R . As shown in Fig. 6 (a), an enhancement of the mobility difference for small DNA fragments (20-120 bp) was observed as illustrated by the increasing slope of the mobility plots on decreasing R from 8/2 to 3/7.

This result indicates that the presence of shorter polymer strands contributed to an effective sieving of small molecules. However, even lower R at 2/8 and 0/10 did not yield a steeper mobility plot. This might be because that the subscale inhomogeneity in the gel gained significance and led to a loss of sieving efficiency. On the other hand, when R increased from 0/10 to 8/2, an enhanced mobility difference for large DNA fragments (140-1500 bp) was observed. It indicates that the presence of longer polymer strands contributed to an effective sieving of large molecules. It is interesting to compare the plots when R equaled to 8/2, 5/5 and 0/10 (Fig. 6 (b)). The mobility plot from the R of 5/5 gel sharply overlapped with parts from the other two. It seems that as long as the suitable polymer strands presented, the corresponding DNA fragments is more likely to receive an enhanced mobility difference. This inspires us in design the sieving matrix: by assembling the different structures in a single network may produce a versatile sieving matrix which is capable of a wide range separation. Overall, as R affects the length of network strand and the structural homogeneity, it is found to be an efficient factor to control the separation speed and resolution of CGE.

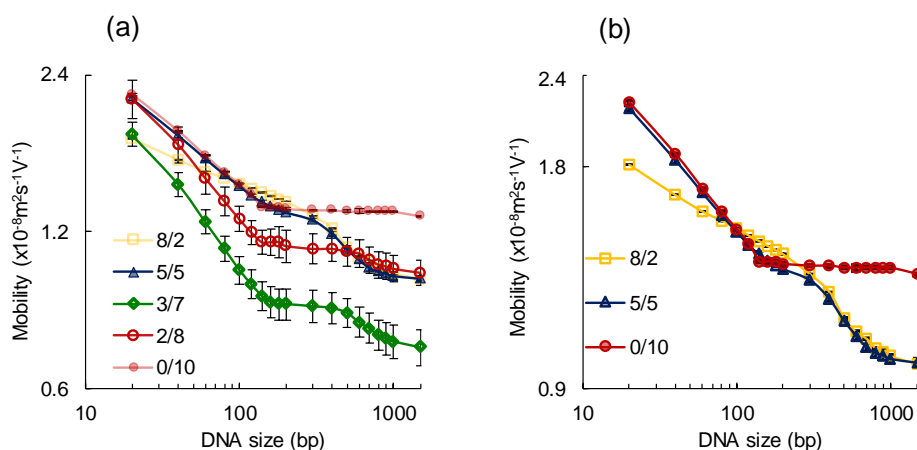


Fig. 6 The mobility plots under different R . (a) R ranged from 8/2 to 0/10. (b) R equaled to 8/2, 5/5 and 0/10.

In addition, it is indicated that R plays a role in modify the DNA fragments' migration regimes since the mobility plots showed a significant variation in Fig. 6. Based on the sigmoidal curve of the double logarithmic mobility-size plot, we take preliminary hypothesis about the migration mechanisms for DNA fragments. It seems that when R was 8/2 the Ogston regime governed the migration behavior of 20-300 bp DNAs; the reptation regime governed the migration behavior of 300-1500 bp DNAs. When R was between 5/5 and 2/8, it seems there were Ogston regime for 20-180 bp DNAs, and reptation regime for 500-1500 bp DNAs. Here the plateau mobility plot between 200 and 400 bp DNA

fragments presumably corresponds to the situation when the radius of gyration of DNA is larger than the pore size (so that sieving is impossible), but at the same time the DNA is too stiff to effectively reptate through the separation matrix^{44, 46}. When R was 0/10, it seems there were Ogston regime for 20-120 bp DNAs and reptation with orientation for the rest DNAs. The hypothesis takes pervious literatures 16-19 as references. And future works are necessary to investigate the related migration mechanisms.

3.4 The effect of crosslinker length

The *copoly*(PEGA/PEGDA) gels were synthesized with different length of PEGDA monomers (L_c), 9G', 14G' and 23G'. Among them, the total weight concentration (w/v) of PEGDA and PEGA were fixed (Table 4). The electropherograms (data not shown) obtained under different L_c showed that the separation range was not obviously affected by changing the crosslinker length. The migration mobility in the gel with 9G' and 14 G' (Fig. 7 (a)) of the DNA ladder got slower and the resolution (Fig. 7 (b)) was slightly higher than in those with longer crosslinkers of 23G'. This result could be interpreted by the calculation in SI and the illustration in Scheme 1 (c): the distance between two crosslinking became longer (Eq. S5) with a longer crosslinker. Here, the pore size (ζ) of the gel structure was enlarged by using a longer crosslinker. In addition, it was induced that the number of these pores decreased with a longer L_c . Therefore, it was supposed that the DNA molecules would experience a less frequent interaction in the polymer network formed by longer L_c being less retarded. This might ascribe to the faster migration velocity of DNA molecules and reduced resolution.

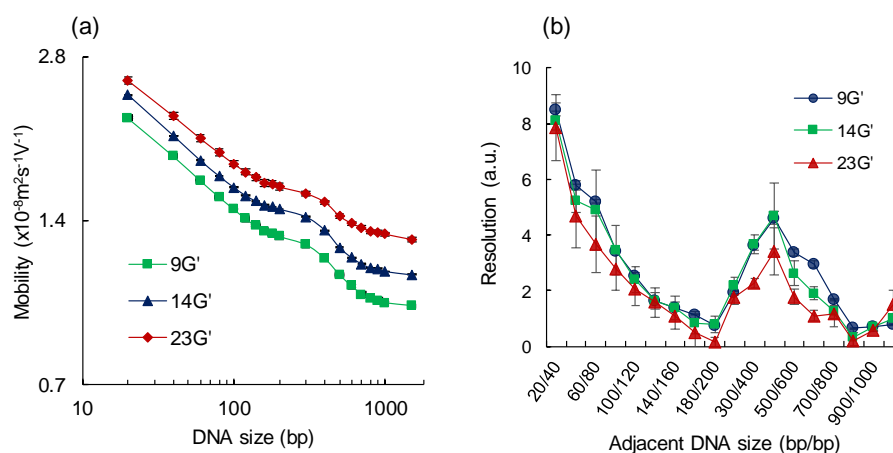


Fig. 7 (a) Mobility plots and (b) the resolution of the adjacent DNA fragments under different L_c .

3.5 Repeatability and reusability

Repeated experiments were carried out to examine the run-to-run, day-to-day, and column-to-column repeatabilities and reusabilities of the *copoly*(PEGA/PEGDA) gel capillaries. The tested gel capillary contained 9% (w/v) of monomers with R of 5/5 (mol/mol). A single gel capillary was tested by 10 times to evaluate the run-to-run repeatability, and by a total 25 times (5 day \times 5 time/day) to for the day-to-day repeatability. Five capillaries were tested for the column-to-column repeatability (5 column \times 5 time/column). The representing electropherograms were shown in Fig. 8. The resulted migration time and resolution of each run were calculated. As a summary of the results, Table 6 listed the relative standard deviations (RSDs) of the migration time and the standard deviation (SD) of resolution. The migration time in the *copoly*(PEGA/PEGDA) gel showed the good run-to-run precision (RSD < 0.9%) and column-to-column precision (RSD < 5.9%). For the resolution, the repeatability of 20-100 bp DNA fragments was demonstrated with the run-to-run precision (RSD < 6.1%) and the column-to-column precision (RSD < 14.6%). The column-to-column RSD for > 100 bp DNAs raised up to 37.3% because the resolution value of some DNA pairs are low, so that a small standard deviation (SD) could result with a large RSD to these DNA pairs. The reproducibility tests showed the possibility of a repeatable separation using *copoly*(PEGA/PEGDA) gel columns.

The reusability was evaluated by comparing the CE results taken immediately after preparation to those taken after a one-month storage. Day-to-day tests were performed immediately after the gel capillary was prepared. Then the capillary was stored for one month in the 0.5x TBE buffer solution and retested. The results in Fig. 8 (b) and table 6 show that the run-to-run precision for the migration time remained a good value (RSD < 4%) after the long-term storage, which was comparable to the newly made capillary (RSD < 5.2%). While the repeatability of resolution decreased along with the separation resolution, especially the large DNA fragments (> 500 bp) lost resolution dramatically (Fig. 8). It is supposed that the gel degraded upon long-term storage and thus caused the decrease in resolution. In brief, a good repeatability of the *copoly*(PEGA/PEGDA) gel capillary was possible with the run-to-run and column-to-column use. The gel capillary can be reused for days with a certain decrease of sieving resolution.

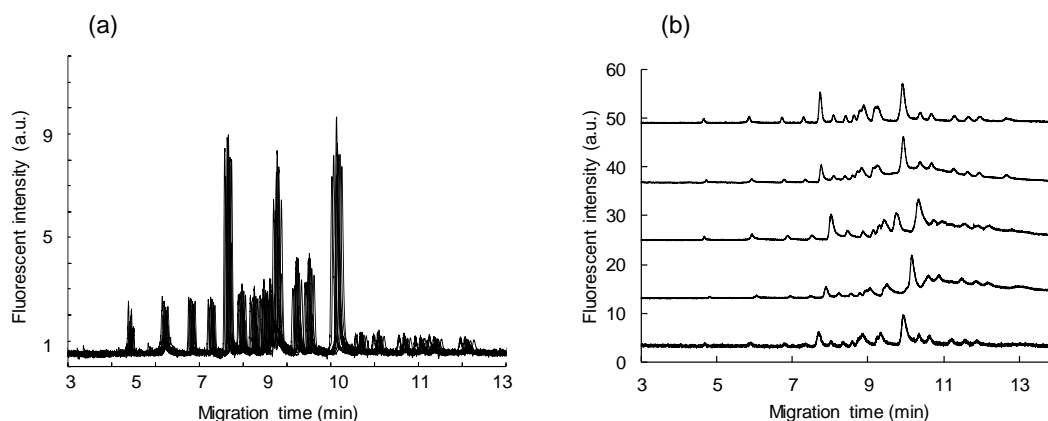


Fig. 8 The electropherograms using (a) a single column for 10 successive runs, (b) a 38-days old column for 5 successive runs. Electric field strength 100 V/cm.

Table 6 The relative standard deviations (RSD, %) of the migration time, resolution (20-1500 bp), and resolution (< 100 bp) under different tests.

	Migration time	Resolution (20-1500 bp)	Resolution (< 100 bp)
Run-to-run	0.7-0.9	2.5-9.9	2.5-6.1
Column-to-column	4.1-5.9	10.4-37.3	10.4-14.6
Day-to-day	3.5-5.2	10.1-50.2	10.1-21.3
Run-to-run (38-days-old)	1.6-4.0	-	16.3-27.3

3.6 Comparison with a polyacrylamide gel

A comparison study regarding to the molecular sieving properties was carried out between the *copoly*(PEGA/PEGDA) gel and a typical PA gel. Although the separation performance of a gel could be further improved by tuning the effective length of capillary, buffer composition, electric field strength, etc., the optimization of these parameters falls out the scope of the present work. As well as the same experimental conditions are applied, the resulted sieving resolution would be used as a comparison study. Here, the PA gels were fabricated with different concentrations (C_{IPA}) ranging from 2 to 14%. Similar to the *copoly*(PEGA/PEGDA) gel, the PA gels also showed the possibility to separate all the DNA fragments in the 20-1500 bp ladder. As shown in Fig. 9 (a), the gels with C_{IPA} ranged between 2 and 8% may afford a good separation range. In addition, Fig. 9 (b) demonstrated the C_{IPA} 's influences on the sieving resolution. The difference between the PA gel and *copoly*(PEGA/PEGDA) gel is found out that the *copoly*(PEGA/PEGDA) gels provided an improved resolution for small DNA fragments (Fig. 10 (a)) by increasing the monomer concentration. However, in the PA gels, the resolution of small

DNA fragments decreased in higher monomer concentration (Fig. 10 (b)). We assumed that this result was due to the volume stability upon polymerization²⁰. As in Fig. 10 (c), the PA gels were much shrunk at higher monomer concentration. When shrinkage occurs in the capillary, bubbles are apt to form after the gelation process or during the run, which may break the electrical circuit and worsen the separation resolution. As a result, the bubble formation was observed under the microscope after the initial run (< 40 min) in the PA gel capillary (14% C_{tPA}). In contrast, no obvious volume shrinkage was observed in *copoly*(PEGA/PEGDA) gels with various C_t s (a typical example in Fig. 10 (d)). In fact, the bubbles were not observed in the *copoly*(PEGA/PEGDA) gel capillary (13% C_t) until an 8 h successive usage. These results indicate that the *copoly*(PEGA/PEGDA) gels in a capillary are more stable than the PA gels against the electric force. Here, we ascribe this stability to the volume stability. It is concluded that the *copoly*(PEGA/PEGDA) gel capillary is able to provide a comparable separation performance for large DNA fragments and a higher resolution for small DNA fragments compared with the PA gel capillaries.

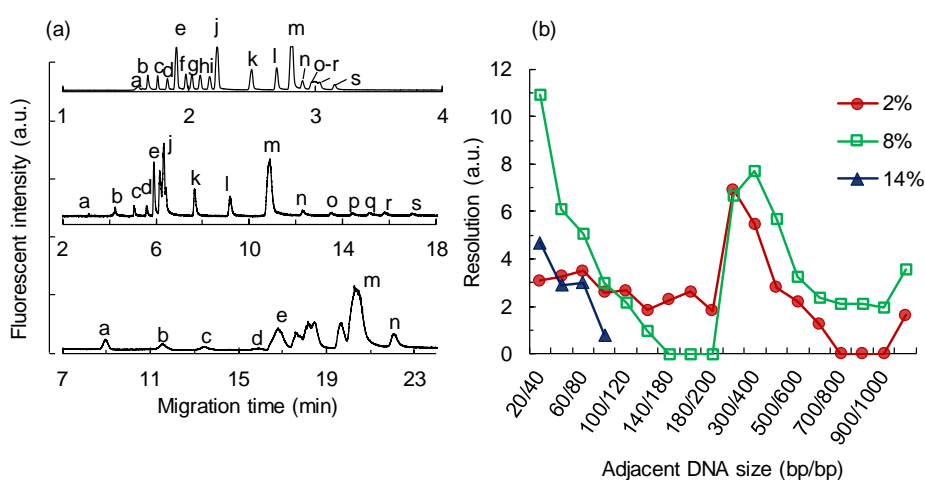


Fig. 9 (a) The electropherogram of the DNA ladder under different acrylamide concentrations (C_{tPA}). From top to bottom: 2%, 8% and 14%. Peaks and DNA sizes (bp): same with Fig. 4. (b) The resolution of the adjacent DNAs under different C_{tPA} . The experiments were carried out under the 100 V/cm separation voltage.

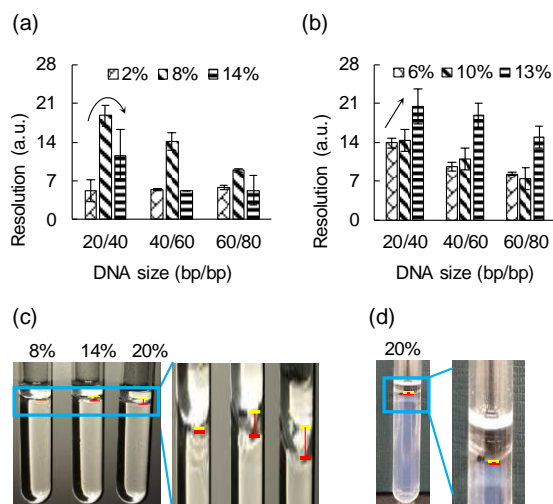


Fig. 10 Resolution of DNA fragments obtained from (a) PA gels with different C_{IPA} and (b) *copoly*(PEGA/PEGDA) gels with different C_t ($R = 5/5$). Evaluating the volume shrinkage of (c) PA gels with different C_{IPA} and (d) the *copoly*(PEGA/PEGDA) gel with $C_t = 20\%$. Yellow line: the interface between the gel synthetic system and the liquid paraffin before polymerization, red line: after polymerization. The distance between the yellow and red line were calculated as 0, 1.03 and 1.22 mm, i.e. 0%, 3.2% and 3.8% of the precursor volume when C_{IPA} equaled to 8%, 14% and 20%. Indicating the volume shrinkage got severe in concentrated PA gel. In contrast, the distance between the yellow and red line were negligible in even the 20% *copoly*(PEGA/PEGDA) gel, as well as the *copoly*(PEGA/PEGDA) gels with $C_t < 20\%$ (picture not shown).

4. Conclusion

We synthesized the *copoly*(PEGA/PEGDA) gels in the 75 μm i.d. capillary for a controllable CGE separation performances. Results proved that the separation range and resolution were influenced by C_{APS} , C_t , R , and L_c . Among these factors, C_t and R showed the significant impact on the separation performance. Worthy to note is that tuning R could effectively improve the separation resolution of small DNAs with shorter analysis time. Furthermore, the proposed gel capillary showed the good run-to-run and column-to-column repeatability owing to a good gel volume stability. After a long-term storage (1 month), the separation of small DNA fragments was still effective. Comparing with typical PA gel capillaries, the *copoly*(PEGA/PEGDA) gel capillary showed a comparable separation performance for large DNA fragments and a better resolution for small DNA fragments. The *copoly*(PEGA/PEGDA) gels described in this work were demonstrated to be a superior candidate as a sieving matrix for CGE. By choosing a proper composition, the *copoly*(PEGA/PEGDA) based CGE can afford a low pre-gel solution viscosity, avoid inefficiencies created by volume shrinkages, and

allow for a wide separation range or high separation resolution of a target range. The method of tuning the network strand could be further applied for the development of new sieving materials.

Appendix

Calculation of the network structure of the copoly(PEGA/PEGDA) gel

Parameters:

np : the number of EG units present in the monomer molecule (1)

np_c : the number of EG units present in the bi-vinyl group monomer (the crosslinker)

np_s : the number of EG units present in the mono-vinyl group monomer (the sidechain)

m : the mass of monomer (g)

m_c : the mass of bi-vinyl group monomer in the precursor solution

m_s : the mass of mono-vinyl group monomer in the precursor solution

M : the molecular weight of the described unit (1)

M_c : the molecular weight of the crosslinker monomer

M_s : the molecular weight of the side chain monomer

M_a : the molecular weight of a EG unit

M_{ac} : the molecular weight of the PEG chain on the bi-vinyl group monomer

M_{as} : the molecular weight of the PEG chain on the mono-vinyl group monomer

M_{bc} : the summary molecular weight of unit b1 and b2

M_{bs} : the summary molecular weight of unit b1 and b3

M_{b1} : the molecular weight of unit b1

M_{b2} : the molecular weight of unit b2

M_{b3} : the molecular weight of unit b3

n : the molar mass of the monomer (mol)

n_c : the molar mass of the crosslinker in the precursor solution

n_s : the molar mass of the sidechain in the precursor solution

L : the length of the described unit (nm)

L_{main} : the summary length of the total main chains

l_{main} : the main chain length contributed by one single vinyl group

L_{mainc} : the summary of main chain length contributed by the crosslinker

L_{mains} : the summary of main chain length contributed by the sidechain

L_c : the length of crosslinker

L_s : the length of side chain

L_a : the length of a EG unit (Fig. A1)

L_{ac} : the length of the PEG chain on the bi-vinyl group monomer

L_{as} : the length of the PEG chain on the mono-vinyl group monomer

L_{bc} : the summary length of the unit b1 and b2

L_{bs} : the summary length of the unit b1 and b3

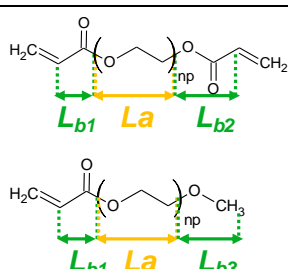
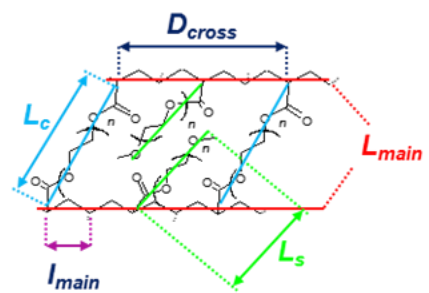
L_{b1} : the length of the unit b1 as described by the Fig. A1

L_{b2} : the length of the unit b2 as described by the Fig. A1

L_{b3} : the length of the unit b3 as described by the Fig. A1

D : the distance between the two crosslinking points (nm)

Table A1 The definition, equation and calculation of the size of the gel components and structure.

Parameter	Structure	Equation	Value (nm)
L_a	 <p>Fig. A1 Illustration of the parameters regarding to the molecular structure of PEGDA (top) and PEGA (bottom).</p>	-	0.366
L_{ac}		$=np_c L_a$ (1)	$0.366np_c$
L_{as}		$=np_s L_a$ (2)	$0.366np_s$
L_{bc}		$=L_{b1}+L_{b2}$ (3)	0.477
L_{bs}	$=L_{b1}+L_{b3}$ (4)	0.369	
L_c	 <p>Fig. A2 Illustration of the parameters regarding to the molecular structure of copoly(PEGA/PEGDA) gel.</p>	$=L_{ac}+L_{bc}$	$0.366np_c+0.477$
L_s		$=np_c L_a+L_{bc}$ (5)	
I_{main}		$=L_{as}+L_{bs}$	$0.366np_s+0.369$
L_{main}		$=np_s L_a+L_{bs}$ (6)	
L_{main}	$=I_{main} NA (2n_c+n_s)$ (7)	$0.225NA (2n_c+n_s)$	
L_{mainc}	-	$=2I_{main} NAn_c$ (8)	$0.45NAn_c$
L_{mains}	-	$=I_{main} NAn_s$ (9)	$0.225NAn_s$

With a prescribed amount of monomers m_c and m_s , and the volume of the precursor solution, the size of the network structure could be estimated. As the molecular weight M of each unit M_a , M_{b1} , M_{b2} , M_{b3} , M_{ac} , M_{as} , M_c and M_s is the known parameter. Also, the spatial dimension L of the molecular unit L_a , L_{b1} , L_{b2} , L_{ac} , L_{bc} and L_{bs} can be calculated as the Table A1 in virtue of the open access calculator.¹ Here the spatial dimension were calculated as the monomer molecule is at the planar zigzag conformation. Table A1 showed the dependence of monomer length on the np and the dependence of main chain length on the molar mass of each monomer.

Suppose all the vinyl groups got polymerized, the average distance between the two crosslinking point can be calculated via dividing the total length of the main chain by the number of crosslinkers.

$$D = \frac{L_{main}}{2NA n_c} = \frac{L_a(n_c+n_s)}{2NA n_c} = \frac{L_a}{2NA} \left(1 + \frac{n_s}{n_c}\right) \quad (10)$$

Where the NA is the Avogadro's constant, the Eq. (10) is divided by 2 because one crosslinker attached two crosslinking points on the main chain. As R is defined as $R = n_s/n_c$, substitute to Eq. 10. We get

$$D = \frac{L_a}{2NA} (1 + R) \quad (11)$$

As the n_s and n_c can be calculated by Eq. (12) and (13). Substitute them into Eq. (10), the Eq. (14) is obtained

$$n_c = m_c(M_{bc} + np_c M_a) \quad (12)$$

$$n_s = m_s(M_{bc} + np_s M_a) \quad (13)$$

$$D = \frac{L_a}{2NA} \left(1 + \frac{m_s M_{bc} + np_s M_a}{m_c M_{bc} + np_c M_a}\right) \quad (14)$$

In Eq. (14), when the monomer concentration (m_s and m_c) and length of side chain (np_s) are fixed, the only variable is np_c . It can be induced that the D increases along with the increasing of the np_c . Also, Eq. (5) induced that the L_c increases with np_c . As shown in Scheme 1 (C), because both the L_c and the D increase, the pore size ζ is enlarged when using a longer crosslinker.

References

- (1) Blesa, S.; Olivares, M. D.; Alic, A. S.; Serrano, A.; Lendinez, V.; González-Albert, V.; Olivares, L.; Martínez-Hervás, S.; Juanes, J. M.; Marín, P.; Real, J. T.; Navarro, B.; García-García, A. B.; Chaves, F. J.; Ivorra, C., Easy one-step amplification and labeling procedure for copy number variation detection. *Clin. Chem.* **2020**, *66*, 463-473.
- (2) da Cunha, M. J. M.; da Conceicao, I.; Abrantes, I. M. D.; Santos, M., Assessment of the use of high-performance capillary gel electrophoresis to differentiate isolates of *Globodera* spp. *Nematology* **2006**, *8*, 139-146.
- (3) Mayes, C.; Seashols-Williams, S.; Hughes-Stamm, S., A capillary electrophoresis method for identifying forensically relevant body fluids using miRNAs. *Legal Medicine* **2018**, *30*, 1-4.
- (4) Demellenne, A.; Napp, A.; Bouillenne, F.; Crommen, J.; Servais, A. C.; Fillet, M., Insulin aggregation assessment by capillary gel electrophoresis without sodium dodecyl sulfate: Comparison with size-exclusion chromatography. *Talanta* **2019**, *199*, 457-463.
- (5) Kubota, K.; Kobayashi, N.; Yabuta, M.; Ohara, M.; Naito, T.; Kubo, T.; Otsuka, K., Identification and characterization of a thermally cleaved fragment of monoclonal antibody-A detected by sodium dodecyl sulfate-capillary gel electrophoresis. *J. Pharm. Biomed. Anal.* **2017**, *140*, 98-104.
- (6) Deeb, S. E.; Wätzig, H.; El-Hady, D. A., Capillary electrophoresis to investigate biopharmaceuticals and pharmaceutically-relevant binding properties. *TrAC, Trends Anal. Chem.* **2013**, *48*, 112-131.
- (7) Woo, N.; Kim, S.-K.; Sun, Y.; Kang, S. H., Enhanced capillary electrophoretic screening of Alzheimer based on direct apolipoprotein E genotyping and one-step multiplex PCR. *J. Chromatogr. B* **2018**, *1072*, 290-299.
- (8) Carli, K. T.; Unal, C. B.; Caner, V.; Eyigor, A., Detection of salmonellae in chicken feces by a combination of tetrathionate broth enrichment, capillary PCR, and capillary gel electrophoresis. *J. Clin. Microbiol.* **2001**, *39*, 1871-1876.
- (9) Vergara-Barberan, M.; Mompo-Rosello, O.; Jesus Lerma-Garcia, M.; Manuel Herrero-Martinez, J.; Francisco Simo-Alfonso, E., Enzyme-assisted extraction of proteins from Citrus fruits and prediction of their cultivar using protein profiles obtained by capillary gel electrophoresis. *Food Control* **2017**, *72*, 14-19.
- (10) Linhardt, R. J.; Toida, T., Tech.Sight. Capillary electrophoresis. Ultra-high resolution separation comes of age. *Science* **2002**, *298*, 1441-1442.
- (11) Smith, M. T.; Zhang, S.; Adams, T.; DiPaolo, B.; Dally, J., Establishment and validation of a microfluidic capillary gel electrophoresis platform method for purity analysis of therapeutic monoclonal antibodies. *Electrophoresis* **2017**, *38*, 1353-1365.
- (12) Haab, B. B.; Mathies, R. A., Single-molecule detection of DNA separations in microfabricated capillary electrophoresis chips employing focused molecular streams. *Anal. Chem.* **1999**, *71*, 5137-5145.
- (13) Luo, F.; Li, Z.; Dai, G.; Lu, Y.; He, P.; Wang, Q., Ultrasensitive biosensing pathogenic bacteria by combining aptamer-induced catalysed hairpin assembly circle amplification with microchip electrophoresis. *Sensors and Actuators B: Chemical* **2020**, *306*, 127577.
- (14) Olivares, J. A.; Nguyen, N. T.; Yonker, C. R.; Smith, R. D., ONLINE MASS-SPECTROMETRIC DETECTION FOR CAPILLARY ZONE ELECTROPHORESIS.

- Anal. Chem.* **1987**, *59*, 1230-1232.
- (15) Lu, J. J.; Zhu, Z. F.; Wang, W.; Liu, S. R., Coupling Sodium Dodecyl Sulfate-Capillary Polyacrylamide Gel Electrophoresis with Matrix-Assisted Laser Desorption Ionization Time-of-Flight Mass Spectrometry via a Poly(tetrafluoroethylene) Membrane. *Anal. Chem.* **2011**, *83*, 1784-1790.
- (16) Rodbard, D.; Chrambach, A., Unified theory for gel electrophoresis and gel filtration. *Proc Natl Acad Sci U S A* **1970**, *65*, 970-977.
- (17) Grossman, P. D.; Soane, D. S., Experimental and theoretical studies of DNA separations by capillary electrophoresis in entangled polymer solutions. *Biopolymers* **1991**, *31*, 1221-1228.
- (18) Viovy, J.-L.; Duke, T., DNA electrophoresis in polymer solutions: Ogston sieving, reptation and constraint release. *Electrophoresis* **1993**, *14*, 322-329.
- (19) Rousseau, J.; Drouin, G.; Slater, G. W., Entropic Trapping of DNA During Gel Electrophoresis: Effect of Field Intensity and Gel Concentration. *Phys. Rev. Lett.* **1997**, *79*, 1945-1948.
- (20) Chung, M.; Kim, D.; Herr, A. E., Polymer sieving matrices in microanalytical electrophoresis. *The Analyst* **2014**, *139*, 5635-5654.
- (21) Dolnik, V.; Cobb, K. A.; Novotny, M., Preparation of polyacrylamide gel-filled capillaries for capillary electrophoresis. *J. Microcolumn Sep.* **1991**, *3*, 155-159.
- (22) Baba, Y.; Matsuura, T.; Wakamoto, K.; Morita, Y.; Nishitsu, Y.; Tshuhako, M., Preparation of polyacrylamide gel filled capillaries for ultrahigh resolution of polynucleotides by capillary gel electrophoresis. *Anal. Chem.* **1992**, *64*, 1221-1225.
- (23) Sudor, J.; Barbier, V.; Thiroit, S.; Godfrin, D.; Hourdet, D.; Millequant, M.; Blanchard, J.; Viovy, J.-L., New block-copolymer thermoassociating matrices for DNA sequencing: Effect of molecular structure on rheology and resolution. *Electrophoresis* **2001**, *22*, 720-728.
- (24) Wan, F.; He, W.; Zhang, J.; Chu, B., Reduced matrix viscosity in DNA sequencing by CE and microchip electrophoresis using a novel thermo-responsive copolymer. *Electrophoresis* **2009**, *30*, 2488-2498.
- (25) Dolnik, V., Wall coating for capillary electrophoresis on microchips. *Electrophoresis* **2004**, *25*, 3589-3601.
- (26) Awada, C.; Sato, T.; Takao, T., Affinity-Trap Polyacrylamide Gel Electrophoresis: A Novel Method of Capturing Specific Proteins by Electro-Transfer. *Anal. Chem.* **2010**, *82*, 755-761.
- (27) Kinoshita, E.; Kinoshita-Kikuta, E.; Koike, T., The Cutting Edge of Affinity Electrophoresis Technology. *Proteomes* **2015**, *3*, 42-55.
- (28) Li, X.; Khairulina, K.; Chung, U. I.; Sakai, T., Migration behavior of rodlike dsDNA under electric field in homogeneous polymer networks. *Macromolecules* **2013**, *46*, 8657-8663.
- (29) Li, X.; Khairulina, K.; Chung, U.; Sakai, T., Electrophoretic Mobility of Double-Stranded DNA in Polymer Solutions and Gels with Tuned Structures. *Macromolecules* **2014**, *47*, 3582-3586.
- (30) Takuya Kubo; Mami Oketani; Yuichi Tominaga; Toyohiro Naito; Otsuka, K., Tunable Molecular Sieving in Gel Electrophoresis Using a Poly(ethylene glycol)-Based Hydrogel. *Chromatography* **2014**, *35*, 81-86.
- (31) Kubo, T.; Nishimura, N.; Furuta, H.; Kubota, K.; Naito, T.; Otsuka, K., Tunable separations based on a molecular size effect for biomolecules by poly(ethylene glycol) gel-based capillary electrophoresis. *J. Chromatogr. A* **2017**, *1523*, 107-113.
- (32) Zarei, M., Application of nanocomposite polymer hydrogels for ultra-sensitive fluorescence

- detection of proteins in gel electrophoresis. *Trac-Trends in Analytical Chemistry* **2017**, *93*, 7-22.
- (33) Yang, S.; Liu, J.; Lee, C. S.; DeVoe, D. L., Microfluidic 2-D PAGE using multifunctional in situ polyacrylamide gels and discontinuous buffers. *Lab on a chip* **2009**, *9*, 592-599.
- (34) Pan, Q.; Yamauchi, K. A.; Herr, A. E., Controlling Dispersion during Single-Cell Polyacrylamide-Gel Electrophoresis in Open Microfluidic Devices. *Anal. Chem.* **2018**, *90*, 13419-13426.
- (35) Shibayama, M.; Ikkai, F.; Shiwa, Y.; Rabin, Y., Effect of degree of cross-linking on spatial inhomogeneity in charged gels. I. Theoretical predictions and light scattering study. *The Journal of Chemical Physics* **1997**, *107*, 5227-5235.
- (36) Stellwagen, N. C., DNA mobility anomalies are determined primarily by polyacrylamide gel concentration, not gel pore size. *Electrophoresis* **1997**, *18*, 34-44.
- (37) Kinoshita, T.; Ishigaki, Y.; Nakano, K.; Yamaguchi, K.; Akita, S.; Nii, S.; Kawaizumi, F., Application of acrylate gel having poly(ethylene glycol) side chains to recovery of gold from hydrochloric acid solutions. *Sep. Purif. Technol.* **2006**, *49*, 253-257.
- (38) Ishigaki, Y.; Kinoshita, T.; Nakano, K.; Yamaguchi, K.; Shibata, N.; Aoi, K.; Nii, S.; Akita, S., Autonomous Stepwise Process for Adsorption, Reduction, and Desorption of Chromium Ions by Using Hydrogel Beads Having Poly(ethylene glycol) Chains. *J. Chem. Eng. Jpn.* **2012**, *45*, 148-153.
- (39) He, H.; Averick, S.; Mandal, P.; Ding, H.; Li, S.; Gelb, J.; Kotwal, N.; Merkle, A.; Litster, S.; Matyjaszewski, K., Multifunctional Hydrogels with Reversible 3D Ordered Macroporous Structures. *Advanced Science* **2015**, *2*, 1500069.
- (40) Pelras, T.; Mahon, C. S.; Nonappa; Ikkala, O.; Groeschel, A. H.; Muellner, M., Polymer Nanowires with Highly Precise Internal Morphology and Topography. *J. Am. Chem. Soc.* **2018**, *140*, 12736-12740.
- (41) Liu, C.; Yamaguchi, Y.; Sekine, S.; Ni, Y.; Dou, X., Precise and simultaneous enumeration of multiplex pathogens using multiplex polymer chain reaction coupled with a novel quantitative capillary electrophoresis. *Sensors and Actuators B: Chemical* **2018**, *258*, 263-269.
- (42) Liu, C.; Yamaguchi, Y.; Zhu, X.; Li, Z.; Ni, Y.; Dou, X., Analysis of small interfering RNA by capillary electrophoresis in hydroxyethylcellulose solutions. *Electrophoresis* **2015**, *36*, 1651-1657.
- (43) Heller, C., Separation of double-stranded and single-stranded DNA in polymer solutions: I. Mobility and separation mechanism. *Electrophoresis* **1999**, *20*, 1962-1976.
- (44) Heller, C., Separation of double-stranded and single-stranded DNA in polymer solutions: II. Separation, peak width and resolution. *Electrophoresis* **1999**, *20*, 1978-1986.
- (45) Shibayama, M.; Norisuye, T.; Nomura, S., Cross-link Density Dependence of Spatial Inhomogeneities and Dynamic Fluctuations of Poly(N-isopropylacrylamide) Gels. *Macromolecules* **1996**, *29*, 8746-8750.
- (46) Heller, C., Finding a universal low viscosity polymer for DNA separation (II). *Electrophoresis* **1998**, *19*, 3114-27.

Chapter III

***Copoly*(poly(ethylene glycol) diacrylate/poly(ethylene glycol) acrylate) based molecularly imprinted polymer for the specific adsorption and selective electrophoretic separation of native cytochrome c**

Abstract

Protein imprinted hydrogel, which is a form of molecularly imprinted polymers (MIPs) using target protein as a template, is an important material for enzyme-linked immunosorbent assay, drug delivery materials, sensors, separation materials, *etc.* In order to obtain a high protein recognition performance, we still have to optimize the compositions of the hydrogel. This work focuses on the *copoly*(poly(ethylene glycol) diacrylates/poly(ethylene glycol) acrylate), in short (*copoly*(PEGDA/PEGA)), based MIP hydrogels targeting the selective recognition of cytochrome c. The presented MIP hydrogels employ a water soluble PEGDA as a crosslinker, PEGA as a side chain, and sodium allylsulfonate as a functional monomer. The fabricated MIP hydrogels and non-imprinted polymer (NIP) hydrogels were treated as the adsorbents for protein adsorption. Factors including the ratio of the template to functional monomer, ionic strength in the adsorption test, crosslinker length and crosslinker ratio of PEGDA/PEGA were investigated for a highly specific recognition. Results showed that a higher template ratio to the functional monomer, shorter crosslinker, and an additional of NaCl (20 mM) in the adsorption solvent provided a higher imprinting effect. A lower crosslinker ratio of no less than 6/4 offered a faster template removing; at the same time, the imprinting effect still remained at a quite high level. As an application, the cytochrome c imprinted *copoly*(PEGDA/PEGA) hydrogel was hybridized with a polyacrylamide gel and applied to the selective separation of native cytochrome c via slab gel electrophoresis.

1. Introduction

Molecularly imprinting technology (MIT) is a facile, economic, and robust approach to the construction of molecular affinity structures for a specified molecule^{1, 2}. Generally, the MIT involves a copolymerization of several types of crosslinkers and functional monomers under the presence of template molecules. The resulting molecularly imprinted polymer (MIP) bears the structural information of the template molecule, including shape, size, and surface distribution pattern of functional groups, exhibiting as a counterpart to the target. When target molecules present, the MIP possesses a specific affinity to the target molecule, and may possess recognizable adsorption³, structural reformation^{4, 5}, or electrochemical characters⁶⁻⁸. In addition, the MIT is recognized as a powerful technology for being able to offer artificial affinity MIPs for theoretically any molecules⁹. So far, the MIP has evolved as sensors¹⁰⁻¹², drug delivery materials¹³⁻¹⁵, sorbent¹⁶⁻¹⁸, separation materials^{19, 20}, etc., by the specific recognition of a variety of molecules.

The MIP has become an important tool in the field of protein recognition because the natural-source antibodies or receptors for protein sensing are sometimes scarce, unstable or difficult to extract. However, to fabricate a protein imprinted MIP, untypical techniques are required due to the large size, structural complexity, and low conformational stability of proteins²¹. One issue is that, in a MIP material, there is supposed to be a densely crosslinked network for conservation of the memorized structural information. Meanwhile, there should be enough room, such as pores in a porous material or pores in a polymer network, to facilitate the removal and rebinding of the protein macromolecule¹. Additionally, water-soluble proteins need to be imprinted and rebind in conditions close to their natural environment in order to guarantee conformational integrity.² Initially, the major MIT methods employed organic porogens. Thus, when we employ an aqueous environment for an MIP, we must also consider the functional monomers and crosslinkers^{22, 23}, to guarantee the effectiveness of polymerization and molecule-functional monomer interaction. Among the successful MIT methods for protein imprinting, including the surface imprinting, epitope-mediated imprinting²⁴⁻²⁶, and nanoparticle imprinting, the protein imprinted hydrogel has merits such as genuine aqueous environment, easy preparation, stimulus repressiveness, permeability, elasticity, etc. Protein imprinted hydrogels employ minimal steps in preparation by simple mixing the templates and monomers before polymerization. The resulting solid can adsorb a large amount of water and has promising application prospects for its potential in smart materials²⁷ and wearable soft materials²⁸⁻³⁰.

As is discussed above, to achieve a balanced imprinting performance and molecular up-and-take efficiency, the fabrication of protein imprinted hydrogel requires an optimization of the polymer network structure based on the compositions of the hydrogel. The *copoly*(poly(ethylene glycol) diacrylate/poly(ethylene glycol) acrylate) (*copoly*(PEGDA/PEGA)) hydrogel is one type of crosslinked polymer networks with PEGDA as a crosslinker and PEGA as side chains, which offers lots of opportunities in obtaining a high imprinting performance. Depending on the unit number (n) of PEG, a variety of commercially available PEGDA and PEGA monomers can be used, thereby provide a flexible way to tune the length of network strands^{31,32}. The length of network strands also relies on the crosslinker ratio. When n is equal to or more than 9, the PEGDA becomes water soluble, thus allows a wide range of crosslinking ratio of PEGDA/PEGA up to 10/0. As one type of PEG based materials, the *copoly*(PEGDA/PEGA) hydrogel is suitable for biomolecule-imprinting and environmental-friendly applications owing to their features such as low toxicity and bio-compatibility. On the other hand, there are prosperous studies using PEG based materials, including PEG materials with ideally controllable structure³³, enhanced mechanical properties^{34,35}, and responsiveness to narrow temperature zone, pH³⁶⁻⁴⁰, and ionic strength⁴¹, etc. Thus, it is worthy to study the PEG based MIPs to promote the diversity of MIP materials. Previously, the PEG based hydrogels has found applications for the carbonhydrates, proteins, and small molecules, by showing specific adsorption³⁶, retention/affinity effect for separation¹⁹, fluorescent response⁴², swelling-deswelling⁴³ behavior to the targets.

In this work, we carry out a fundamental study with the *copoly*(PEGDA/PEGA) hydrogel^{31,44} for the fabrication of a protein imprinted MIP hydrogel. PEGDAs with different lengths ($n = 9, 14, 23$) were employed as crosslinkers, PEGA with $n = 9$ was employed as side chain. Cytochrome c was employed as a model template and sodium allylsulfonate was employed as a functional monomer in order to form ionic interaction with proteins. The obtained MIP hydrogels were used as adsorbent for the specific adsorption of cytochrome c and also applied to slab gel electrophoresis (SGE) for the selective separation of native proteins. A few factors, including the functional monomer-template ratio, crosslinker length, crosslinker ratio of PEGDA/PEGA, and NaCl concentration in the adsorption test (to adjust the ionic strength of protein rebinding condition), were investigated for a high level of specific molecular adsorption. The limit of detection (LOD) and selectivity against non-target proteins were also evaluated in this study. So far, it is urgent to find new approaches to separate native proteins with high resolution. For SGE, this work develops a method to make an MIP and non-imprinted polymer (NIP)-acrylamide hybrid slab gel for native protein separation.

2. Experimental

2.1 Chemicals

Tris-HCl powder was purchased from Takara (Shiga, Japan). Trypsin from bovine pancreas and cytochrome c from equine heart was purchased from Sigma-Aldrich (St. Louis, USA). Sodium chloride, ammonium peroxodisulfate (APS), *N,N,N',N'*-tetramethylethylenediamine (TEMED), and coomassie brilliant blue (CBB) solution (quick CBB plus) were purchased from Wako Pure Chemical Industries (Osaka, Japan). PEGDA (namely 9G', 14G', and 23G' when *n* equaled to 9, 14 and 23, respectively) and PEGA (namely AM-90G, *n* = 9) were donated from Shin-Nakamura Chemical (Wakayama, Japan). The 40% acrylamide/bis solution and sodium chloride (NaCl) were from Nacalai Tesque (Kyoto, Japan). And sodium allylsulfonate (SA) were from Tokyo Chemical Industry (Tokyo, Japan).

Table 1 Compositions of MIP gels with different template-functional monomer ratios.

14G' (μL)	Cytochrome c (mM)	10% SA (μL)	1 mM tris-HCl (mL)	20% (w/w) APS (μL)	TEMED (μL)
	0.03				
	0.3				
214.3 (111 mM)	0.425	29.5 (6.8 mM)	3	6	1
	0.68				
	1.5				

The SA and APS was dissolved into water before use.

2.2 Fabricating MIP gels

The compositions of MIP hydrogels were listed in Table 1-3. For reference, NIP hydrogels were also fabricated without adding the protein template to the precursor solution. The prescribed compositions (except for TEMED) were added into one glass bottle and mixed by several repeats of pipetting. The mixture solution was degassed by performing 20 min Ar bubbling and then 10 min vacuum under 0.1 MPa. Immediately after degas, the prescribed amount of TEMED was well mixed into the mixture. The mixture solution was quickly transferred into a slab gel mold and kept still for 24 h to complete the polymerization. The resulted gel was peeled off and cut into disks with 7 mm diameter. The gel was 1 mm thickness thus one piece of gel disk had an initial volume around 38.5 μL .

Table 2 Compositions of MIP gels with different crosslinker lengths.

Crosslinker	Crosslinker volume (μL)	Cytochrome c (mM)	10% SA (μL)	1 mM tris-HCl (mL)	20% (w/w) APS (μL)	TEMED (μL)
9G'						
14G'	214.3	0.297	29.5 (6.8 mM)	3	6	1
23G'						

Table 3 Compositions of MIP gels with different crosslinker ratios (mass ratio).

Crosslinker ratio	23G' (mg)	AM-90G (μL)	Cytochrom c (mM)	10% SA (μL)	1 mM tris-HCl (mL)	TEMED/20 % APS (μL)
8/2	188.6 (55.2 mM)	42.9 (22.2 mM)				
6/4	141.4 (41.1 mM)	85.7 (44.4 mM)	0.297	29.5 (6.8 mM)	3	1/6
4/6	94.3 (27.6 mM)	128.6 (66.7 mM)				

2.3 Template removing

To remove the templates from the MIP gels, the gel pieces were immersed into 1 M NaCl which volumes more than 50 times of the gel's volume. The washing solution with gels was kept at 40 °C temperature and refreshed every 24 h for total 6 times. At last, the gels were conditioned in a buffer solution for another 24 h under 40 °C then followed by the adsorption test. The buffer solution was employed in the final step wash because the identical compositions of a buffer solution was used to prepare protein samples in the adsorption test. As a control reference, the NIP gels were washed with the same manner.

2.4 Adsorption test

The proteins, including cytochrome c, lysozyme, trypsin and BSA, were dissolved into a buffer solution to make an adsorption solution. The buffer solution contained protein, pH 7.4 tris-HCl (1 mM otherwise indicated) and different concentrations of NaCl. Protein concentration was 0.018 mM otherwise indicated. To test the protein adsorption ability, the gels were put into the adsorption solution and kept shaking for 24 h. The supernatant of the adsorption solvent was examined under a UV spectrometer to detect the concentration of remaining proteins. Each test was conducted with three

repeats. In this study, although the removing of template required a 7-day-long washing and was more efficient at 40 °C, the adsorption of protein into the gel would be completed within one day. For the detection of lysozyme, trypsin, and BSA the UV absorbance at 280 nm was examined; for cytochrome c the UV absorbance at 411 nm was examined. The adsorption amount and imprinting factor (IF) were calculated as following:

$$\text{Adsorption amount} = (\text{protein concentration before adsorption} - \text{protein concentration after adsorption}) \times \text{volume of adsorption solution} \quad (1)$$

$$\text{Imprinting factor} = \frac{\text{Adsorption amount of MIP gel}}{\text{Adsorption amount of NIP gel}} \quad (2)$$

2.5 Slab gel electrophoresis

The MIP and NIP gels were cut into pieces with 1 mm × 1 mm × 5 mm size. The gel pieces were placed next to the comb, between the glass plates mold, aiming at forming a gel barrier at the bottom of sample wells. The 8% acrylamide precursor solution (Table 4) was poured into the glass slide mold. After removing the bubbles and 10 h polymerization, the resulted hybrid gel was applied to the SGE test. The running buffer was 10 mM tris-HCl. The separation voltage was 100 V. To visualize the electrophoretic bands of proteins, the hybrid gel was first washed with distilled water for 15 min, stained with a CBB solution for 30 min, and washed with distilled water for 30 min.

Table 4 Compositions of the 8% acrylamide gel.

40% acrylamide/bis (mL)	1 M tris-HCl (μL)	H ₂ O (mL)	TEMED/20% APS (μL)
2	10	8	2/20

3. Results and discussion

3.1 Template removal

The importance of a proper template removing process cannot be emphasized more because the remaining templates may occupy the MIP sites to block the target molecule to access, or leak to the circumstance to interfere with the molecular recognition performance. As previously reported, for an

ionic gel, the mass density of the MIP network and the ionic strength of the washing solution influences the template removing efficiency. The mass density of the MIP structure is supposed to be low enough to allow a fast macromolecule elution, also should be high enough to offer an operable mechanical strength. The ions in the washing solution will induce a shrinkage of the ionic gel, and consequently reduce the pore size of the polymer network. Thus, it is suggested to balance the composition of the washing solution until the ionic strength is strong enough for the template elution, as well as moderate enough to keep the ionic gel from severe shrinkage. Based on our previous study, this work employed the mass density of 64.9 mg/mL, and 1 M NaCl as washing solution^{36, 41}.

Through unsystematic experiments we found that the temperature also affected the elution efficiency of templates. To specify, we achieved an efficient template removal by elevating the temperature to 40 °C. Our result showed that the gels eluted under 40 °C showed a higher IF than those eluted under room temperature (data not shown). As indicated in Fig. 1 (a), after the MIP gels was eluted with 1 M NaCl under 40 °C for two days, its color-fade was more significant comparing to the one eluted under room temperature. Here we note that the color-fade was not a thermal-induced color change, as a cytochrome c solution did not fade under 40 °C for up to 3 days. We would like to ascribe the fast color-fade of the MIP gel to the faster dissociation of cytochrome c from the functional monomer under a high temperature, because a dissociation reaction is an endothermic process. As a result, Fig. 1 (b) and (c) show typical gels after template removing and after cytochrome c rebinding, respectively. It can be seen that after removing the template, the MIP gel swelled more significantly than the NIP gel due to the loss of templates to confine the ionic repelling force. After cytochrome c rebinding, the MIP and NIP gels returned to close sizes.

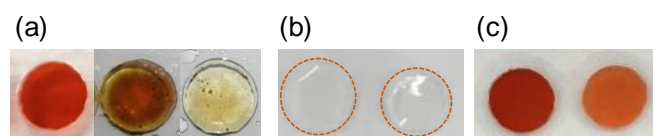


Fig. 1 (a) The pictures of MIP gel before wash (left), after a 2 day wash by 1 M NaCl under room temperature (middle) and after a 2 day wash by 1 M NaCl under 40 °C (right). (b) The picture of MIP (left) and NIP (right) gels after template removal. Circles indicating the size of gels are used to guide the eye. (c) The picture of MIP (left) and NIP (right) gels after cytochrome c adsorption.

3.2 Ratio of template to functional monomer and ionic strength in the adsorption solvent

The ratio of the template to functional monomer and the ionic strength in the adsorption solvent were studied for their effects on the IFs. The MIP gels were prepared with different ratio (Table 1), and put into adsorption tests with different NaCl concentrations. The adsorption amount of the MIP and NIP gels was examined and the IF was calculated. Results showed that a higher ratio of the template to functional monomer would improve the adsorption amount (Fig. 2 (a)) and thus the IF (Fig. 2 (b)). However, the increase of the adsorption amount was gentle when the template concentration was higher than 0.3 mM. In addition, during the template removal process, we noticed that a higher template concentration required longer washing time. Thus, we chose the template concentration of 0.3 mM for following study.

To modify the ionic strength, different concentrations of NaCl from 0 to 50 mM were added into the adsorption solvent. From Fig. 2 (a) it was observed that the adsorption amount decreased along with the increase of the NaCl concentration, which proved that the presence of NaCl competed with the ionic interaction between protein-functional monomer. As a result, the IF changed upon the change of the NaCl concentration (Fig. 2 (b)), and an optimum IF was found under the presence of 20 mM NaCl.

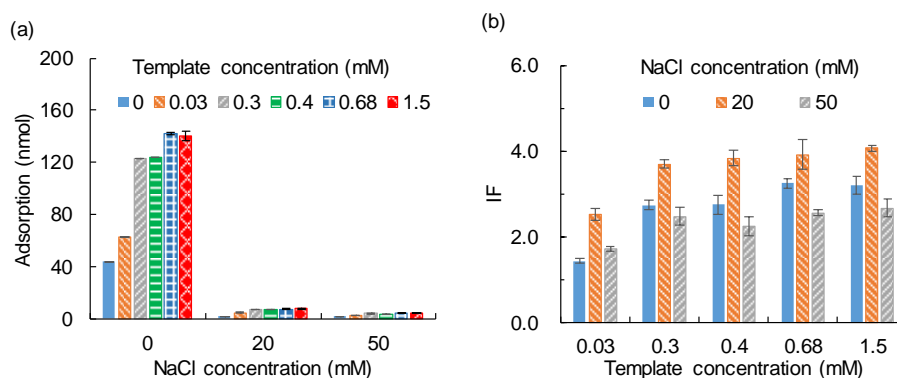


Fig. 2 (a) The adsorption amount of MIP and NIP gels tested under different NaCl concentrations. Each bar also indicated the adsorption amount in a gel fabricated with one template concentration. (b) The imprinting factor (IF) of the MIP gels fabricated with different template concentrations. Each bar also indicated the IF tested under a different NaCl concentration.

3.3 Crosslinker length

The effect of the crosslinker length on the adsorption ability was investigated in this section. The crosslinkers employed here was 9G' ($n = 9$), 14G' ($n = 14$), and 23G' ($n = 23$) and the crosslinker ratio

of PEGDA/PEGA was fixed to 10/0 (Table 2). Fig. 3 (a) illustrated the ideal structure of PEGDA gels, given the same mass density, when using a shorter crosslinker, the side chain length decreases, and the main chain length increases³¹. Thus, this structural difference might have an impact on the molecular recognition character of the MIP gel.

Adsorption test was carried out with the three types of PEGDA gels under 20 mM NaCl, 0.5 mM tris-HCl, and results were shown in Fig. 3 (b). It was observed that when the length of the crosslinker decreased, the MIP gels' adsorption ability to cytochrome c increased by a large margin; while the NIP gels' adsorption ability varied at a slightly difference. As a result, we found that the MIP gels fabricated by shorter crosslinker 9G' showed the highest specificity among the three types of gels. This result is consistent with the previous result that the shorter crosslinker provided a more rigid polymer structure thus the MIP sites would be more robust.

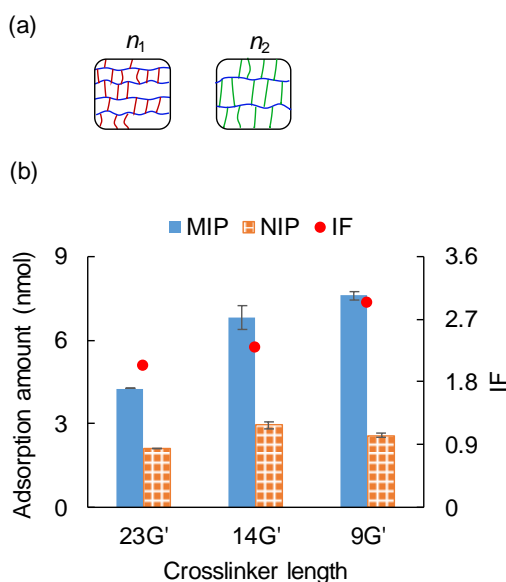


Fig. 3 (a) An illustration of the polymer network when the crosslinker length changed. Here, $n_1 < n_2$, *i.e.*, the left illustration represents the shorter crosslinker polymer network, the right one represents the longer crosslinker polymer network. (b) The adsorption amount and imprinting factor (IF) of the gels fabricated with different crosslinkers.

3.4 Crosslinker ratio

The effect of the crosslinker ratio of PEGDA/PEGA on the molecular recognition performance was investigated in this section. The crosslinker ratio was changed ranging from 10/0 to 4/6, with 23G' (PEGDA, $n = 23$) served as the crosslinker and the AM-90G (PEGA, $n = 9$) as the polymer chain (Table 3). As illustrated in Fig. 4 (a), given a fixed mass density, the lower crosslinker ratio brought the longer

polymer length between two crosslinking point, as well as the larger pore size of the polymer network. Thus, using a less crosslinked gel might facilitate the molecular elution and uptake. As a typical evidence, after a 3-day 1 M NaCl washing, the less crosslinked gel exhibited a lighter color (Fig. 4 (b)). This indicated that the lower crosslinker ratio, the more efficient elution of cytochrome c.

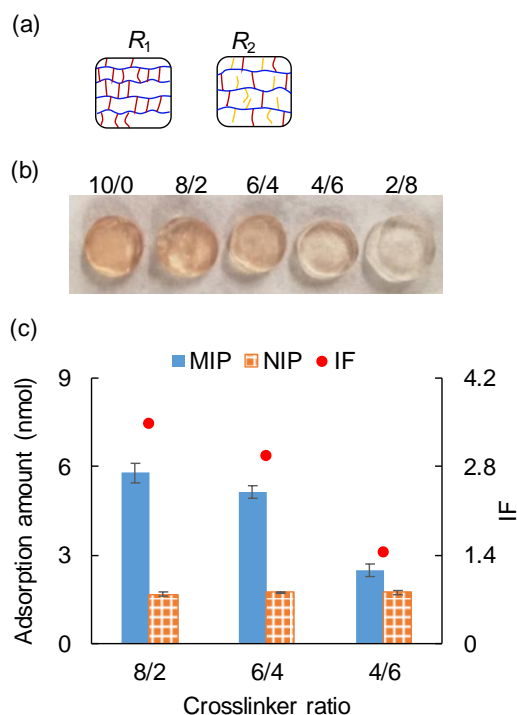


Fig. 4 (a) A illustration of the polymer network when the crosslinker ratio changed. Here, $R_1 > R_2$, *i.e.*, the left illustration represents the dense crosslinker polymer network, the right one represents the light crosslinker polymer network. (b) Picture of gels washed by 1 M NaCl for 3-days. The crosslinker ratio was indicated by the number above the gel. (c) The adsorption amount and imprinting factor (IF) of the gels fabricated with different crosslinker ratios of PEGDA/PEGA.

After completing the template removal, each MIP and NIP gels was immersed into a solution (500 μ L) containing 0.03 mM cytochrom c, 20 mM NaCl, and 1 mM tris-HCl for the adsorption test. From the result of the adsorption test, we found that when the crosslinker ratio increased, the NIP gels showed no significant variation in the adsorption ability, while the MIP gels exhibited a higher adsorption to cytochrome c. This suggested that the crosslinker ratio influenced the adsorption ability of the MIP gels, because a larger population of rigid MIP cavities might form with the higher crosslinker ratio. By examining the IF, it was found that a quite specific recognition to cytochrome c ($IF > 1.5$) still can be obtained when the crosslinker was higher than 6/4. In brief, by using the crosslinker ratio 6/4, a faster elution would be obtained while maintain the specificity ($IF > 1.5$) of the molecular recognition.

3.5 Limit of detection

As an adsorbent material, the LOD is also a parameter of interest. As was demonstrated by this work, the adsorption performance of an ionic gel may be controlled by the ionic strength of adsorption solution. When the NaCl concentration increased, the adsorption of an ionic gel to protein decreased, and vice versa. We can take advantage of this character to optimize the specificity, *i.e.*, the IF of the ionic gel³⁶. As another application, it is possible to modify the LOD of the gel by adjusting the ionic strength.

Here, the LOD was defined to a concentration beyond which the IF fell below 1.5. The gel volume for this test was set as 115.4 μL , the adsorption solution volume was 500 μL . Here we examine the lower LOD under the presence of 20 mM NaCl. This is because the gel showed a higher specificity to target protein with low abundance, although it was apt to saturate under a high concentration. As is shown in Fig. 5, when testing the lower LOD, we found a linear relation between the sample concentration and adsorption amount in both MIP and NIP gels. The data were fitted into fitting lines of Eqs. (3) and (4), and the lower LOD was calculated as following:

$$A_{\text{MIP}}(c) = 419.5c + 0.1208 \quad (3)$$

$$A_{\text{NIP}}(c) = 106.6c + 0.1027 \quad (4)$$

$$F(c) = A_{\text{MIP}}(c)/A_{\text{NIP}}(c) \quad (5)$$

where c was the sample concentration, $A_{\text{MIP}}(c)$ and $A_{\text{NIP}}(c)$ were the adsorption amounts of the MIP and NIP gels at the sample concentration c , respectively. Eq. (3) was the fitting line of the sample concentration-adsorption amount in the MIP, and Eq. (4) was that in the NIP. When Eq. (5) = 1.5, we obtained the $c = 1.4 \mu\text{M}$ (18 ng/ μL), *i.e.*, the value of lower LOD. The higher LOD was obtained without

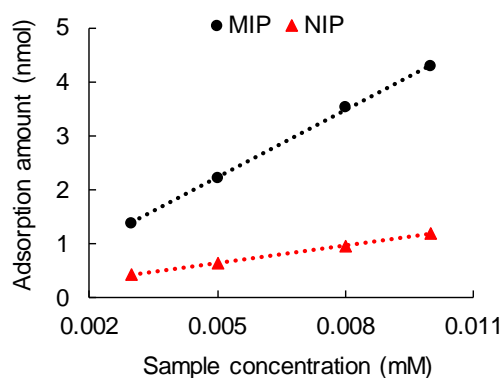


Fig. 5 The adsorption amount of the MIP and NIP gels obtained with different sample concentrations. A linear relationship was found in both MIP and NIP gels.

the presence of NaCl concentration in the adsorption solution. This is because the gel was able to take up a large amount of protein without being saturated under a circumstance with low ionic strength (Section 3.2). Results show that the MIP gels exhibited IF >1.5 under cytochrome c concentration up to 100 μ M (1.2 mg/ μ L).

3.6 Selectivity

The selectivity of the cytochrome c imprinted hydrogel was tested with non-target proteins of lysozyme, trypsin and BSA. As shown in Table 5, cytochrome c, lysozyme, and trypsin have similar isoelectric point (pI) and carry positive charge under pH 7.4 (the working pH in this work), where they may show affinity to the sulfonate functional monomer. BSA has pI of 4.7, thus carry negative charge under pH 7.4. The MIP gel with compositions shown in Table 2 (14G') was employed here. Each adsorption solution had a volume of 500 μ L and contained 0.03 mM sample protein and 1 mM tris-HCl.

Table 5 Molecular weight and isoelectric point of proteins.

Protein	Molecular weight (kDa)	Isoelectric point, pI
Cytochrome c	12.3	10.2
Lysozyme	14.4	10.8
Trypsin	23.8	10.6
BSA	66.0	4.7

At first, 20 mM NaCl was added into the adsorption solution, and the result was shown in Fig. 6 (a). Comparing with cytochrome c, it was found that the adsorption amount of the MIP and NIP gels was much lower when it came to BSA, which is a molecule with the positive charge. This indicated that the ionic repelling force occurred to resist the adsorption of BSA. The MIP gel also showed lower adsorption to trypsin which is a larger molecule with close pI . This indicated that small cavities formed in the MIP gels and the cavities could block large molecules to access the specific sites. The MIP and NIP gels showed higher adsorption ability to lysozyme. This may be because that the lysozyme has similar molecular size and pI with cytochrome c, consequently it could access the cytochrome c imprinted cavities easily. On the other hand, the NIP gel showed a higher adsorption to lysozyme too, which suggested that compared to cytochrome c, lysozyme inherently had easier access to the sulfonate group under the presented conditions.

Then, we employed no NaCl in the adsorption solution for an enhanced ionic interaction to proteins. As shown in Fig. 6 (b), the adsorption amount of lysozyme became lower than the target cytochrome c. The increased adsorption to cytochrome c indicated that the cytochrome c imprinted cavities remembered the surface pattern of the ionic sites on cytochrome c, thereby suppressed the unspecific adsorption to lysozyme. While, the IF to lysozyme was still high. As a brief conclusion, it was demonstrated that the cytochrome c imprinted PEGDA hydrogel showed a high selectivity to cytochrome c amongst trypsin and BSA (larger molecules even with close pI); while, it is difficult to distinguish cytochrome c from lysozyme (small molecules with close pI) under the present conditions.

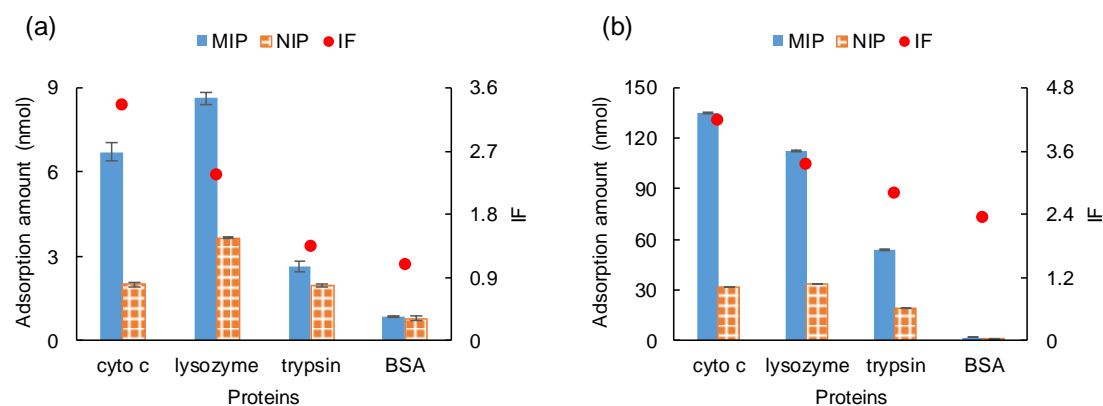


Fig. 6 The adsorption amount and imprinting factor (IF) of different proteins tested under (a) 20 mM NaCl with 1 mM tris-HCl, and (b) 0 mM NaCl with 1 mM tris-HCl. Cytochrome c was indicated as cyto c for short.

3.7 Selective electrophoretic separation

A MIP/NIP-acrylamide hybrid slab gels were prepared by embedding a small piece of the MIP or NIP gels at the bottom of sample well, *i.e.*, at the top of separation lane. So that before the sample enter the zone of the acrylamide gel, it should pass through the MIP or NIP gels. For reference, the hybrid slab gel also contained lanes without any MIP nor NIP, for short, the none lane. By measuring the migration of cytochrome c in the different lanes, we evaluate the affinity of the MIP and NIP gels to cytochrome c. The sample loading had a high amount of 20 μg so that the inherent color of cytochrome c is strong enough for the visualization of the electrophoretic band. The examined parameter was the migration distance (D_{MIP} , D_{NIP} and D_{none} in each lane). During electrophoresis, the sample wells were first filled with 1 mM tris-HCl for 10 min and then gently supplied with 10 mM tris-HCl.

Because the native cytochrome c carries the positive charge at pH 7.4, it migrates with a direction from the anode to cathode. Fig. 7 (a) showed the picture of cytochrome c in the MIP, NIP, and none lanes at 10 min, respectively. It can be seen that with 1 mM tris-HCl, the MIP lane trapped cytochrome c in the MIP gel, the NIP lane allowed cytochrome c to pass through the NIP gel but showed a certain retention effect compared with the none lane. Fig. 7 (b) showed the picture of cytochrome c after 10 mM tris-HCl was supplied to the sample wells, this result demonstrated that using 10 mM tris-HCl as a background buffer solution, cytochrome c would be eluted from the MIP gel and continued to migrate in the acrylamide gel zone. By this method, we realized an online preconcentration of cytochrome c using the MIP hydrogel.

SGE was also conducted with non-target proteins of lysozyme and trypsin (sample loading: 50 ng). After 40 min electrophoresis (the sample wells were filled with 1 mM tris-HCl for 20 min and then supplied with 10 mM tris-HCl for another 20 min), the slab gel was stained by CBB to visualize the native protein bands. The result in Fig. 8 showed that among the none lanes D_{none} of cytochrome c was longest and D_{none} of trypsin was shortest. This result is consistent with the fact that cytochrome c has the smallest molecular weight and trypsin has the largest molecular weight among the three proteins (Table 5), which indicated that a size sieving effect occurred in the acrylamide gel. In the MIP and NIP lanes,

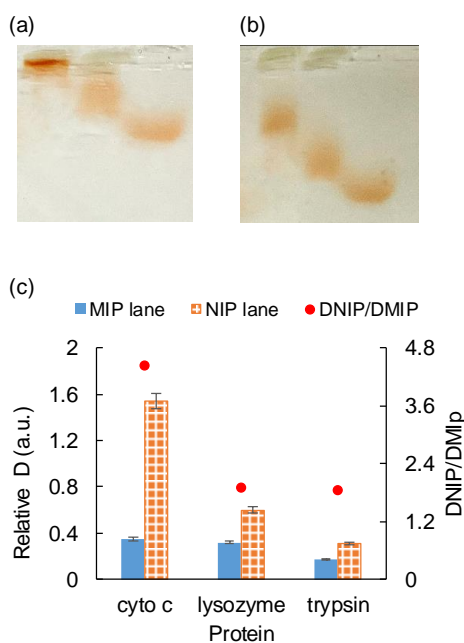


Fig. 7 The image of the hybrid slab gel after (a) 10 min electrophoresis with the sample well filled with 1 mM tris-HCl and (b) an additional 30 min electrophoresis with the sample well supplied with 10 mM tris-HCl. (c) The relative migration distance (D) of proteins in the MIP and NIP lanes, and the value of $D_{\text{NIP}}/D_{\text{MIP}}$. Cytochrome c was indicated as cyto c for short.

the migration distances still were longest with cytochrome c and shortest with trypsin. While, when we divided D_{NIP} by D_{MIP} of each protein (Fig. 7 (c)), the data revealed a fact that the MIP gel retarded cytochrome c by a more significant content than it did to lysozyme and trypsin. As the identical protein would migrate with the same velocity in the acrylamide gel zone, we ascribe the difference between D_{NIP} and D_{MIP} to the retention effect from the MIP and NIP gels. In other words, the higher D_{NIP}/D_{MIP} evidenced a stronger affinity force to cytochrome c in the MIP gel. Comparing the results in Fig. 7 (b) to in Fig. 6, we found a selectivity to cytochrome c amongst lysozyme and trypsin via the electrophoretic approach.

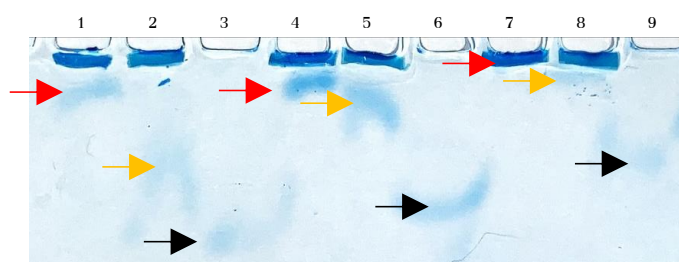


Fig. 8 The picture of the hybrid hydrogel after CBB stain. Lane 1, 4 and 7: MIP lanes; lane 2, 5 and 8: NIP lanes; lane 3, 6 and 9: none lanes. Sample loading: Lane 1-3: cytochrome c; lane 4-6: lysozyme; lane 7-8: trypsin. The blue strip at the top of the MIP and NIP lanes were the MIP and NIP gels, respectively, because the copoly(PEGDA/PEGA) would be stained to blue by CBB. Arrows indicate the position of protein bands: red arrow, protein in the MIP lanes; yellow arrow, protein in the NIP lanes; black arrow, protein in the none lanes. Some bands showed a smiling shape possibly caused the act of buffer exchange.

4. Conclusion

This work involves a fundamental study about the *copoly*(PEGDA/PEGA) based MIP hydrogel. Cytochrome c was employed as a model template and sodium allylsulfonate was employed as an ionic functional monomer. The effect of experimental factors, including the ratio of the template to functional monomer, NaCl concentration in the adsorption solution (to adjust the ionic strength), crosslinker length and crosslinker ratio toward the imprinting effect, was investigated. Results showed that a higher imprinting effect would be obtained when using a higher ratio of the template to functional monomer, 20 mM NaCl with 1 mM tris-HCl as the adsorption solution, and a shorter crosslinker length. A lower crosslinker ratio facilitated the template removal; it was found that when using PEGDA/PEGA higher than 6/4, the imprinting factor still remained a relatively high value. When using 115.4 μ L MIP hydrogels, as little as 17 ng/ μ L cytochrome c would be recognized. When employing the presented MIP hydrogel

as an adsorbent, it showed a high selectivity amongst trypsin and BSA; but apt to adsorb small protein like lysozyme. When employing the presented MIP hydrogel for the electrophoretic separation, it exhibited the ability to distinguish cytochrome c from lysozyme and a high selectivity. This study showed the possibility to use the *copoly*(PEGDA/PEGA) hydrogel as the MIP materials. The presented cytochrome c imprinted MIP material would be applied for the specific adsorption and selective electrophoretic separation of native cytochrome c.

References

- (1) Chen, L.; Xu, S.; Li, J., Recent advances in molecular imprinting technology: current status, challenges and highlighted applications. *Chem. Soc. Rev.* **2011**, *40*, 2922-42.
- (2) Chen, L.; Wang, X.; Lu, W.; Wu, X.; Li, J., Molecular imprinting: perspectives and applications. *Chem. Soc. Rev.* **2016**, *45*, 2137-211.
- (3) Kloskowski, A.; Pilarczyk, M.; Przyjazny, A.; Namiesnik, J., Progress in development of molecularly imprinted polymers as sorbents for sample preparation. *Crit. Rev. Anal. Chem.* **2009**, *39*, 43-58.
- (4) Chen, W.; Ma, Y.; Pan, J. M.; Meng, Z. H.; Pan, G. Q.; Sellergren, B., Molecularly imprinted polymers with stimuli-responsive affinity: progress and perspectives. *Polymers* **2015**, *7*, 1689-1715.
- (5) Bai, W.; Gariano, N. A.; Spivak, D. A., Macromolecular amplification of binding response in superaptamer hydrogels. *J. Am. Chem. Soc.* **2013**, *135*, 6977-6984.
- (6) Jia, L.; Mao, Y.; Zhang, S. Q.; Li, H.; Qian, M.; Liu, D. B.; Qi, B., Electrochemical switch sensor toward ephedrine hydrochloride determination based on molecularly imprinted polymer/nafion-MWCNTs modified electrode. *Microchem. J.* **2021**, *164*.
- (7) Herrera-Chacon, A.; Ceto, X.; del Valle, M., Molecularly imprinted polymers - towards electrochemical sensors and electronic tongues. *Anal. Bioanal. Chem.* **2021**.
- (8) Yoshimi, Y.; Yagisawa, Y.; Yamaguchi, R.; Seki, M., Blood heparin sensor made from a paste electrode of graphite particles grafted with molecularly imprinted polymer. *Sens. Actuators, B* **2018**, *259*, 455-462.
- (9) Advincula, R. C., Engineering molecularly imprinted polymer (MIP) materials: Developments and challenges for sensing and separation technologies. *Korean J. Chem. Eng.* **2011**, *28*, 1313-1321.
- (10) Ahmad, O. S.; Bedwell, T. S.; Esen, C.; Garcia-Cruz, A.; Piletsky, S. A., Molecularly imprinted polymers in electrochemical and optical sensors. *Trends Biotechnol.* **2019**, *37*, 294-309.
- (11) Whitcombe, M. J.; Chianella, I.; Larcombe, L.; Piletsky, S. A.; Noble, J.; Porter, R.; Horgan, A., The rational development of molecularly imprinted polymer-based sensors for protein detection. *Chem. Soc. Rev.* **2011**, *40*, 1547-1571.
- (12) Uzun, L.; Turner, A. P. F., Molecularly-imprinted polymer sensors: realising their potential. *Biosens. Bioelectron.* **2016**, *76*, 131-144.
- (13) Bodoki, A. E.; Iacob, B. C.; Bodoki, E., Perspectives of molecularly imprinted polymer-based drug delivery systems in cancer therapy. *Polymers* **2019**, *11*.
- (14) Sellergren, B.; Allender, C. J., Molecularly imprinted polymers: A bridge to advanced drug delivery. *Adv. Drug Deliver. Rev.* **2005**, *57*, 1733-1741.
- (15) Qin, Y. T.; Feng, Y. S.; Ma, Y. J.; He, X. W.; Li, W. Y.; Zhang, Y. K., Tumor-sensitive biodegradable nanoparticles of molecularly imprinted polymer-stabilized fluorescent zeolitic imidazolate framework-8 for targeted imaging and drug delivery. *ACS Appl. Mater. Inter.* **2020**, *12*, 24585-24598.
- (16) Sun, X. L.; Wang, M. H.; Yang, L. X.; Wen, H. P.; Wang, L. G.; Li, T.; Tang, C. L.; Yang, J. J., Preparation and evaluation of dummy-template molecularly imprinted polymer as a potential sorbent for solid phase extraction of imidazole fungicides from river water. *J. Chromatogr. A* **2019**, *1586*, 1-8.

- (17) Panjan, P.; Monasterio, R. P.; Carrasco-Pancorbo, A.; Fernandez-Gutierrez, A.; Sesay, A. M.; Fernandez-Sanchez, J. F., Development of a folic acid molecularly imprinted polymer and its evaluation as a sorbent for dispersive solid-phase extraction by liquid chromatography coupled to mass spectrometry. *J. Chromatogr. A* **2018**, *1576*, 26-33.
- (18) Beltran, A.; Borrull, F.; Cormack, P. A. G.; Marce, R. M., Molecularly-imprinted polymers: useful sorbents for selective extractions. *Trac-Trends in Analytical Chemistry* **2010**, *29*, 1363-1375.
- (19) Xing, R.; Wang, S.; Bie, Z.; He, H.; Liu, Z., Preparation of molecularly imprinted polymers specific to glycoproteins, glycans and monosaccharides via boronate affinity controllable-oriented surface imprinting. *Nat. Protoc.* **2017**, *12*, 964-987.
- (20) Iacob, B. C.; Bodoki, E.; Oprean, R., Recent advances in capillary electrochromatography using molecularly imprinted polymers. *Electrophoresis* **2014**, *35*, 2722-2732.
- (21) Khumsap, T.; Corpuz, A.; Nguyen, L. T., Epitope-imprinted polymers: applications in protein recognition and separation. *RSC Adv.* **2021**, *11*, 11403-11414.
- (22) Qin, L.; He, X.-W.; Zhang, W.; Li, W.-Y.; Zhang, Y.-K., Macroporous thermosensitive imprinted hydrogel for recognition of protein by metal coordinate interaction. *Anal. Chem.* **2009**, *81*, 7206-7216.
- (23) Bereli, N.; Andaç, M.; Baydemir, G.; Say, R.; Galaev, I. Y.; Denizli, A., Protein recognition via ion-coordinated molecularly imprinted supermacroporous cryogels. *J. Chromatogr. A* **2008**, *1190*, 18-26.
- (24) Pasquardini, L.; Bossi, A. M., Molecularly imprinted polymers by epitope imprinting: a journey from molecular interactions to the available bioinformatics resources to scout for epitope templates. *Anal. Bioanal. Chem.* **2021**.
- (25) Wang, X.; Chen, G.; Zhang, P.; Jia, Q., Advances in epitope molecularly imprinted polymers for protein detection: a review. *Anal. Methods* **2021**, *13*, 1660-1671.
- (26) Nishino, H.; Huang, C.-S.; Shea, K. J., Selective protein capture by epitope imprinting. *Angew. Chem. Int. Ed.* **2006**, *45*, 2392-2396.
- (27) Whitcombe, M. J., Molecularly imprinted polymers smart hydrogel crystal gardens. *Nat. Chem.* **2011**, *3*, 657-658.
- (28) Zhang, Q. W.; Jiang, D. F.; Xu, C. S.; Ge, Y. C.; Liu, X. H.; Wei, Q. Q.; Huang, L. P.; Ren, X. Q.; Wang, C. D.; Wang, Y., Wearable electrochemical biosensor based on molecularly imprinted Ag nanowires for noninvasive monitoring lactate in human sweat. *Sens. Actuators, B* **2020**, *320*, 128325.
- (29) Parlak, O.; Keene, S. T.; Marais, A.; Curto, V. F.; Salleo, A., Molecularly selective nanoporous membrane-based wearable organic electrochemical device for noninvasive cortisol sensing. *Sci. Adv.* **2018**, *4*, eaar2904.
- (30) Liu, Y. L.; Liu, R.; Qin, Y.; Qiu, Q. F.; Chen, Z.; Cheng, S. B.; Huang, W. H., Flexible electrochemical urea sensor based on surface molecularly imprinted nanotubes for detection of human sweat. *Anal. Chem.* **2018**, *90*, 13081-13087.
- (31) Liu, C.; Kubo, T.; Naito, T.; Otsuka, K., Controllable molecular sieving by copoly(poly(ethylene glycol) acrylate/poly(ethylene glycol) diacrylate)-based hydrogels via capillary electrophoresis for DNA fragments. *ACS Appl. Polym. Mater.* **2020**, *2*, 3886-3893.
- (32) Li, X.; Khairulina, K.; Chung, U.-i.; Sakai, T., Electrophoretic mobility of double-stranded DNA in polymer solutions and gels with tuned structures. *Macromolecules* **2014**, *47*, 3582-3586.

- (33) Sakai, T.; Matsunaga, T.; Yamamoto, Y.; Ito, C.; Yoshida, R.; Suzuki, S.; Sasaki, N.; Shibayama, M.; Chung, U. I., Design and fabrication of a high-strength hydrogel with ideally homogeneous network structure from tetrahedron-like macromonomers. *Macromolecules* **2008**, *41*, 5379-5384.
- (34) Jiang, L.; Liu, C.; Mayumi, K.; Kato, K.; Yokoyama, H.; Ito, K., Highly stretchable and instantly recoverable slide-ring gels consisting of enzymatically synthesized polyrotaxane with low host coverage. *Chem. Mater.* **2018**, *30*, 5013-5019.
- (35) Bin Imran, A.; Esaki, K.; Gotoh, H.; Seki, T.; Ito, K.; Sakai, Y.; Takeoka, Y., Extremely stretchable thermosensitive hydrogels by introducing slide-ring polyrotaxane cross-linkers and ionic groups into the polymer network. *Nat. Commun.* **2014**, *5*, 5124.
- (36) Kubo, T.; Arimura, S.; Tominaga, Y.; Naito, T.; Hosoya, K.; Otsuka, K., Molecularly imprinted polymers for selective adsorption of lysozyme and cytochrome c using a PEG-based hydrogel: selective recognition for different conformations due to pH conditions. *Macromolecules* **2015**, *48*, 4081-4087.
- (37) Liu, H. Q.; Li, Y. J.; Yang, R.; Gao, X. J.; Ying, G. G., pH-responsive polyethylene glycol monomethyl ether-epsilon-polylysine-G-poly (Lactic Acid)-based nanoparticles as protein delivery systems. *Plos One* **2016**, *11*, e0159296.
- (38) Ijaz, Q. A.; Abbas, N.; Arshad, M. S.; Hussain, A.; Shahiq uz, Z.; Javaid, Z., Synthesis and evaluation of pH dependent polyethylene glycol-co-acrylic acid hydrogels for controlled release of venlafaxine HCl. *J. Drug Deliv. Sci. Tec.* **2018**, *43*, 221-232.
- (39) Cui, W.; Liu, R.; Jin, H. Q.; Lv, P.; Sun, Y. Y.; Men, X.; Yang, S. N.; Qu, X. Z.; Yang, Z. Z.; Huang, Y. N., pH gradient difference around ischemic brain tissue can serve as a trigger for delivering polyethylene glycol-conjugated urokinase nanogels. *J. Controll. Release* **2016**, *225*, 53-63.
- (40) Weng, J. J.; Huang, Z. B.; Pu, X. M.; Chen, X. C.; Yin, G. F.; Tian, Y. P.; Song, Y., Preparation of polyethylene glycol-polyacrylic acid block copolymer micelles with pH/hypoxic dual-responsive for tumor chemoradiotherapy. *Colloids Surf., B* **2020**, *191*, 110943.
- (41) Tominaga, Y.; Kubo, T.; Sueyoshi, K.; Hosoya, K.; Otsuka, K., Synthesis of poly(ethylene glycol)-based hydrogels and their swelling/shrinking response to molecular recognition. *J. Polym. Sci., Part A: Polym. Chem.* **2013**, *51*, 3153-3158.
- (42) Kubo, T.; Watanabe, N.; Liu, C.; Ikari, S.; Kanao, E.; Naito, T.; Sano, T.; Otsuka, K., Fluorescent detection of the target protein via a molecularly imprinted hydrogel. *Anal. Methods* **2021**.
- (43) Miyata, T.; Hayashi, T.; Kuriu, Y.; Uragami, T., Responsive behavior of tumor-marker-imprinted hydrogels using macromolecular cross-linkers. *J. Mol. Recognit.* **2012**, *25*, 336-343.
- (44) Kinoshita, T.; Ishigaki, Y.; Nakano, K.; Yamaguchi, K.; Akita, S.; Nii, S.; Kawaizumi, F., Application of acrylate gel having poly(ethylene glycol) side chains to recovery of gold from hydrochloric acid solutions. *Sep. Purif. Technol.* **2006**, *49*, 253-257.

Chapter IV

Fabrication of protein recognition structures by grafting molecularly imprinted polymer on a crosslinked hydrogel

Abstract

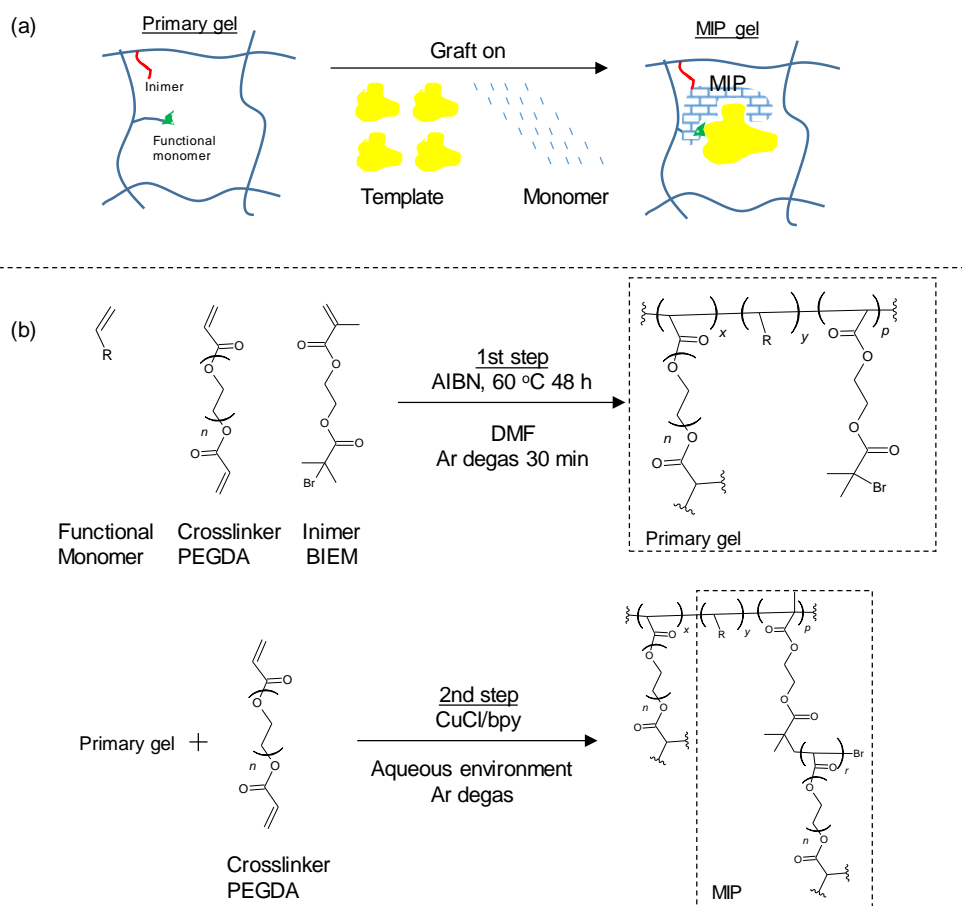
Protein imprinted polymer is one type of molecularly imprinted polymers (MIPs) for protein recognition. Despite the several successful methods to synthesize MIPs, the fabrication of MIPs for proteins is challenging due to the difficulty in balancing the specificity and product yield efficiency. In an attempt to find new approaches, we study to fabricate MIPs via grafting MIP structures on a hydrogel network. A two-step synthesis is involved: a hydrogel network was synthesized via a free radical polymerization, forming an artificial scaffold in the 1st step. In the 2nd step, MIP structures grow from the inimer, around the templates, via the atom transfer radical polymerization. The hydrogel obtained from the 1st step reaction was designed with low monomer density, aiming at a faster molecule diffusion and thus higher molecular recognition efficiency. The MIP structure obtained from the 2nd step reaction provided a specific recognition with target molecules. Both MIP and non-imprinted polymer (NIP) gels were regarded as adsorbents and put into a solution containing the target molecule for the adsorption test. As a result, the newly developed MIP gels offered a higher adsorption ability to the target molecule than the NIP gels when using either trypsin or cytochrome c as a template.

1. Introduction

Protein imprinted polymer is one type of molecularly imprinted polymers (MIPs) for protein recognition. The MIP capable of protein recognition may serve as a substitute of antibody or receptor but also has merits of robust structure, facile preparation, stable for long-term storage, etc. Generally, there are three major approaches to fabricate MIP structures for protein recognition: fabricate MIP structures in a gel bulk^{1, 2}, on a solid phase^{3, 4} or fabricate MIP nanoparticles⁵⁻⁷ in a solution. Regarding to the bulk form of MIP, the gel bulks usually present with a rigid network, which has too small pore size to allow a fast diffusion of biomolecules, as the MIP structure requires a high crosslinking degree to form rigid MIP sites. This impedes the up and take interaction between targets and MIP sites, and affects the elution efficiency of analyte molecule removal.⁸ By synthesizing MIP structures on a solid phase, it is possible to realize a quick mass transfer for target molecules. The solid phase may be a capillary surface⁹, silica spheres^{10, 11}, nanoparticles¹², graphene^{13, 14}, etc. Here, one disadvantage of the solid phase synthesis is the limited number of MIP site due to the small surface area of the supporting solid phase. The technology for MIP nanoparticles involves a polymerization reaction in a large volume of solution. Initially, this technology requires tremendous dialysis steps for collecting the nanoparticle products, it suffers from low imprinting efficiency as a number of unspecific products present. A new strategy was proposed to solve these problems by using a magnet-particle as a core¹⁵. The highly specific MIP structures, which attached on the magnet-particle could be easily collected by a simple magnet control. The products' imprinting specificity was guaranteed, as only the MIP particles attached to the magnet-particle would be selected.

The postsynthesis modification method has attracts considerable interests for its ability to introduce new functionalities to a primary framework¹⁶. The primary framework is infiltrated with monomers, which can graft on as side chains, thereby gets functionalized. Depending on the compositions of the side chain, the primary framework can be altered to functional materials with hydrophobic, fluorescent, conducting, or temperature responsive properties¹⁷. Inspired by the postmodification approach, the present work proposes a method to synthesis MIP structures in a primary gel, in other words, to graft MIP structures on a polymer network. The present method involves a two-step reaction. The 1st step synthesizes a hydrogel network to provide a scaffold (1st gel). In addition, the 1st gel is copolymerized with inimer for the next step of synthesis. In the 2nd step, MIP structures grow from the inimer, which are immobilized on the scaffold (2nd gel). The large pore size of the 1st gel obtained from the 1st step

allows a faster molecule diffusion. Meanwhile, the MIP structure reaching from the scaffold polymer provides a specific recognition with target molecules.



Scheme 1. (a) An illustration of the proposed method to synthesize MIP structures via an postmodification of a primary network. (b) An illustration of the two-step reaction via a radical reaction (1st step) and an ATRP reaction (2nd step).

As shown in Scheme 1, in the 1st step, poly(ethylene glycol diacrylate) (PEGDA), 2-(2-bromoisobutyryloxy)ethyl methacrylate (BIEM), sodium allylsulfonate (SA), and 2,2'-azobis(2-methylpropionitrile) (AIBN) were employed as a crosslinker, inimer (for the 2nd step polymerization), functional monomer, and initiator (for the 1st step polymerization), respectively. In the 2nd step, MIP structures grow from the inimers, around the templates, via the atom transfer radical polymerization (ATRP) approach. PEGDA was employed as a monomer for the structural backbone, copper(I) chloride/bipyridine was employed as a catalyst, trypsin or cytochrome c was employed as a template in the aqueous environment. This work finds out reaction conditions for the 2nd reaction. The postmodification was confirmed by examining the physical chemical properties on the resulting gel

including the optical transmittance and the thermal response. The success of grafting MIP on the primary gel was demonstrated via the higher adsorption to the target molecules.

2. Experimental

2.1 Chemicals

Tris-HCl powder was purchased from Takara (Shiga, Japan). Trypsin from bovine pancreas, cytochrome c from equine heart, bipyridine (bpy), and 2-(2-Bromoisobutyryloxy)ethyl methacrylate (BIEM) were purchased from Sigma-Aldrich (St. Louis, USA). 2,2'-Azobisisobutyronitrile (AIBN) and copper (I) chloride (CuCl) were purchased from Wako Pure Chemical Industries (Osaka, Japan). The PEGDA (namely 9G' and 23G' when n equaled to 9 and 23, respectively) were donated from Shin-Nakamura Chemical (Wakayama, Japan). Sodium chloride (NaCl) was from Nacalai Tesque (Kyoto, Japan). Sodium allylsulfonate (SA) was from Tokyo Chemical Industry (Tokyo, Japan).

2.2 Synthesis of the primary gel (1st reaction)

The primary gel was fabricated by mixing the prescribed compositions in a glass beaker. The mixture was bubbled with Ar for 30 min and then transferred into a glass slide model (1 mm thickness). The glass slide model was then kept at 60 °C for 48 h to complete the polymerization. The resulted gel was peeled off from the glass slide and then cut into disks with 7 mm diameter. The gel disks were washed by 50% dimethylformamide (DMF) in H₂O for 12 h and 1 mM tris-HCl for another 12 h.

2.3 Synthesis of the MIP hydrogel (2nd reaction) and template removing

The fabrication of MIP structures was conducted by mixing 1 mL of prescribed solution with 3 pieces of primary gel disks. In detail, the protein, monomer, solvent and gel disks were first placed into a sealed glass tube and bubbled by Ar for 2 h. The catalyst of CuCl and bpy were dissolved in DMF (28 μ L) before use and transferred into the tube followed by another 6 h of Ar bubbling. As a control reference, the NIP gels were fabricated without the use of protein.

To remove the templates from the MIP gels, the gel pieces were immersed into 1 M NaCl which volumes more than 50 times of the gel's volume. The washing solution with gels was kept at 40 °C temperature and refreshed every 24 h for total 6 times. At last, the gels were conditioned in a buffer

solution for another 24 h under 40 °C then followed by the adsorption test. The buffer solution was employed in the final step wash because the identical composition of the buffer solution was used to prepare protein samples in the adsorption test. As a control reference, the NIP gels were washed with the same manner.

2.4 Adsorption test

The protein, cytochrome c or trypsin, was dissolved into a buffer solution to make an adsorption solution. The protein concentration was 0.018 mM, the buffer solution contained 20 mM NaCl and 1 mM tris-HCl (pH7.4)², otherwise indicated. To test the protein adsorption ability, the gels were put into the adsorption solution and kept shaking for 24 h. The supernatant of the adsorption solvent was examined under a UV-Vis spectrometer to detect the concentration of remaining proteins. Each test was conducted with three repeats. In this study, although the removing of template required a 7-day-long washing and was more efficient at 40 °C, the adsorption of protein into the gel would be completed within one day. For the detection of trypsin, the UV absorbance at 280 nm was measured; for cytochrome c at 411 nm. The adsorption amount and imprinting factor (IF) were calculated as following:

$$\text{Adsorption amount} = (\text{protein concentration before adsorption} - \text{protein concentration after adsorption}) \times \text{volume of adsorption solution} \quad (1)$$

$$\text{Imprinting factor} = \frac{\text{Adsorption amount of MIP gel}}{\text{Adsorption amount of NIP gel}} \quad (2)$$

3. Results and discussion

3.1 Confirmation of the effectiveness of the 2nd reaction

The physical characterization of the gel was changed after the 2nd step reaction. As shown in Fig. 1 (a), the decreased gel's optical transmittance at 608 nm of the 2nd gel was found compared to the 1st gel. Also, different 9G' monomer concentrations, including 10% and 20% (vol/vol), were used to prepare the 2nd gels (compositions of gels were listed in Table 1 and 2). As the concentration of 9G' monomer increased from 10% to 20%, the gel became more obscure (Fig. 1 (b)). This indicated that it was possible to control the thickness of the 2nd gel by adjusting the monomer concentration.

The PEG polymer is a thermal responsive component. For example, the 9G' oligo, which was used in the 2nd step reaction, was reported to have a lower critical solution temperature (LCST) around 90 °C¹⁸. Thus, when the temperature was elevated from 25 to 63.5 °C, the gel generally got immiscible and showed a decreased optical transmittance. From Fig. 1 (b), it was found that the transmittance of the 2nd gels decreased more significantly than the 1st gel, which evidenced the success of the 2nd reaction.

Table 1 Compositions of the 1st gel.

ATM-E35 (μL)	AM-90G (μL)	10% BIEM (μL)	H ₂ O (mL)	20% APS (μL)	TEMED (μL)
56.4 (16.8 mM)	21.6 (26.0 mM)	10 (2.3 mM)	2	15 (0.3% w/w)	1

Table 2 Compositions of the 2nd gel.

9G' (μL)	CuCl (mg)	Bpy (mg)	H ₂ O (mL)
200 (216 mM)	1.8 (9.1 mM)	59.1 (189.2 mM)	1.8
400 (432 mM)			1.6

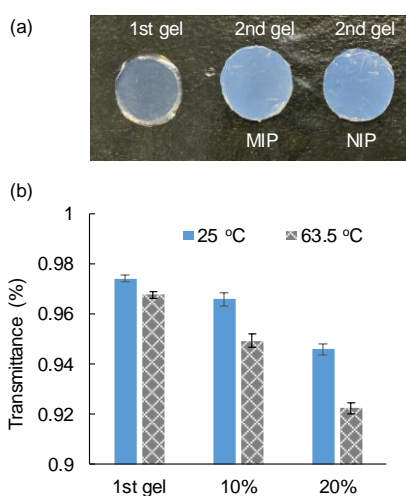


Fig. 1 (a) Picture of a 1st gel (left), 2nd gel with MIP (middle) and 2nd gel with NIP (right). The picture of MIP and NIP gels were taken after template removal. (b) The optical transmittance of the 1st gel and 2nd gels with NIP at 25 °C and 63.5 °C, respectively. The 2nd gels were synthesized under 10% and 20% (vol/vol) 9G' monomer.

3.2 Specific recognition to cytochrome c

As the thickness of the grafted polymer may affect the size of MIP cavities, the crosslinker concentration in the 2nd reaction was adjusted for optimizing the protein recognition performance. Three

MIP gels were prepared with 9G' concentration at 10, 20 and 30% (vol/vol), respectively (Table 3 and 4). Adsorption tests were conducted and results showed that when increasing the monomer concentration from 10 to 30%, the adsorption amount of both MIP and NIP gels decreased. At the same time, the IF increased from 0.9 to 1.9. This suggested that the unspecific adsorption was restricted when a high monomer concentration was employed.

Table 3 Compositions of the 1st gel.

23G' (mg)	BIEM (μL)	DMSO (mL)	10% SA (μL)	AIBN (mg)
406 (58.1 mM)	32.5 (23.2 mM)	6.5	209.6 (22.2 mM)	10.1

Table 4 Compositions of the 2nd gel with MIP. The 2nd gel with NIP was prepared without the presence of cytochrome c.

Cytochrome c	9G' (μL)	CuCl (mg)	Bpy (mg)	H ₂ O (mL)
	300 (216 mM)			2.7
0.3 mM	600 (432 mM)	2.7 (9.1 mM)	88.65 (189.2 mM)	2.4
	900 (648 mM)			2.1

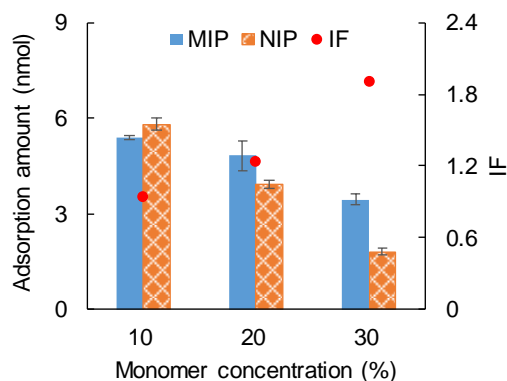


Fig. 2 The Adsorption amount and imprinting factor (IF) of the MIP gels and NIP gels prepared with different monomer concentrations. The template was cytochrome c.

Comparing the adsorption amount of the 1st to 2nd gels which was prepared under 30% (vol/vol) of 9G', it was found that the NIP gel exhibited a lower adsorption than the 1st gel, while the MIP gel exhibited a higher adsorption than the 1st gel (Fig. 3 (a)). This result suggests that the 2nd reaction successfully led to a modification of the 1st gel. To specify, in the NIP gel, when enough polymers were grafted on the main strand of the 1st gel, they might shield the main strand of the 1st gel, forming a rigid barrier to keep the large protein from accessing the functional monomer (SA). In the MIP gel, the grafted

polymers formed cavities to allow a specific rebinding of the target molecule to the functional monomer. For a better illustration, Fig. (b) and (c) plotted possible structures of the MIP and NIP gels.

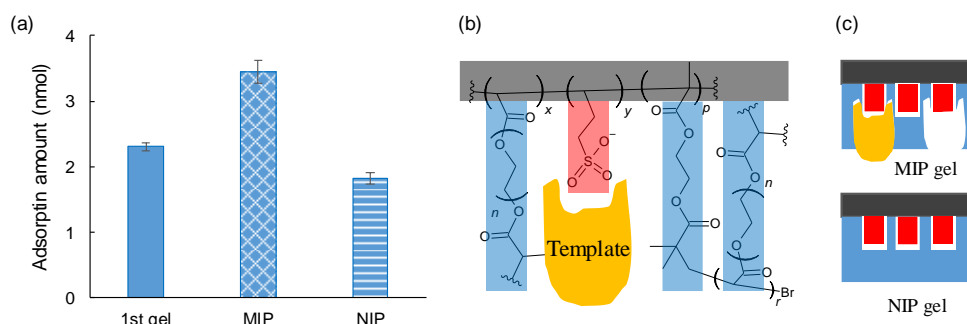


Fig. 3 (a) The adsorption amount of the 1st and its 2nd gels with MIP and NIP. (b) A possible MIP sites indicated by the molecular formula of the 2nd gel. (c) Illustrations of a possible MIP and NIP gels.

3.3 Specific adsorption to trypsin

To show the effectiveness of the postmodification approach in preparing MIP gel, trypsin was employed as a template and the specific recognition was realized. In detail, the 1st and 2nd gels were prepared with compositions shown in Tables 5 and 6. Adsorption test was carried out with a sample solution containing 0.03 mM trypsin and 1 mM HCl (to protect trypsin from degradation). As evidenced by the result in Fig. 4, a higher adsorption in the MIP gel than in the NIP gel was achieved, which evidenced a specific recognition to the target protein of trypsin.

Table 5 Compositions of the 1st gel.

23G' (μL)	10% SA (μL)	BIEM (μL)	DMSO (mL)	AIBN (mg)
240 (58.1 mM)	128 (22.2 mM)	20 (23.2 mM)	4	6

Table 6 Compositions of the 2nd gel with MIP. The 2nd gel with NIP was prepared without the presence of trypsin.

Trypsin	14G' (μL)	CuCl (mg)	Bpy (mg)	1 mM HCl (mL)
1 mM	150 (216 mM)	0.03 (2.25 mM)	1.05 (4.5 mM)	1.5

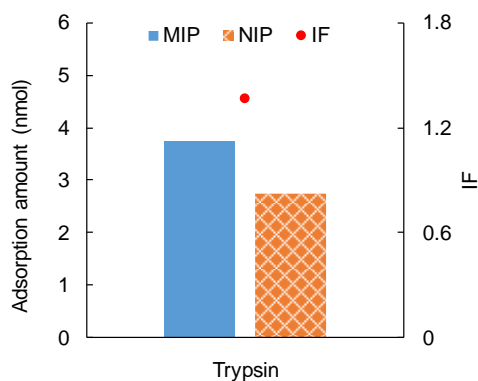


Fig. 4 The adsorption amount and imprinting factor (IF) of the MIP gels and NIP gels prepared with trypsin as template.

4. Conclusion

This work proposed an approach to prepare the MIP hydrogel via a postmodification of a primary gel network. The primary gel was prepared by the copolymerization of a crosslinker, inimer, and functional monomer. Here, the crosslinker was employed to form the main crosslinked polymer structure of the primary network; the inimer was employed for the initiation of the postmodification reaction; the functional monomer was employed to anchor templates on the polymer strands of the primary network, so that MIP sites may form during the postmodification reaction. The post modification required to infiltrate the primary gel with a monomer and a template. Here, the monomer was employed to form structural grafts via the ATRP reaction. With the presence of templates, the grafts may leave cavities as molecularly imprinted sites. This work demonstrated the effectiveness in MIP fabrication using cytochrome c and trypsin as templates. The results showed that the monomer concentration in the postmodification affected the imprinting efficiency.

References

- (1) El-Sharif, H. F.; Phan, Q. T.; Reddy, S. M., Enhanced selectivity of hydrogel-based molecularly imprinted polymers (HydroMIPs) following buffer conditioning. *Anal. Chim. Acta* **2014**, *809*, 155-161.
- (2) Kubo, T.; Arimura, S.; Tominaga, Y.; Naito, T.; Hosoya, K.; Otsuka, K., Molecularly imprinted polymers for selective adsorption of lysozyme and cytochrome c using a PEG-based hydrogel: selective recognition for different conformations due to pH conditions. *Macromolecules* **2015**, *48*, 4081-4087.
- (3) Zhang, Z.; Zhang, X.; Liu, B.; Liu, J., Molecular Imprinting on Inorganic Nanozymes for Hundred-fold Enzyme Specificity. *J. Am. Chem. Soc.* **2017**, *139*, 5412-5419.
- (4) Dong, C.; Shi, H.; Han, Y.; Yang, Y.; Wang, R.; Men, J., Molecularly imprinted polymers by the surface imprinting technique. *Eur. Polym. J.* **2021**, *145*, 110231.
- (5) Fresco-Cala, B.; Batista, A. D.; Cardenas, S., Molecularly Imprinted Polymer Micro- and Nano-Particles: A Review. *Molecules* **2020**, *25*.
- (6) Hoshino, Y.; Kodama, T.; Okahata, Y.; Shea, K. J., Peptide Imprinted Polymer Nanoparticles: A Plastic Antibody. *J. Am. Chem. Soc.* **2008**, *130*, 15242-15243.
- (7) Canfarotta, F.; Poma, A.; Guerreiro, A.; Piletsky, S., Solid-phase synthesis of molecularly imprinted nanoparticles. *Nat. Protoc.* **2016**, *11*, 443-455.
- (8) Chen, L.; Xu, S.; Li, J., Recent advances in molecular imprinting technology: current status, challenges and highlighted applications. *Chem. Soc. Rev.* **2011**, *40*, 2922-42.
- (9) Xing, R.; Wang, S.; Bie, Z.; He, H.; Liu, Z., Preparation of molecularly imprinted polymers specific to glycoproteins, glycans and monosaccharides via boronate affinity controllable-oriented surface imprinting. *Nat. Protoc.* **2017**, *12*, 964-987.
- (10) Titirici, M.-M.; Sellergren, B., Thin Molecularly Imprinted Polymer Films via Reversible Addition-Fragmentation Chain Transfer Polymerization. *Chem. Mater.* **2006**, *18*, 1773-1779.
- (11) Zhao, X.; He, Y.; Wang, Y.; Wang, S.; Wang, J., Hollow molecularly imprinted polymer based quartz crystal microbalance sensor for rapid detection of methimazole in food samples. *Food Chem.* **2020**, *309*, 125787.
- (12) Zhang, G.; Yu, Y.; Zhang, L.; Lin, B.; Wang, Y.; Guo, M.; Cao, Y., Precise detection of prostate specific antigen in serum: A surface molecular imprinted sensor based on novel cooperated signal amplification strategy. *Sensors and Actuators B: Chemical* **2020**, *302*, 126998.
- (13) Roy, E.; Patra, S.; Tiwari, A.; Madhuri, R.; Sharma, P. K., Introduction of selectivity and specificity to graphene using an inimitable combination of molecular imprinting and nanotechnology. *Biosens. Bioelectron.* **2017**, *89*, 234-248.
- (14) Zeng, Y.; Zhou, Y.; Zhou, T.; Shi, G., A novel composite of reduced graphene oxide and molecularly imprinted polymer for electrochemical sensing 4-nitrophenol. *Electrochim. Acta* **2014**, *130*, 504-511.
- (15) Mahajan, R.; Rouhi, M.; Shinde, S.; Bedwell, T.; Incel, A.; Mavliutova, L.; Piletsky, S.; Nicholls, I. A.; Sellergren, B., Highly Efficient Synthesis and Assay of Protein-Imprinted Nanogels by Using Magnetic Templates. *Angew. Chem. Int. Ed.* **2019**, *58*, 727-730.
- (16) Cuthbert, J.; Beziau, A.; Gottlieb, E.; Fu, L.; Yuan, R.; Balazs, A. C.; Kowalewski, T.; Matyjaszewski, K., Transformable Materials: Structurally Tailored and Engineered

-
- Macromolecular (STEM) Gels by Controlled Radical Polymerization. *Macromolecules* **2018**, *51*, 3808-3817.
- (17) He, H.; Averick, S.; Mandal, P.; Ding, H.; Li, S.; Gelb, J.; Kotwal, N.; Merkle, A.; Litster, S.; Matyjaszewski, K., Multifunctional Hydrogels with Reversible 3D Ordered Macroporous Structures. *Advanced Science* **2015**, *2*, 1500069.
- (18) Lutz, J.-F., Polymerization of oligo(ethylene glycol) (meth)acrylates: Toward new generations of smart biocompatible materials. *J. Polym. Sci., Part A: Polym. Chem.* **2008**, *46*, 3459-3470.

General conclusion

The electrophoretic technology is advancing with improved separation performance, more integrative form, and more compatible manner with upward and downward analysis. With these aims, this thesis reports several fundamental studies about electrophoretic analyses as following:

Chapter I targets at an accurate quantitative analysis via an online fluorescent detection-based CE system. The analytes' inequivalent photobleaching was detected with the assistance of an online image detection system. To avoid the interference of analytes' inequivalent photobleaching with quantitative determination, this work plotted an image process method for tracing the real-time fluorescent intensity of analytes. The proposed method allowed to collect the analytes' fluorescent intensities at equivalent photo exposure duration, thus the inequivalent photobleaching was avoided and the accuracy of quantitative analysis would be improved. As a result, this work improved the relative error to 0.3-3.2% and a more practical operation because the efforts to restrict the photobleaching were exempted.

Chapter II attempts to develop a fast and high resolution CE protocol by using a new size sieving matrix, which is a *copoly*(PEGDA/PEGA) hydrogel with a tunable network structure. The size sieving performance was evaluated with a standard DNA ladder. Results showed that the *copoly*(PEGDA/PEGA) hydrogel was able to provide comparable separation resolution with the authentic PA hydrogel. In addition, the results demonstrated that both fast and high resolution could be obtained in a *copoly*(PEGDA/PEGA) gel with the low polymer concentration and high crosslinker ratio. The *copoly*(PEGDA/PEGA) gel showed a high repeatability in CE separation, owing to the merit of less volume shrinkage upon polymerization.

Chapter III focuses on the development of MIP hydrogels for the specific recognition of target proteins, and then the MIP hydrogels were used in SGE to offer an affinity to target protein. The *copoly*(PEGDA/PEGA) hydrogel was employed as a new MIP material and the gel compositions were adjusted for improving the specificity of molecular recognition to cytochrome c. Shorter crosslinker and crosslinker ratio of no less than 6/4 were demonstrated to provide high specificity. A hybrid slab gel was developed containing MIP gel zone for the selective retardation of target protein and PA gel zone for the size sieving separation, with which a selective electrophoretic separation of cytochrome c was realized.

Chapter IV proposes a new method to fabricate MIP structures, which is the grafting of MIP

structure on a crosslinked network. A reaction system was reported to be successful to realize the postmodification of a hydrogel. A controllable MIP grafting method was demonstrated by using cytochrome c as template and different concentrations of PEGDA as monomer. Although further progress is still demanded, the present result has shown a specific molecular recognition when using cytochrome c and trypsin as templates.

List of publications

Chapter I

Liu, C.; Yamaguchi, Y.; Wang, Y.; Dou, X.; Kubo, T.; Otsuka, K.:

Online fluorescence imaging method by reducing the inequivalent photobleaching for quantitative capillary electrophoresis,

Sens. Actuator B-Chem. **2020**, *319*, 128035. [DOI: 10.1016/j.snb.2020.128035]

Chapter II

Liu, C.; Kubo, T.; Naito, T.; Otsuka, K.:

Controllable molecular sieving by *copoly*(poly(ethylene glycol) acrylate/poly(ethylene glycol) diacrylate) based hydrogels via capillary electrophoresis for DNA fragments,

ACS Appl. Polym. Mater. **2020**, *2*(9), 3886-3893. [DOI: 10.1021/acsapm.0c00567]

Chapter III

Liu, C.; Kubo, T.; Otsuka, K.:

Copoly(poly(ethylene glycol) diacrylate/poly(ethylene glycol) acrylate) based molecularly imprinted polymer for the specific adsorption and selective electrophoretic separation of native cytochrome c. (under submission)

Chapter IV

Liu, C.; Kubo, T.; Otsuka, K.:

Fabrication of protein recognition structures by grafting molecularly imprinted polymer on a crosslinked hydrogel.

(in preparation)

Other publications

1. Original research paper

Kubo, T.; Watanabe, N.; Ikari, S.; Liu, C.; Kanao, E.; Naito, T.; Sano, T.; Otsuka, K.:

Fluorescent Detection of the Target Protein via a Molecularly Imprinted Hydrogel,

Anal. Methods **2021**, in press. [DOI: 10.1039/D0AY02341H]

2. Review

Liu, C.; Kubo, T.; Otsuka, K.:

Hydrogels in electrophoresis: Applications and advances,

Anal. Sci. **2021**, 37(6), 807-816. [DOI: 10.2116/analsci.20R004]

Acknowledgments

The present thesis is a summary of the author's research work from April 2018 to June 2021. These studies were conducted in Department of Material Chemistry, Graduate School of Engineering, Kyoto University under the supervision of Professor Koji Otsuka. Here, the author would like to express her gratitude to Professor Otsuka for his generous supporting, warm understanding, and kind instruction during the composition period of this thesis.

The author is grateful to Professor Kazunari Akiyoshi (Graduate School of Engineering, Kyoto University) for providing the experimental apparatus and for his thoughtful comments and discussions, and Professor Seiji Matsubara (Graduate School of Engineering, Kyoto University) for his splendid comments and discussions.

The author would like to express her appreciation to Associate Professor Takuya Kubo (Graduate School of Engineering, Kyoto University) for his daily discussion and inspiring suggestions throughout this work. The author feels grateful to Dr. Toyohiro Naito (Graduate School of Engineering, Kyushu University) and Dr. Tetsuya Tanigawa and Dr. Yoshiyuki Watabe (Graduate School of Engineering, Kyoto University) for their valuable comments and instructions about the experimental details in this work.

The author would like to take this opportunity to thank Professor Emeritus Toshikazu Takigawa and Associate Professor Junichi Horinaka (Graduate School of Engineering, Kyoto University) for their generous offering of the use of experimental equipment.

The author feels thankful to Dr. Eisuke Kanao (Graduate School of Pharmaceutical Sciences, Kyoto University), the other members (present and graduated) of the Otsuka Lab, and author's roommate for their accompany and encouragement during these days in Japan.

The author would like to acknowledge the financial supports from the Japan Society for the Promotion of Science (JSPS) through the JSPS Fellowship for Young Scientists, the Monbukagakusho Honors Scholarship, the National Natural Science Foundation of China [grant number 21804042], and the Otsuka Lab.

Finally, the author thanks her family member and friends for their encouragement that helped her to continue academic career.

As the saying goes “*how can there be peace in life, it just because someone is weight-bearing ahead for you!*”. The author is grateful to the world’s peace.

June 2021

Chenchen Liu